

Dynamic weighing calibration method for liquid flowmeters – A new approach

Dissertation

zur Erlangung des akademischen Grades

**Doktoringenieur
(Dr.-Ing.)**

vorgelegt der
Fakultät für Maschinenbau der
Technischen Universität Ilmenau

von Herrn
Dipl.-Ing. Jesús Jaime Aguilera Mena
geboren am 16.09.1979 in Durango/Mexiko

Tag der Einreichung: 13.12.2011

Tag der Verteidigung: 14.06.2012

Doktorvater: Univ.-Prof. Dr.-Ing. habil. Thomas Fröhlich / TU Ilmenau

2. Gutachter: Dir. u. Prof. Dr. Roman Schwartz / PTB Braunschweig

3. Gutachter: Univ.-Prof. Dr.-Ing. habil. Tino Hausotte / FAU Erlangen-Nürnberg

urn:nbn:de:gbv:ilm1-2012000461

Danksagung

Die vorliegende Arbeit entstand während meiner Tätigkeit als wissenschaftlicher Angestellter im Fachbereich „Flüssigkeiten“ der Physikalisch-Technischen Bundesanstalt (PTB) in Braunschweig.

Sehr herzlich möchte ich mich bei Herrn Univ. Prof. Dr.-Ing. habil. Thomas Fröhlich, Leiter des Fachgebietes Prozessmess- und Sensortechnik der TU Ilmenau, für die intensive Betreuung und die Unterstützung bei der Bearbeitung des Themas bedanken.

Mein außerordentlicher Dank gilt Herrn Dir. u. Prof. Dr.-Ing. Roman Schwartz, Leiter der Abteilung „Mechanik und Akustik“, Dr.-Ing. Gudrun Wendt, Leiterin des Fachbereichs „Flüssigkeiten“, und Dr.-Ing. Rainer Engel, Leiter der Arbeitsgruppe „Rückführung Flüssigkeitsmessungen“ für die Gelegenheit und Motivation im Ausführen meiner Doktorarbeit an der PTB.

Bei Frau Dipl.-Phys. Angelika Täubner, wissenschaftliche Mitarbeiterin im Fachbereich „Darstellung Beschleunigung und Stoßdynamik“, sowie Herrn Klaus Middlestädt und Herrn Andreas Hein aus dem Fachbereich „Flüssigkeiten“ danke ich sehr für Ihre Kooperation und Unterstützung bei meinen experimentellen untersuchen.

Frau Dr.-Ing. Iryna Marfenko und Herrn Dr.-Ing. Jann Neumann danke ich ebenfalls herzlich für die hilfreichen fachlichen Hinweise und die Korrektur meines Manuskripts.

Meine große Anerkennung gilt meiner Frau und meiner Familie in Mexiko und der Ukraine, die mich stets aufgemuntert und unterstützt haben, um meine Doktorarbeit erfolgreich zu vollenden.

Jesús Jaime Aguilera Mena

Zusammenfassung

Das Ziel dieser Doktorarbeit ist es, die ersten Schritte zur Umsetzung einer neuen Kalibriermethode für Durchflussmessgeräte zu beschreiben. Diese Forschungsarbeit wurde im Fachbereich „Flüssigkeiten“ der Physikalisch-Technischen Bundesanstalt durchgeführt. Sie realisiert ein dynamisches Wägeverfahren, welches es ermöglicht, den Massendurchfluss mehrmals unter stationären und quasistationären Bedingungen zu messen. Eine somit verkürzte Kalibrierzeit bringt einen wichtigen Vorteil für Durchfluss-Kalibrierlaboratorien, um ihre Kalibrierkosten, den Energieverbrauch und die Arbeitsbelastung zu reduzieren.

Die vorgeschlagene Kalibriermethode beruht auf einer gründlichen Analyse der Wechselwirkung zwischen den durchflussinduzierten Kräften im Messprozess und der Dynamik des Wägesystems. Basierend auf dieser Analyse wird anschließend eine Reihe von Signalverarbeitungstechniken angewandt, um sowohl die Stärke der unerwünschten, durch den Durchfluss induzierten Kräfte zu verringern, als auch das Messrauschen im Ausgangssignal zu dämpfen. Damit kann die Messgröße einerseits sehr genau und andererseits auch als Funktion der Zeit ermittelt werden.

Die Wirksamkeit der neuen Kalibriermethode für Durchfluss-Messgeräte wird durch numerische und experimentelle Tests validiert. Die Ergebnisse zeigen, dass eine Genauigkeit kleiner als 0,1 % erreichbar ist. Außerdem gibt die vorliegende Arbeit Empfehlungen, wie das vorgeschlagene Messprinzip zukünftig noch weiter verbessert werden kann.

Abstract

The aim of this dissertation is to describe the first steps made towards the realization of a new calibration method for liquid flowmeters. Such the research work carried out at the liquid flow department of the Physikalisch-Technische Bundesanstalt implements a dynamic weighing approach, to estimate the mass flow rate several times under stationary and quasi-steady conditions, thus shortening the calibration time. The latter statement represents a significant benefit for flow calibration laboratories, which seek to reduce their calibration costs, energy consumption, and workload.

The proposed calibration method relies on a thorough analysis of the interaction between the acting flow-induced forces present in the measurement process, and the dynamics of the weighing system. Then, a series of signal processing techniques based on such an analysis are implemented in order to attenuate the magnitude of the undesired flow-induced forces as well as the embedded measurement noise from the system's output signal, so the measurand can be determined as a time-varying state variable.

The effectiveness of this new flowmeter calibration method is validated by a series of numerical and experimental tests in which, according to their results, it reveals that an accuracy level smaller than 0,1% is attainable by applying the proposed method. Furthermore, this document offers a guideline of how to improve the performance of the proposed measurement principle at a future date.

CONTENTS

| | | |
|-----------|--|-----------|
| 1. | INTRODUCTION..... | 1 |
| 1.1 | The importance of fluid flow measurements..... | 1 |
| 1.2 | Motivation of the research work..... | 2 |
| 1.3 | Structure of the research work..... | 2 |
| 2. | CURRENT SITUATION AND GOAL OF THE RESEARCH WORK..... | 4 |
| 2.1 | Definition of mass and volumetric flow..... | 4 |
| 2.2 | Definition of a flowmeter..... | 5 |
| 2.3 | Traceability chain of fluid flow measurements..... | 7 |
| 2.4 | Working principle of a liquid flow primary standard..... | 8 |
| 2.5 | Current situation..... | 11 |
| 2.5.1 | Gravimetric and volumetric flying start-and-stop liquid flow primary standard..... | 11 |
| 2.5.2 | Gravimetric and volumetric standing start-and-stop liquid flow primary standard..... | 12 |
| 2.5.3 | Dynamic level gauging volumetric liquid flow primary standard..... | 14 |
| 2.5.4 | ISO dynamic gravimetric liquid flow primary standard..... | 15 |
| 2.5.5 | Dynamic weighing liquid flow primary standard with immersed pipe..... | 17 |
| 2.5.6 | Dynamic weighing liquid flow primary standard assisted by an in-line flowmeter..... | 18 |
| 2.6 | The proposed dynamic weighing liquid flow primary standard..... | 20 |
| 3. | INPUT SIGNAL, MODELING OF THE DYNAMIC WEIGHING LIQUID FLOW STANDARD AND THE CONNECTING VOLUME EFFECT..... | 22 |
| 3.1 | Input signal..... | 24 |
| 3.1.1 | Collected water mass force..... | 24 |
| 3.1.2 | Hydrodynamic force..... | 25 |
| 3.1.3 | Buoyancy force..... | 27 |
| 3.1.4 | Total fluid force and its block diagram representation..... | 27 |
| 3.2 | The weighing system and its numerical representation..... | 28 |

| | | |
|-----------|---|-----------|
| 3.2.1 | Spring force..... | 30 |
| 3.2.2 | Inertial force and system total mass..... | 31 |
| 3.2.3 | Damping force..... | 32 |
| 3.2.4 | 1-Degree-of-Freedom motion equation of the weighing system..... | 33 |
| 3.2.5 | Technical considerations in regards to the modeling of the weighing system..... | 37 |
| 3.2.6 | General representation of the weighing system internal filter and the discrete time representation of its output signal..... | 38 |
| 3.3 | The connecting volume effect in liquid flow measurements..... | 42 |
| 3.3.1 | Accuracy considerations in relation to the connecting volume effect in dynamic liquid flow measurements..... | 46 |
| 4. | FILTERING TECHNIQUES FOR THE DETERMINATION AND ACCURACY OF MASS FLOW RATE (PROCESS MODEL)..... | 49 |
| 4.1 | Derivation of a process noise filter for the attenuation of the hydrodynamic force effect upon the balance output response and the determination of mass flow rate..... | 51 |
| 4.2 | Proposed filter algorithms for an improved mass flow rate calculation based on the identification and reduction of measurement noise..... | 57 |
| 4.2.1 | Central moving average filter..... | 58 |
| 4.2.2 | Least-Mean-Square adaptive filter..... | 60 |
| 4.2.3 | Linear Kalman filter..... | 65 |
| 4.3 | Summary..... | 73 |
| 5. | NUMERICAL DETERMINATION OF MASS FLOW RATE AND THE RESPONSE OF THE DYNAMIC WEIGHING LIQUID FLOW STANDARD..... | 74 |
| 5.1 | Fluid forces acting upon the weighing system (input signal)..... | 75 |
| 5.2 | Frequency response of the weighing system..... | 77 |
| 5.3 | Continuous time and discrete time response of the balance..... | 81 |
| 5.4 | Hydrodynamic force filter..... | 85 |
| 5.5 | Proposed measurement noise filters..... | 87 |
| 5.5.1 | Central moving average filter..... | 87 |
| 5.5.2 | Least-Mean-Square adaptive filter..... | 89 |
| 5.5.3 | Linear Kalman filter..... | 91 |
| 5.5.4 | Summary..... | 95 |

| | | |
|-----------|---|------------|
| 5.6 | The influence of the data sampling frequency and the low pass filter cutoff frequency upon the mass flow rate estimate values and its measurement accuracy enhancement..... | 96 |
| 6. | EXPERIMENTAL RESULTS..... | 102 |
| 6.1 | Transfer standard used for the liquid flow comparison..... | 102 |
| 6.2 | Data acquisition system..... | 104 |
| 6.3 | Implementation of an accelerometer to detect the initial time of the measurement process..... | 105 |
| 6.4 | Usage of a non-contact laser displacement sensor to characterize the water jet impact height..... | 107 |
| 6.5 | Characterization of the weighing system's stiffness and damping coefficients..... | 109 |
| 6.6 | Results..... | 111 |
| 6.6.1 | Hydrodynamic force filter..... | 112 |
| 6.6.2 | Analytical and experimental estimation of the hydrodynamic force..... | 114 |
| 6.6.3 | Estimation of the collected mass force..... | 115 |
| 6.6.4 | Time offset correction..... | 117 |
| 6.6.5 | Summary..... | 122 |
| 7. | CONCLUSIONS AND OUTLOOK..... | 126 |
| | NOMENCLATURE..... | 130 |
| | REFERENCES..... | 135 |

1. Introduction

1.1 The importance of fluid flow measurements

Liquid flow measurement technology is an important area of engineering that involves all industrial sectors wherein fluids, such as water, hydrocarbons, bio-fuels, and so on, are transported and/or traded. The main purpose of this area consists in providing reliable technology that can technically assure the amount of fluid flowing through a conduit agrees with the magnitude claimed by a system or an individual [1].

Flow measurement technology has significantly matured in the past decades because it is an effective way to commercialize valuable fluids, and it improves the efficiency, quality, and safety in any industrial or scientific process. Nowadays, the main tasks of this sector are focused on the development of more precise flow measurement devices, the improvement of flow calibration rigs in order to characterize flowmeters more accurately, the implementation of new manufacturing as well as calibration methods that deliver more affordable and reliable flow metering technologies to the industry.

A liquid flow calibration rig plays a fundamental role in all the tasks mentioned above, as this is the only system capable to reproduce the unit of flow by itself. The latter is because the flow rate unit is a derived quantity that is realized by the direct traceability to the fundamental units of time, mass, length, and temperature. As a remark, such a primary standard can reproduce the flow unit by either using a weighing approach to obtain mass flow (kg/s), or by dimensional means to directly obtain the volumetric flow (m³/s). Once the primary standard is under operation, it can proceed with its final goal of disseminating the measurand by the calibration of flowmeters in different industry sectors.

1.2 Motivation of the research work

The motivation for carrying out this dissertation is focused on the first steps made towards the realization of a dynamic weighing method, which estimate the time-varying mass flow rate, and allows the calibration of liquid flowmeters in a shorter time.

At present, the start-and-stop flowmeter calibration systems define the flow unit as an average quantity, given by metering the difference between the initial and final quantity of the liquid and the time taken for such a collection. One of the main goals of this research work is the development of a measurement principle that allows using the existing gravimetric start-and-stop flowmeter calibration facilities to determine the flow unit several times within a single measurement run. This means, a calibration method that will measure the time-varying mass flow rate (under stationary and quasi-steady flow conditions) by analyzing the fluid-mechanical system dynamics, and the output signal response of the weighing system. The latter will benefit the flow calibration laboratories in reducing their calibration time, and thus, the calibration costs, energy consumption, and work load. Another important goal of this research work is to present an alternative calibration method that can avoid the bypass valve timing error, which is considered to be the most striking measurement uncertainty contributor, and one of the most difficult components to characterize in a start-and-stop flowmeter calibration system.

1.3 Structure of the research work

The following research work is divided into six parts: **Chapter 2** for instance presents a general overview in the field of flow primary standards, and the state-of-the-art proposed by some national measurement Institutes (NMIs) and calibration laboratories, in regards to weighing and volumetric calibration methods. Then in **Chapter 3**, the manuscript depicts the main variables (input) involved in the measurement process as well as a general numerical representation of the liquid flow standard. **Chapter 4** deals with the derivation and application of the process equation to calculate the mass flow rate estimate via dynamic weighing as well as the performance assessment of some filter algorithms to attenuate the measurement noise from the measurand. The latter is with the aim to make the estimate calculations more accurate. The following part of this research work (**Chapter 5**) describes the numerical simulation and sequence of the measurement process, comprising the input variables of the process, the flow standard response (system), the estimation of the mass flow rate, and the attenuation of measurement noise from the measurand.

Thereafter, the document describes in **Chapter 6** the components of a prototype flow primary standard used for the application of this new calibration method. Moreover, it shows a series of experimental tests made in order to compare and to validate the results given by proposed calibration method, with those results obtained by a PTB traceable transfer standard.

The final part of this work (**Chapter 7**) addresses the conclusions and remarks reached after analyzing the new calibration method, numerically and experimentally. Additionally, an outlook of the investigation is given in order to underline the advantages and limitations of the proposed calibration method, and how the current results and experiences could help to improve it.

2. Current situation and goal of the research work

2.1 Definition of mass and volumetric flow

The conservation of mass is a fundamental concept of macroscopic physics, which states that the amount of mass existing in a defined or arbitrary space can neither be created nor destroyed. Additionally, the mass is characterized for having two physical properties: its occupying volume and density. For the case of a fluid mass enclosed in a conduit, it is agreed that its density, volume, and its shape can move and change within the time domain. Furthermore, in accordance to the continuity law (**Eq. 2.1**), it is established that the mass flow rate of a fluid entering \bar{m}_{wIN} and leaving \bar{m}_{wOUT} the finite volume tube is the same, as long as the finite volume remains constant in time [1]. Note that the subindex w is used in the equation below to indicate that the fluid in use is water.

$$\underbrace{\bar{m}_{wIN}}_{\rho_{wIN} \cdot \bar{u}_{IN} \cdot A_{IN}} = \underbrace{\bar{m}_{wOUT}}_{\rho_{wOUT} \cdot \bar{u}_{OUT} \cdot A_{OUT}} \quad (2.1)$$

As a definition, the mass flow rate \dot{m}_w is a process variable in which its magnitude is equal to arbitrary cross section of the tube A , wherein the fluid mass passes at an average velocity \bar{u} , and a density ρ_w (**Fig. 2.1**). Moreover, according to the equation of continuity, if there is a constant volume flow rate for a given area change (change in pipe size), then the average velocity will inversely change. On the other hand, the volumetric flow rate through the pipe (finite volume) can be calculated by just multiplying the cross section area of the pipe A , and the average velocity at that location, as shown in **Eq. 2.2**.

$$\bar{V}_w = \bar{u} \cdot A \quad (2.2)$$

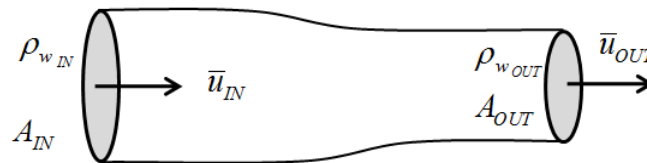


Fig. 2.1 The mass/volume flow rate relationship to the tube cross sectional area and average fluid velocity

2.2 Definition of a flowmeter

A flowmeter is a device that measures the flow rate or the quantity of moving fluid in a closed conduit, and it consists of primary and secondary elements. The flowmeter primary element is a device mounted externally or internally to the fluid conduit. Therefore, it can produce a signal that has a defined relationship to the fluid flow. The latter is in accordance with known physical laws, which relate the interaction of the fluid with the presence of the primary element. The secondary element is the part of the flowmeter that receives a signal from the primary element and displays, records, and/or transmits it as a measure of either mass or volumetric flow rate [2,3].

For the sake of explanation, the turbine flowmeter can be used to illustrate in practical terms the tasks of these two elements. In **Fig. 2.2**, the turbine flowmeter depicts a multi-bladed rotor (primary element) located in the central part of the fluid stream, so as the fluid impinges on the blades, this causes the rotor to spin at an angular velocity approximately proportional to the flow rate [4].

Each of these blades has an embedded ferromagnetic element in order to form a magnetic circuit with the permanent magnet and pickoff coil (secondary elements) in the meter housing [5]. Then, the voltage induced in the coil has the form of a sine wave whose frequency is proportional to the angular frequency of the blades. Thereafter, the output signal is passed through a signal conditioner in order to have a constant amplitude square wave signal of variable frequency. Finally, such a square wave frequency signal and a meter factor are used to calculate the flow rate.

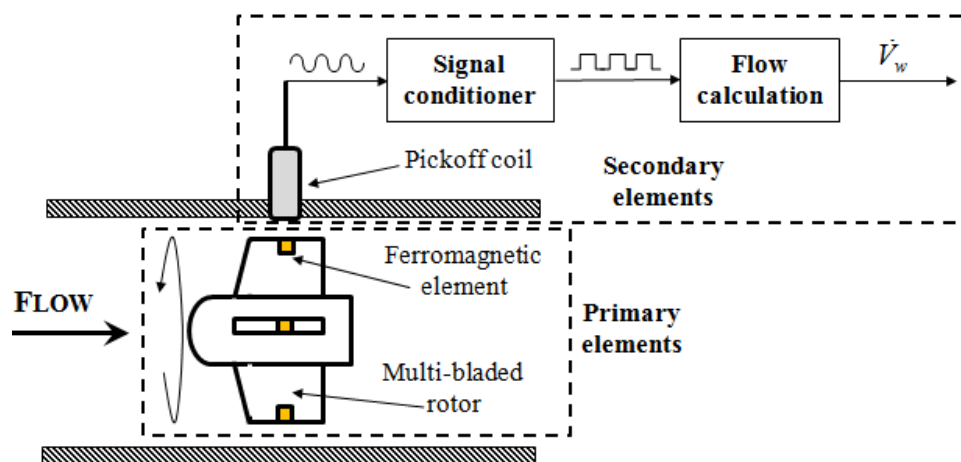


Fig. 2.2 Example of primary and secondary elements of a flowmeter (turbine) [3, 5]

The meter factor is a value used to scale the reading of a flowmeter into a quantity that corresponds to the current magnitude of the measurand flow rate. Such a factor is determined when comparing the flow metering device output signal to a flow calibration rig (flow standard) of known accuracy and measurement uncertainty.

As for the different types of flowmeters, **Table 2.1** presents a classification chart, wherein the flow metering devices are divided into three groups depending on their sensing principle. These are: mass, volume, and differential pressure.

As the name suggests, the mass and volumetric flowmeters are based on the measurement of motion of mass or a volume quantity in a defined time. On the other hand, the measurement principle of the differential pressure flowmeters is based on the pressure difference between the upstream and downstream side of the meter (caused by the contraction/expansion of the fluid), and its proportional response with the flow passing through the meter. The determination of flow rate by means of using differential pressure flowmeters is given by a theoretical equation, in which the dimensions and geometry of the meter body are taken into account, as well as the pressure, temperature and fluid density. Additionally, the calculation is corrected by an experimental factor called the discharge coefficient, which aims to include the frictional flow factor, and a more realistic magnitude of the cross section area of the fluid into the equation [4,6]. As a remark, the quantity yield by the differential pressure flowmeters can be either calculated as mass or volumetric flow rate, as long as the fluid density is known.

| Mass | Volume | Differential pressure |
|----------------------------|---------------------------------|---------------------------------------|
| Thermal flowmeter | Positive displacement flowmeter | Orifice plate |
| Angular momentum flowmeter | Turbine flowmeter | Venturi nozzle |
| Coriolis flowmeter | Vortex flowmeter | Sonic nozzle |
| | Electromagnetic flowmeter | Variable area flowmeter (Rotameter ®) |
| | Ultrasonic flowmeter | Pitot tube |
| | | Laminar flow element |

Table 2.1 Flowmeter classification [7]

Despite the given classification of flowmeters listed in **Table 2.1**, one must be aware that each of those metering devices works with different physical principles, construction designs, fluids, and installation conditions. A further description of this topic can be found in: Spitzer's [5], Baker's [7], and Miller's [8] flow measurement handbooks.

2.3 Traceability chain of fluid flow measurements

In order to ensure the accuracy level of a flowmeter in a measurement process, it is necessary first to calibrate the device periodically against either a national flow standard or an accredited flow calibration rig. Thus, after the calibration [9] has been carried out, the characterized flowmeter can claim to be traceable [10]. By definition, traceability means that the result of a flow measurement, no matter where it is made, can be related to a national flow measurement standard as long as the so called traceability chain is not broken, and each of the different standards involved have a stated uncertainty.

This concept can be exemplified in **Fig. 2.3**, wherein national flow standards have direct traceability to the fundamental standards of mass, time, temperature and length, which are necessary to define the flow unit. As shown in **Fig. 2.3**, such standards are located at the top of the diagram, in order to emphasize their highest level of measurement accuracy. Moreover, for the sake of metrological assurance, the national flow standards must undergo a periodical measurement comparison program among other national flow labs with similar accuracy (i.e., NEL in the UK, NIST in the USA, and PTB in Germany), with the aim to ensure that the flow unit is disseminated with the claimed measurement uncertainty [11].

Then, below the national standards are linked the state-approved primary and secondary flow standards, which feature the lowest measurement uncertainty that a private calibration laboratory or flowmeter manufacture can achieve. Finally, at the bottom of the diagram are the flowmeters or flow measuring rigs, which hold a relatively low measurement accuracy (compared to the two previous groups) but acceptable for industrial process applications. Note that the combined measurement uncertainty level attained after calibrating the flowmeter will eventually depend on the linearity, repeatability, reproducibility of the meter itself [12], but also in great part of the standard used to characterize the measuring device.

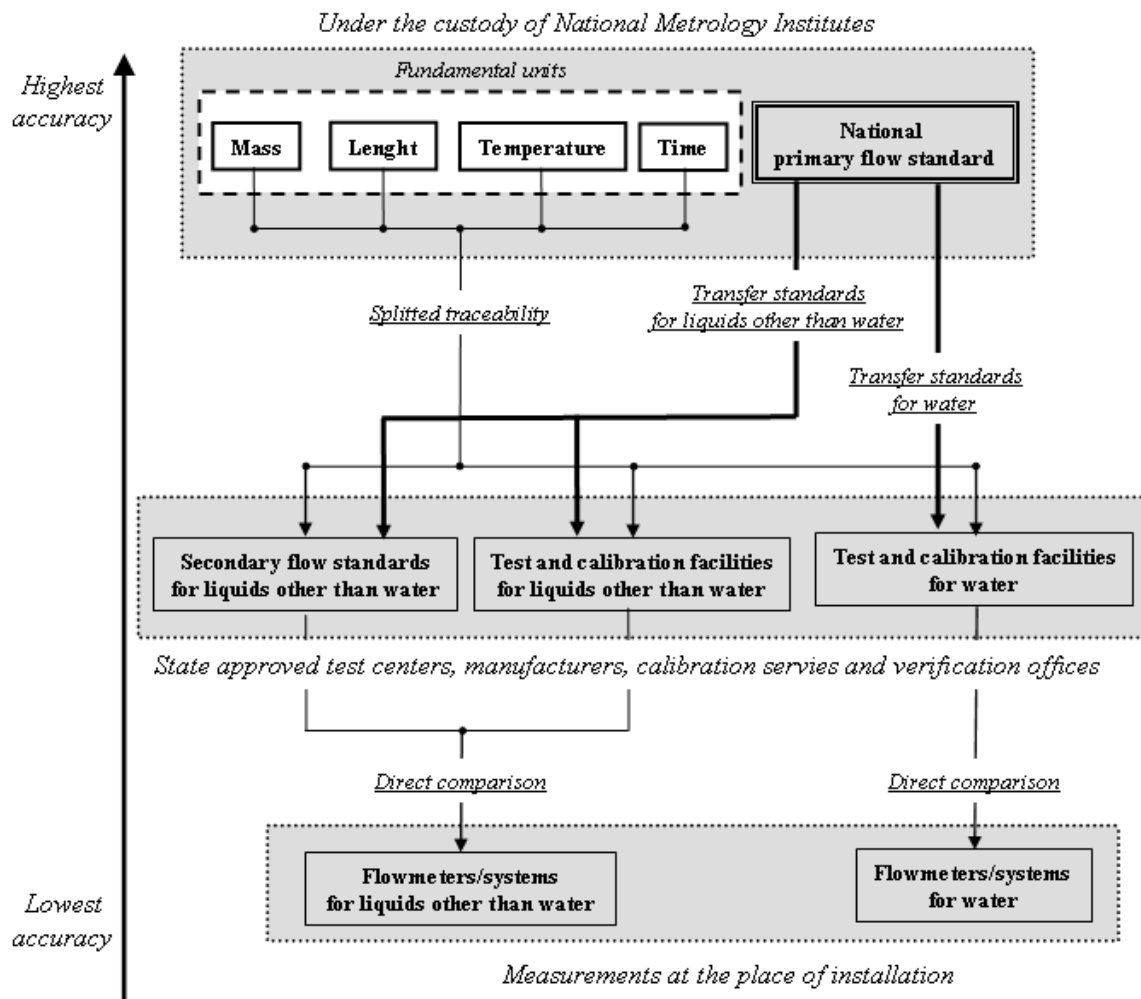


Fig. 2.3 Flow traceability chain and the hierarchy of measurement standards [13]

2.4 Working principle of a liquid flow primary standard

One very important characteristic of a primary flow standard already recalled in text is that unlike secondary and working standards, the primary standard is capable to reproduce the flow unit by itself, without reference to some other standard of the same quantity (but only to the fundamental units) [12].

In terms of its conceptual design (Fig. 2.4), the primary flow standard is a hydraulic circuit in which the liquid is driven by a pumping system, and a control valve is responsible of setting up the operational flow rate as well as keeping it quasi steady during a calibration. Then, the pumped liquid circulates through a pipeline of different diameter sizes and geometries, with the goal to transfer the fluid from the meter under calibration to the mass or volume reference standard.

The Meter Under Calibration (MUC) section shown in **Fig. 2.4** is a straight pipeline, which holds the flowmeter to be calibrated and is long enough to allow the flow profile to be swirl-free [7]. In some cases, due to high flow disturbances caused by the upstream fittings (i.e. valves), and/or limited space to install a long pipeline, a flow straightener is used in order to guarantee a uniform fully developed turbulent flow profile.

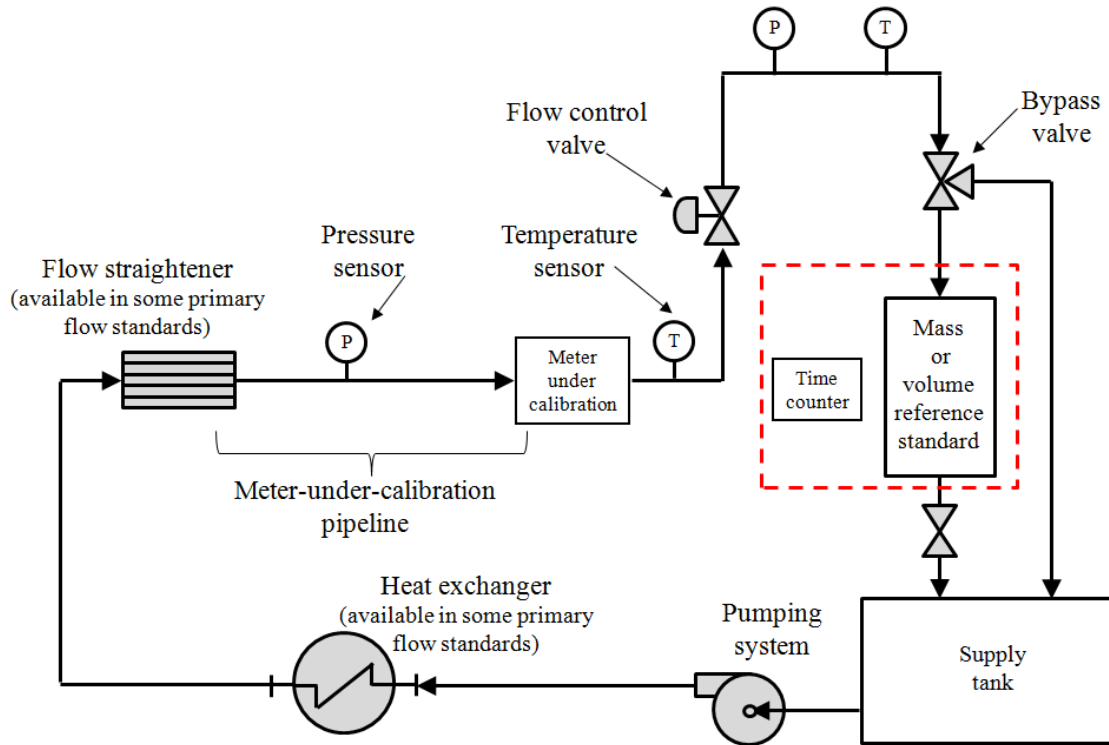


Fig. 2.4 Schematic diagram of the main components of a liquid flow primary standard

Once the circulating fluid passes the flowmeter, it is discharged by a bypass valve into a mass or volume reference standard for effects of flow calculation. Thereafter, when the reference standard reaches a certain level, the fluid is re-directed into a supply tank to continue the liquid circulation. The outcome from this process is either an average flow rate resulting from the totalized mass m_{Total} or volume V_{Total} contained in the reference standards and the time t_{Total} taken to collect such an amount of fluid (**Eq. 2.3** and **Eq. 2.4**).

$$\bar{m}_w = \frac{m_{Total}}{t_{Total}} \quad (2.3)$$

$$\bar{V}_w = \frac{V_{Total}}{t_{Total}} \quad (2.4)$$

The mass flow rate can be converted into volumetric flow rate (or vice versa) if the fluid density is known. In this case, a relationship between the liquid temperature and its density is developed for this purpose by means of analyzing the density of a liquid sample at different temperatures, consulting some standard temperature-density tables, or by installing an online densitometer [14].

The calibration of flowmeters by using primary flow standards is based on the principle of mass conservation applied to a control volume. The conservation of mass principle here states that over a time increment, the change in the mass/volume contained in the reference standards is equal to the mass/volume that flows through control volume defined by: the MUC, the connecting pipe, and the mass/volume reference standard.

When performing a calibration, the primary flow standard must provide the most stable conditions in terms of flow, temperature, and pressure, so that the MUC cannot be highly-influenced by the pulsatile flow [2], fluid density gradients due to temperature variations and so on. The ambient temperature is also an important process parameter in order to avoid slight changes on the calibration factor due to the thermal expansion/contraction of the flowmeter body (i.e. flowmeter internal diameter).

In some cases, the primary flow standards are equipped with heat exchangers in order to keep the fluid temperature as constant as possible [14], and/or an air conditioning system to avoid large temperature gradients among the MUC, connecting pipe, and the mass/volume reference standards.

During the operation of a dynamic liquid flow primary standard is rather important to keep the best possible conditions of *quasi-steady and quasi-stationary flow and temperature*, in order to calibrate a flowmeter [15]. In this instance, the term quasi-steady flow implies a flow, wherein the fluid temperature, pressure, and cross section area of the pipe may differ from point to point, but the flow will slightly change with time. On the other hand, the term quasi-uniform flow stands for the fluid velocity, which is nearly equal at all points along the straight and constant cross section area of the meter-under-calibration pipeline.

If a fully steady uniform flow were achieved by a liquid flow primary standard, the dynamic measurements would be simply assumed to be the same at all times, and at any point of the pipeline, and therefore equal to a mean value. In practice, this is not the case because, the flow is in a turbulent regime, the pumping system and pipe fittings produced an inherent pulsating flow, fluid temperature gradients are mostly present in the system, and so on.

2.5 Current situation

There are different approaches for the realization of the measurand flow. **Table 2.2** serves as a guide for the classification of the primary standards, categorizing the facilities by static and dynamic, and subdividing them into gravimetric and volumetric. The dynamic weighing primary standard is the new calibration approach, in which this investigation is concentrated on. The accuracy issues of these types of facilities are not included in the classification, because the metrological features of a standard depend upon the calibration requirements, and the technological capabilities of each flow laboratory. A general description of each calibration approach is given in the following sections.

| | Gravimetric (Weighing system) | Volumetric (Scaled tank) |
|--|---|------------------------------------|
| Static Flying start-and-stop | Static weighing +diverter | Level gauging +diverter |
| Static Standing start-and-stop | Static weighing | Level gauging |
| Dynamic | ISO definition | Dynamic Level gauging |
| | Dynamic weighing | |

Table 2.2 Classification of liquid flow primary standards [16]

2.5.1 Gravimetric and volumetric flying start-and-stop liquid flow primary standard

This type of primary standards (gravimetric and volumetric) comprise three main components for the determination of flow rate: a bypass valve also known in the flow metrology field as a

diverter valve [17], a collection vessel, and either a balance or a calibrated volumetric tank for the determination of mass or volumetric flow rate, respectively (**Fig. 2.5**).

The method of operation consists in measuring the initial vessel mass or the volume before the filling of liquid starts. At the same time, the fluid circulates through the system, until flow reaches a quasi-steady flow condition **(a)**. This requirement is mandatory for the accurate measurement of flow rate, and thus, a reliable characterization of the MUC. When process conditions are stable, a trigger signal is sent to activate the diverter valve, and thus driving the liquid into the vessel, and to start counting the collection time by means of a timer **(b)**. When a certain amount of fluid is gathered into the weighing vessel or the volumetric tank, a second trigger signal is sent to re-direct the liquid flow back to the supply tank, and to stop the timer **(c)**. Once the collected water reaches an equilibrium condition, the totalized mass or volume of liquid is measured and divided by the collection time, in order to obtain the average mass or volumetric flow rate [5,18].

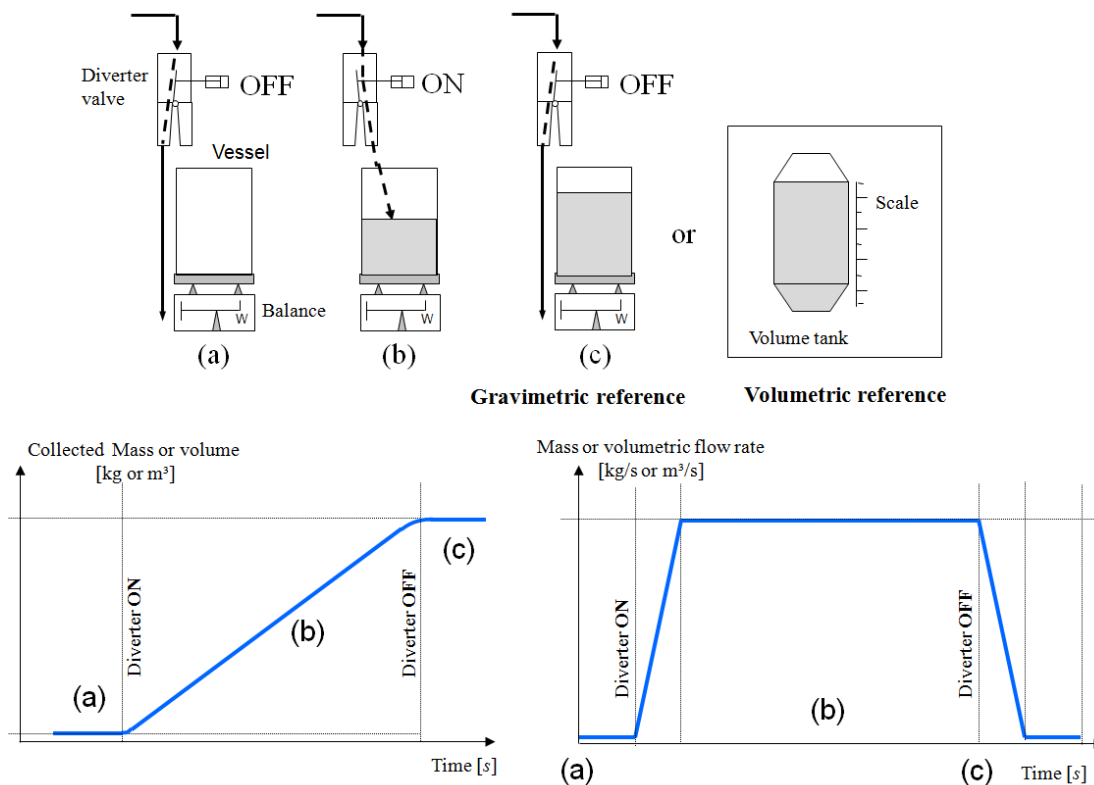


Fig. 2.5 Gravimetric and volumetric flying start-and-stop primary standard

2.5.2 Gravimetric and volumetric standing start-and-stop liquid flow primary standard

The gravimetric standing start-and-stop primary standard determines the average mass flow rate by collecting an amount of fluid in the collection vessel within a fixed period of time, and then measuring the collected mass or volume by a balance or a scaled volumetric tank, respectively [7,18].

In this type of systems, the measurement run starts by setting a reference fluid level with the assistance of a weir (transfer point), as shown in **Fig. 2.6(a)**. When the flow is stable and the reference level is properly set, the block valve is opened; the fluid passes through the weirs, and it gets into the vessel **(b)** [19]. After a defined period of time, the block valve is closed, and the minor weir sets once again the fluid reference level by pouring the remaining water into the collection vessel **(c)**. As soon as the contained fluid reaches an equilibrium condition, a totalized mass or volume is measured by a weighing system or scaled tank, respectively. The calculation of mass or volumetric flow rate is in this case given as the quotient of the totalized mass or volume, and the fixed collection time.

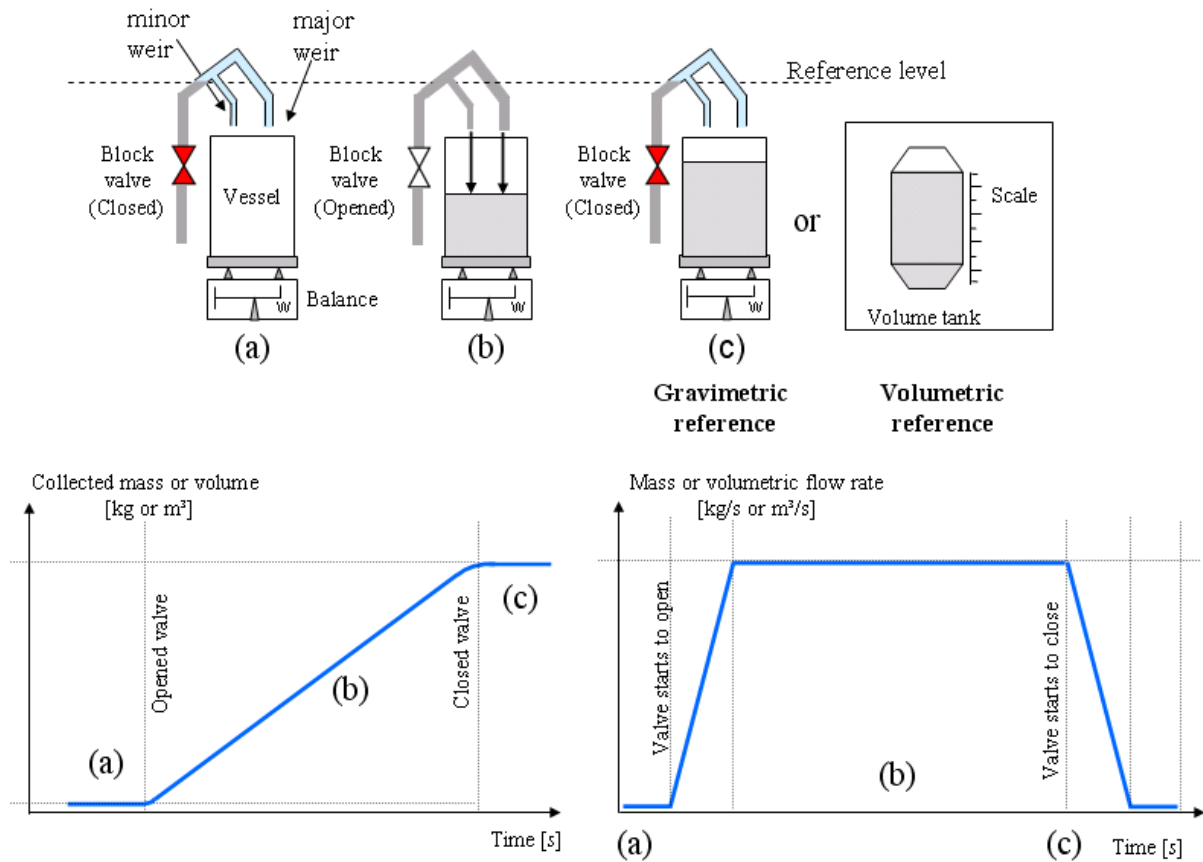


Fig. 2.6 Gravimetric standing start-and-stop primary standard

For this kind of facility (either gravimetric or volumetric), it is essential to assure that the amount of fluid passing through the MUC is the same as for the mass or volume reference standard, so the continuity law can be applied.

Therefore, in order to accomplish this main requirement, particular attention is paid in the design of weirs, which can guarantee that the start and stop reference levels triggered by the stop valve coincide before and after the calibration run (**Fig. 2.6(a)** and **Fig. 2.6(c)**).

2.5.3 Dynamic level gauging volumetric liquid flow primary standard

This dynamic level gauging volumetric primary standard, also known as a piston prover [7] is described as a circular cylinder of a known and uniform internal diameter, which encompasses a sealed piston (**Fig. 2.7**). The determination of flow rate is based on the measurement of the fluid volume out of the cylinder, which is equal to the product of the piston displacement (x_{Piston}) and the crossed section area (A_{Piston}), and the time taken for the piston to travel from one reference point to another (t_{Piston}) [20, 21]. Alternatively, the volumetric flow calculation by a piston prover can be also seen as the product of the piston velocity (\dot{x}_{Piston}), and the crossed section area of the cylinder.

In practical terms, the piston prover operation [22] is graphically depicted in **Fig. 2.7(a)**. At the initial stage of the measurement (**a**), the poppet valve of the piston is opened to allow the circulation of fluid through the cylinder, until quasi-steady flow conditions are achieved. The measurement of flow rate starts when the poppet valve is closed and the piston is driven forward. During the first stage of the stroke, the piston undergoes acceleration due to the inertial force of the downstream fluid illustrated in **Fig. 2.7(b)**. This is considered to be a small region wherein the flow is suddenly increased, so that, it is preferred to skip it from the measurement process.

Shortly thereafter, the piston acceleration reduces basically to zero [23] and its velocity is fairly constant, the actuator reaches the start switch and the calibration time begins (**Fig. 2.7(b)**). Within the region of measurement, the length scale (linear encoder) is responsible for tracking the displacement of the piston, and the system keeps time-stamped record for each length step. At the last stage of the measurement, the actuator approaches the stop switch, which sends the order to stop the timer, and to open the poppet valve (**c**).

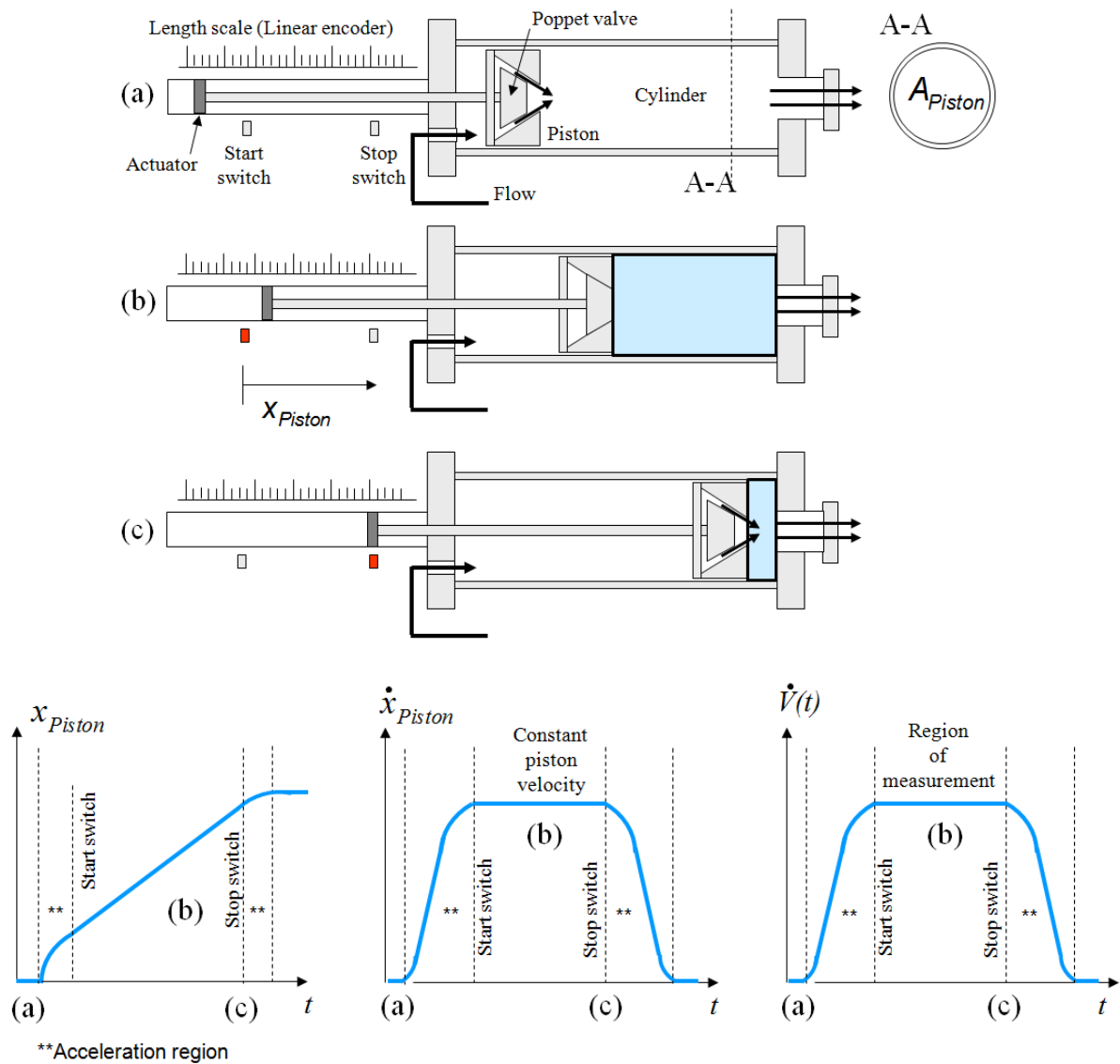


Fig. 2.7 Dynamic level gauging primary standard (Piston prover) [19]

2.5.4 ISO dynamic gravimetric liquid flow primary standard

At present, some of the liquid flow primary standards operate under the ISO definition of a dynamic gravimetric liquid flow calibrator [18]. The main reason that encourages some primary flow laboratories for the implementation of this method is to avoid the tedious characterization of a bypass valve (diverter valve) [17], which is not longer required since the mass flow rate is determined by the time taken to match the magnitude of a reference mass with the magnitude given by the balance readout. This procedure is quite different to the static principle, which considers the totalized liquid mass and the time taken to collect it.

In this type of facility, exemplified in **Fig. 2.8** [24], the liquid circulates until the flow is stable, and a reference mass named as m_{ISO} is placed upon the balance platform **(a)**. As soon as the quasi-steady flow condition is achieved, the drain valve is closed, and the liquid starts being collected in the vessel **(b)**. At some point during the filling, the collected liquid reaches a pre-set initial mass denoted as m_{Tr1} , and triggers a timer to begin the flow measurement **(b)**. The liquid continues being poured into the vessel until the fluid matches a second pre-set mass m_{Tr2} , which generates a trigger signal to lift the reference mass from the balance platform but carrying on with the filling process **(c)**. Finally, after some time during the collection, the pre-set initial mass m_{Tr1} is reached once again, and it gives the order to stop the timer as well as the filling process **(d)**. Thereafter, the *average mass flow rate* is calculated as the quotient of the reference mass m_{ISO} , and the period of time between the triggering points t_{ISO} [25].

The illustration of this type of liquid flow primary standard (**Fig. 2.8**) is based on an electronic load cell as a weighing system. On the other hand, mechanical calibrators based on a lever mechanism are also available for the determination of the flow unit [26, 27], and work under the same ISO measurement principle depicted in the mass-time and flow-time graphs below.

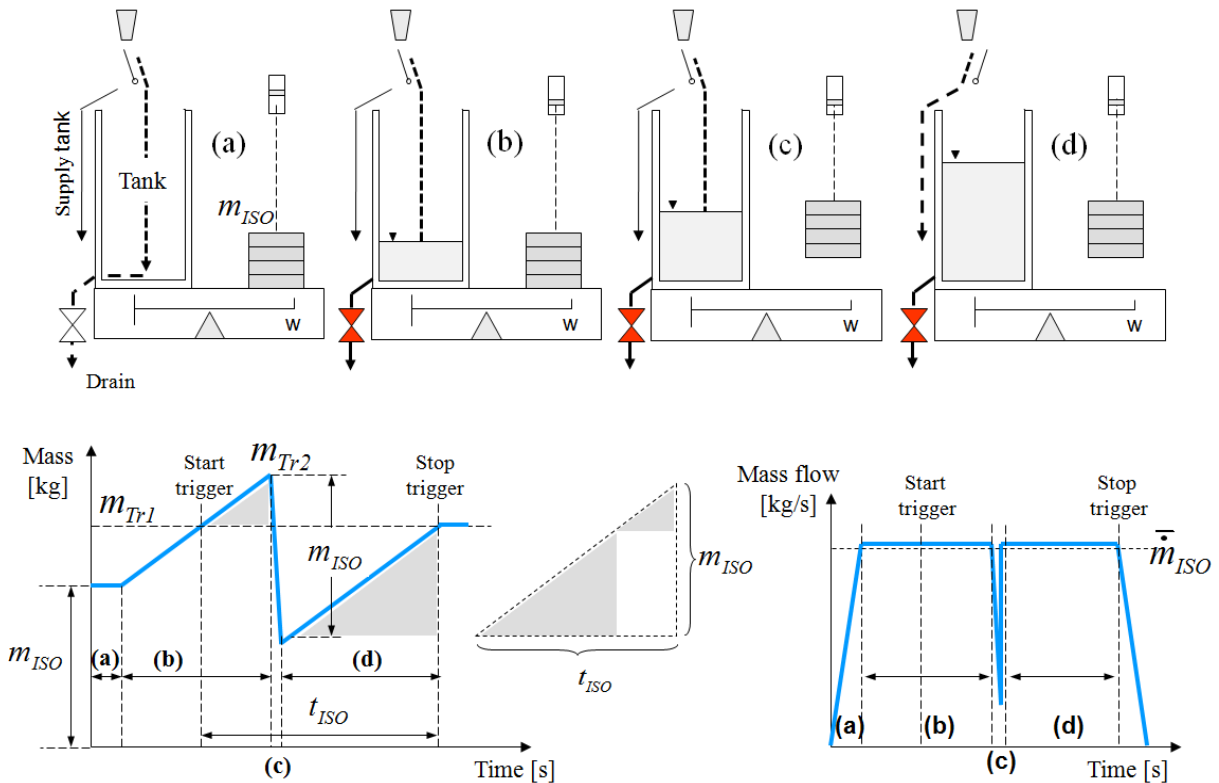


Fig. 2.8 ISO dynamic gravimetric primary standard

In the last paragraph is written the term *average* is used because despite this primary standard operates during the filling process, it still relies on a reference mass for the calculation of a single mass flow rate measurement, and it disregards the fluctuations of flow rate during t_{ISO} .

2.5.5 Dynamic weighing liquid flow primary standard with immersed inlet pipe

This primary standard developed by the company Rota Yokogawa [28] features four main components in its design: a weighing system, a flow control valve, a collection vessel, and an immersed inlet pipe (**Fig. 2.9**). Unlike the recalled liquid flow calibrators, this primary standard deals with the minimization of the flow-induced force effect upon the weighing system response, so that the mass flow rate can be determined as a instant quotient of the balance readout and time.

The first step of this measurement process is related to the designation of the operational mass flow rate, taking into account that before starting a calibration run, the flow must be set at a quasi-steady condition. Once the set up conditions are achieved, the filling process can take place.

The second step addresses an inherent design problem, which is the counter pressure exerted by the collected liquid to the discharging flow at the pipe outlet (**Fig. 2.9**). If this problem were not treated, the primary standard would simply undergo a continuous decrement of mass flow rate, and therefore a flowmeter calibration would be impossible to be carried out.

The solution found in order to overcome this problem is the installation of a flow control valve [26], which can overcome in real time the increasing counter pressure at the pipe outlet, and hence, assuring a nearly constant pressure and mass flow rate along the filling process.

Another remarkable part in the design of this primary standard is its ability to mechanically attenuate the normal impacting force caused by the water jet. The mechanical concept consists in placing inside the vessel, a vertical inlet pipe, which supplies the water mass flow, and it does not have any contact with the vessel structure (**Fig. 2.9**). At the pipe outlet, a deflecting plate is attached with the objective to redirect the normal fluid force into a radial direction, so that, the water stream will spread out to the side walls of the vessel. The advantage of this application is a radial fluid force that has a lower effect on the weighing system vibration and balance output

signal, in addition to a faster dissipation of the water jet kinetic energy when spreading the water throughout the collected water [29]. The other fluid forces taking place in the process are the product of the continuous increment of liquid mass (desired output quantity), and the local acceleration of gravity.

Finally, the measurand mass flow rate is calculated in a differentiation form between the balance readout and time $\hat{m}(t)$. The *hat symbol* on the liquid mass variable is added to indicate that the magnitude given by the weighing system is a close estimation of the real time-varying mass flow rate. If none flow-induced forces were present at all in the process, the balance readout would be equal to the time-varying liquid mass.

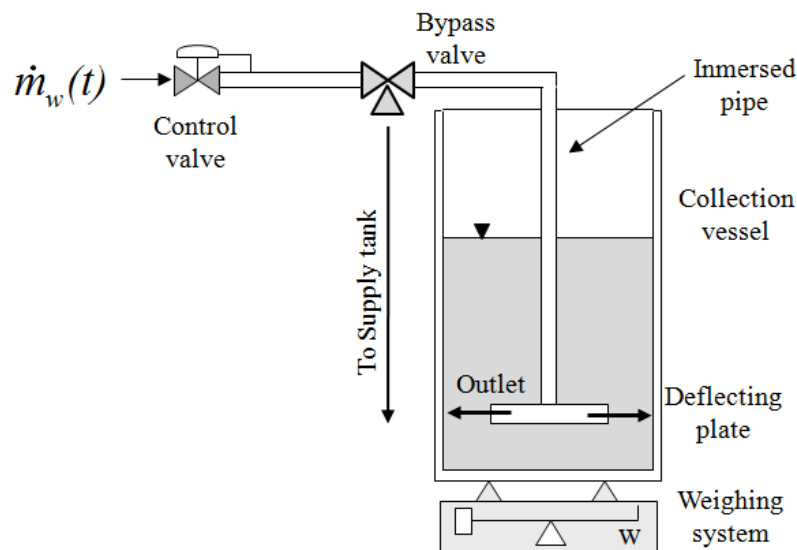


Fig. 2.9 Dynamic weighing liquid flow primary standard with immersed inlet pipe

2.5.6 Dynamic weighing liquid flow primary standard assisted by an in-line flowmeter

The U.S. National Institute of Standards and Technology (NIST) has proposed a dynamic weighing concept for the calibration of liquid flowmeters, which uses the same provisions as for a conventional static weighing system [30] (a collection vessel, a weighing system, and a bypass valve), in addition to a flowmeter.

Such a dynamic flow measurement procedure can be described by the following sequence. First, a calibrated flowmeter is installed upstream the reference weighing system, as illustrated in

Fig. 2.10. Then, after the flow reaches a certain flow stability criterion, the bypass valve drives the fluid stream into the collection vessel to start the filling process. During the collection, a data acquisition system records the three main process variables: the output signal of the weighing system, the flowmeter output signal, and time. The measurement run finishes as soon as the fluid level matches a preset value defined by the user.

The criterion employed for the calculation of dynamic mass flow rate is divided into two parts: the rough estimation of mass flow rate and the time-varying flow correction. The rough estimation of mass flow rate is in this instance, the quotient of the difference between the two fluid forces measured by the weighing system at a time t_n and t_{n+1} , and the local acceleration of gravity. At this stage of the mass flow calculation, the influences of the water jet impact force as well as the dynamic response of the weighing system have not yet been treated [31]. Therefore, the calculated measurand is significantly affected in terms of its precision and accuracy.

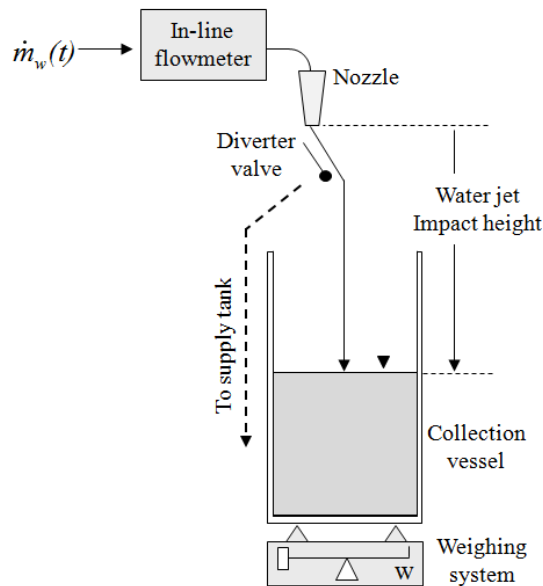


Fig. 2.10 Dynamic weighing liquid flow primary standard assisted by an in-line flowmeter

The second part of the process model deals with the precision and accuracy issues mentioned in the last paragraph, by analyzing separately the error attributed to the dynamic response of the weighing system and the error originated by the water jet impact force. In order to overcome the influence of the weighing system dynamics upon the flow measurement, such a primary standard uses a flowmeter as an alternative form to correct the imprecision of the mass flow rate

estimation. In other words, during a measurement run, the reference flowmeter delivers a value, which is assumed to follow the time-varying mass flow rate [32]. On the other hand, the unwanted force magnitude of the water jet impact force (which affects the measurement accuracy) is estimated by an experimental function relating the water jet impact height, the weighing system readout, mass flow rate (given by the flowmeter), and time.

2.6 The proposed dynamic weighing liquid flow primary standard

The characteristics of this new liquid flow calibration approach will be described in full detail in **Chapter 3** and **Chapter 4**. However, at this point it is appropriate to mention some unique features of the proposed primary standard as well some similarities with its above mentioned counterparts. For instance:

- Unlike the static primary standards and the ISO-based dynamic standard, the calibration time by the proposed primary standard will be reduced, because the flow unit can be reproduced several time during a single collection (**Section 1.2**),
- The fast actuation and thorough characterization of a diverter valve is not longer required, since the measurand is a function of the system dynamics and flow-induced force, and not a function of a totalized amount of mass and time,
- For the static primary standards as well as the ISO-based dynamic standard, the time-varying mass flow rate is considered as an uncertainty contributor. For the proposed dynamic weighing liquid flow primary standard, the time-varying mass flow rate is an inherent characteristic of the measurand,
- The effect of fluid evaporation in the proposed primary standard will be relatively low, due to the fact that the measurement is carried out in a shorter time, in comparison to the static primary standards,
- The proposed dynamic weighing liquid flow primary can be implemented into a conventional static-weighing liquid flow calibration system, and it does not imply any changes in its mechanical design.

In order to summarize all the recalled information, **Table 2.3** offers an overview of the measurement approaches for liquid flow, and a way to compare them (in terms of their advantages and limitations) with the proposed dynamic weighing liquid flow primary standard.

| | Static weighing + diverter | Static weighing | Level gauging + diverter | Level gauging | ISO dynamic weighing | Dynamic level gauging | Dynamic weighing |
|--|-------------------------------|-----------------|-----------------------------|---------------|-------------------------|--------------------------|---------------------|
| Measurement type | <i>Mass</i> | | <i>Volume</i> | | <i>Mass</i> | <i>Volume</i> | <i>Mass</i> |
| Average flow rate | <i>Yes</i> | <i>Yes</i> | <i>Yes</i> | <i>Yes</i> | <i>Yes</i> | <i>Yes</i> | <i>Yes</i> |
| Time-varying mass flow rate | <i>No</i> | <i>No</i> | <i>No</i> | <i>No</i> | <i>No</i> | <i>Yes</i> | <i>Yes</i> |
| Time of calibration | <i>Long</i> | <i>Long</i> | <i>Long</i> | <i>Long</i> | <i>Medium</i> | <i>Short</i> | <i>Short</i> |
| Fluid and mechanical influences | | | | | | | |
| Diverter error | <i>Yes</i> | <i>No</i> | <i>Yes</i> | <i>No</i> | <i>No</i> | <i>No</i> | <i>No</i> |
| Flow-induced forcedisturbance | <i>No</i> | <i>No</i> | <i>No</i> | <i>No</i> | <i>Medium</i> | <i>Low</i> | <i>High</i> |
| Connecting pipe | <i>Medium</i> | <i>Medium</i> | <i>Medium</i> | <i>Medium</i> | <i>Medium</i> | <i>Medium</i> | <i>Medium</i> |
| Fluid evaporation | <i>Medium</i> | <i>Medium</i> | <i>Medium</i> | <i>Medium</i> | <i>Medium</i> | <i>No</i> | <i>Low</i> |
| Flow instability | <i>Medium</i> | <i>High</i> | <i>Medium</i> | <i>High</i> | <i>Medium</i> | <i>Low</i> | <i>Medium</i> |
| Air buoyancy effect | <i>Low</i> | <i>Low</i> | <i>Low</i> | <i>Low</i> | <i>Low</i> | <i>No</i> | <i>Low</i> |
| Temperature variation | <i>Medium</i> | <i>Medium</i> | <i>Medium</i> | <i>Medium</i> | <i>Medium</i> | <i>High</i> | <i>Low</i> |

Table 2.3 Characteristics of different liquid flow primary standards

3. Input signal, modeling of the dynamic weighing liquid flow standard, and the connecting volume effect

As a starting point of this research, it must be stated that the input signal of the measurement process is a fluid force quantity. However, in order to make present the force quantity in this dynamic process, it is necessary to produce fluid motion. Therefore, the mass flow rate $\dot{m}_w(t)$ is in this instance the core variable, or command input of the system [1]. For the sake of early clarification, it is important to explain that mass flow rate is also the desired output signal of the measurement process. However, due to the undergoing dynamic conditions in the liquid flow standard, the system is unable to directly yield the measurand but an estimate value of $\hat{\dot{m}}_w(t)$ (the subindex w denotes water as a fluid in use). The term of estimate measurand is used to remark that in practice, despite the treatment of fluid forces and the system instrumentation, part of the magnitude of these variables will be unavoidably present in the measurand. Such fluid forces present in the liquid flow standard are described in the following sections of this chapter, with the purpose to understand their relevance in the measurement process, and ultimately, its impact upon the measurand.

Fig. 3.1 describes in a block diagram the dynamic weighing liquid flow standard, wherein its working principle is explained by three series-connected subsystems. The command input is in this case the mass flow rate $\dot{m}_w(t)$. Then, the command input enters the first subsystem called **input elements**. Such a block of input elements represents the summation of different mass flow-induced fluid forces $F_T(t)$ that will interact with the next subsystem, the **weighing system** (or balance). This second subsystem deals with the mechanical dynamic response of balance, and the effect of such a behavior upon the fluid force measurement. The third subsystem known as **process model** has the task to dynamically estimate the mass flow rate magnitude $\hat{\dot{m}}_w(t_n)$ based on an *inverse-problem approach* [2]. In this case, the inverse-problem approach takes into account the process parameters from the two previous subsystems (defined by theory and experimental observations), in order to derive a model that can identify and attenuate the unwanted process variables embedded in the system response $F_{Bal}(t_n)$, and thus obtaining an

accurate estimate of the measurand. The detail explanation of this last subsystem will be given in the next **Chapter 4**.

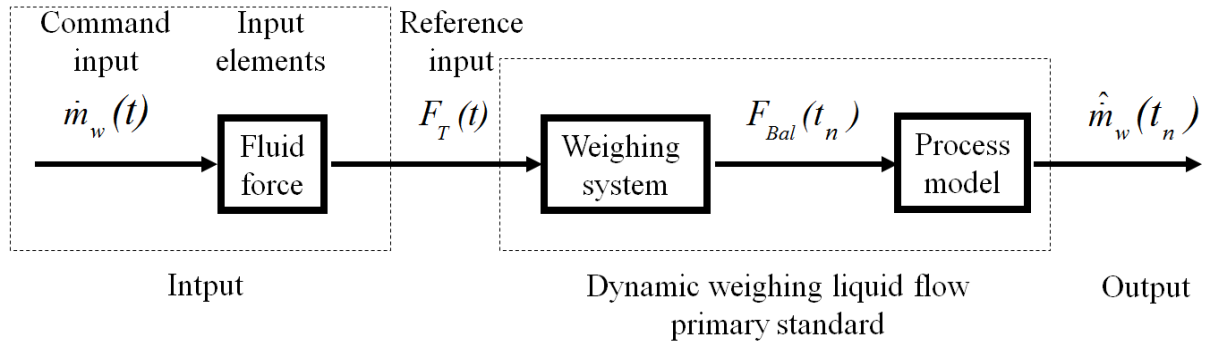


Fig. 3.1 General block diagram representation of the dynamic weighing liquid flow primary standard and its three main subsystems

Fig. 3.2 shows the dynamic weighing liquid flow standard prototype that will be used in this investigation, with the aim to analyze the key variables involved in this measurement process and to realize the level of accuracy that can be achieved by using the proposed calibration method. Such a prototype comprises an air temperature, relative humidity, and absolute pressure sensors that serve to calculate the air density, and subsequently to correct the mass reading from air buoyancy effects. Additionally, a nozzle and a bypass valve (with no fast actuation) are used to discharge the water mass and drive the fluid to either, a 10-L collection vessel or back to a reservoir tank. In terms of fluid mass transfer, the prototype features a 25-mm pipeline, which connects a flowmeter with direct traceability to the PTB primary flow standard to the weighing system. The goal of the flowmeter (transfer standard) is to provide a reference of how the mass flow rate is slightly fluctuating, within its claimed measurement uncertainty, and thus comparing its results with the given by the prototype system for validation purposes (full description in **Chapter 6**). In this case, the weighing system employed is a 30-kg electromagnetic force compensation balance (**section 3.2**), which holds the collection vessel, and it features a resolution of 0,1g, with a characterized linearity of $\pm 0,4g$, and a repeatability $\pm 0,1g$.

In relation to the process conditions, such a prototype uses the PTB primary standard's pumping system, which ensures a stationary and quasi-steady mass flow rate as well as fluid temperature. In addition to these control provisions, an electro-pneumatic control valve is installed upstream the collection vessel, in order to finely adjust the flow within a range from 3 kg/min to 8 kg/min.

Moreover, the system features two auxiliary devices, a laser displacement sensor and an accelerometer, which besides monitoring the system's dynamic response, they serve as tools to improve the accuracy of the mass flow rate measurement. A further description about the usage of these auxiliary devices as well as the dedicated data acquisition system is given in **Chapter 6**, which regards the experimental tests and results of the dynamic weighing calibration method.

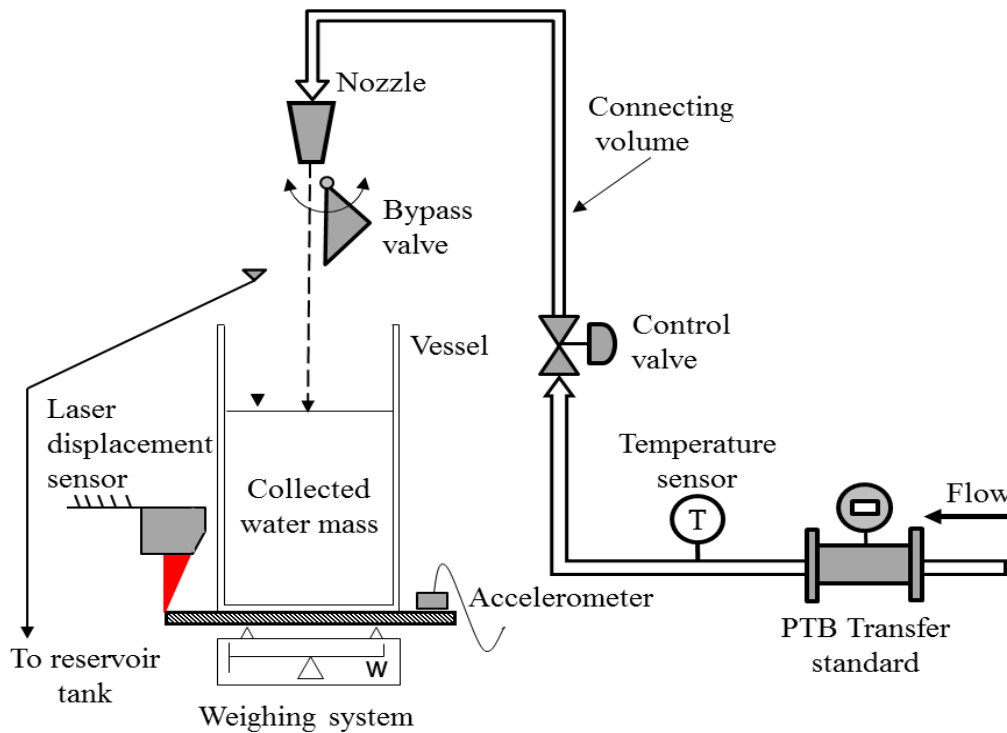


Fig. 3.2 Dynamic weighing liquid flow primary standard prototype

3.1 Input signal

3.1.1 Collected water mass force

The first fluid force variable $F_m(t)$ is related with the collection of water mass inside the vessel through the measurement run, and the effect of the local acceleration of gravity g [3]. In regards to the water mass $m_w(t)$, it is considered to be a time-varying variable due to the continuous increment of its magnitude during the filling process. Moreover, this fluid mass variable is agreed to behave as a ramp function (**Eq. 3.1**), because the mass flow rate $\dot{m}_w(t)$ (seen as a slope) is performed by the liquid flow primary standard under stationary and quasi-steady condition. In this instance, the term stationary and quasi-steady flow refers to the highest level of

stability that a primary standard can achieve. Therefore, in practical terms and for the purpose of mathematical simplification, the mass flow rate can be assumed to be a constant variable $\dot{m}_w(t) \equiv \text{const}$ in the measurement process.

$$\begin{aligned} F_m(t) &= \int_0^t \dot{m}_w(t) \cdot g \cdot dt \\ &= \dot{m}_w \cdot g \cdot (t - t_0) \end{aligned} \quad (3.1)$$

In **Eq. 3.1**, the lower and upper limits of the integral correspond to the initial and current time of the filling process, respectively.

3.1.2 Hydrodynamic force

The second variable involved in the measurement process is known as hydrodynamic force $F_d(t)$, which is caused by the continuous impact of the falling water jet upon the water surface or the vessel bottom at the initial stage of the collection. In the measurement process, the hydrodynamic force can be represented in a simplified form as [4]:

$$F_d(t) = \dot{m}_w(t) \cdot u_i(t) \quad (3.2)$$

where $u_i(t)$ stands for the normal impact velocity of the water jet, and in accordance to Bernoulli's law [5] this is equal to:

$$u_i(t) = \sqrt{u_n^2(t) + 2 \cdot g \cdot h_i(t)} \quad (3.3)$$

In **Eq. 3.3**, $u_n(t)$ and $h_i(t)$ denote respectively, the initial velocity of the falling water jet at the nozzle outlet, and its impact height (see **Fig. 3.3**). As for $u_n(t)$, its magnitude will depend on the constant crossed section area of the nozzle outlet A_n , the density of the fluid ρ_w , and the mass flow rate $\dot{m}_w(t)$ (**Eq. 3.4**).

$$u_n(t) = \frac{\dot{m}_w(t)}{\rho_w \cdot A_n} \quad (3.4)$$

The time-varying water jet impact height $h_i(t)$ can be depicted in a simplified form (**Eq. 3.5**) as the difference between initial impact height $h_i(0)$, and the continuously increasing height of the water surface $h_w(t)$. Thus,

$$h_i(t) = h_i(0) - h_w(t) \quad (3.5)$$

On the other hand, $h_w(t)$ is described by **Eq. 3.6** as a related function of the current collected water mass, the cross section area of the vessel A_v , and the fluid density ρ_w . Hence,

$$h_w(t) = \frac{\int_0^t \dot{m}_w(t) \cdot dt}{\rho_w \cdot A_v} \quad (3.6)$$

Therefore:

$$h_i(t) = h_i(0) - \frac{\int_0^t \dot{m}_w(t) \cdot dt}{\rho_w \cdot A_v} \quad (3.7)$$

Finally, after substituting **Eq. 3.3**, **Eq. 3.4** and **Eq. 3.7** into **Eq. 3.2**, it is found that the hydrodynamic force is a dependent function of the mass flow rate, the fluid density, the local acceleration of gravity as well as the dimensions and geometry of the nozzle outlet, the collection vessel, and the constant initial water impact height (**Eq. 3.8**).

$$F_d(t) = \dot{m}_w(t) \cdot \left\{ \left(\frac{\dot{m}_w(t)}{\rho_w \cdot A_n} \right)^2 + 2 \cdot g \cdot \left(h_i(0) - \frac{\int_0^t \dot{m}_w(t) \cdot dt}{\rho_w \cdot A_v} \right) \right\}^{1/2} \quad (3.8)$$

3.1.3 Buoyancy force

So far, the forces recalled are related to the same direction given by the gravitational force. Nevertheless, there is still one process variable called Buoyancy force $F_b(t)$, which also acts upon the collected water volume but in upward direction as shown in **Fig. 3.3**. This force is caused by the lifting effect (or floating effect) the air has upon the water mass, it is agreed to be equal to the product of the increasing displaced volume by the water $V_w(t)$, the local acceleration of gravity g , and the air density ρ_A . Then, according to **Eq. 3.9**, the buoyancy force [6] is expressed as:

$$F_b(t) = V_w(t) \cdot \rho_A \cdot g \quad (3.9)$$

Alternatively, **Eq. 3.9** can be expressed in terms of the liquid density and the mass flow rate in order to yield:

$$F_b(t) = \left(\frac{\rho_A}{\rho_w} \right) \cdot g \cdot \int_0^t \dot{m}_w(t) \cdot dt \quad (3.10)$$

3.1.4 Total fluid force and its block diagram representation

As seen in **Fig. 3.3**, the liquid flow primary standard cannot longer be treated as a static system where the collected mass is totalized; but instead, as a dynamic system driven by the summed fluid forces of the increasing collected mass force, the hydrodynamic force caused by the water jet impact, and the upward-oriented force of buoyancy (**Eq. 3.10**). Hence, the total fluid force $F_T(t)$ acting upon the system is:

$$F_T(t) = F_m(t) + F_d(t) - F_b(t) \quad (3.11)$$

The second and third terms of **Eq. 3.11** correspond to the hydrodynamic and buoyancy force, which are considered in this measurement process as unwanted variables. In other words, these are the variables that have to be minimized in their magnitude by the dynamic weighing liquid flow standard, in order to estimate with a reasonable accuracy the real mass flow rate $\hat{m}_w(t)$.

The following **Fig. 3.3** summarizes in a free body diagram and a block diagram, the graphical representation of all considered forces and parameters involved in the measurement process. Note that the block diagram representation of fluid forces resembles a feedforward loop, wherein all input elements are primarily dependent of the command input, mass flow rate.

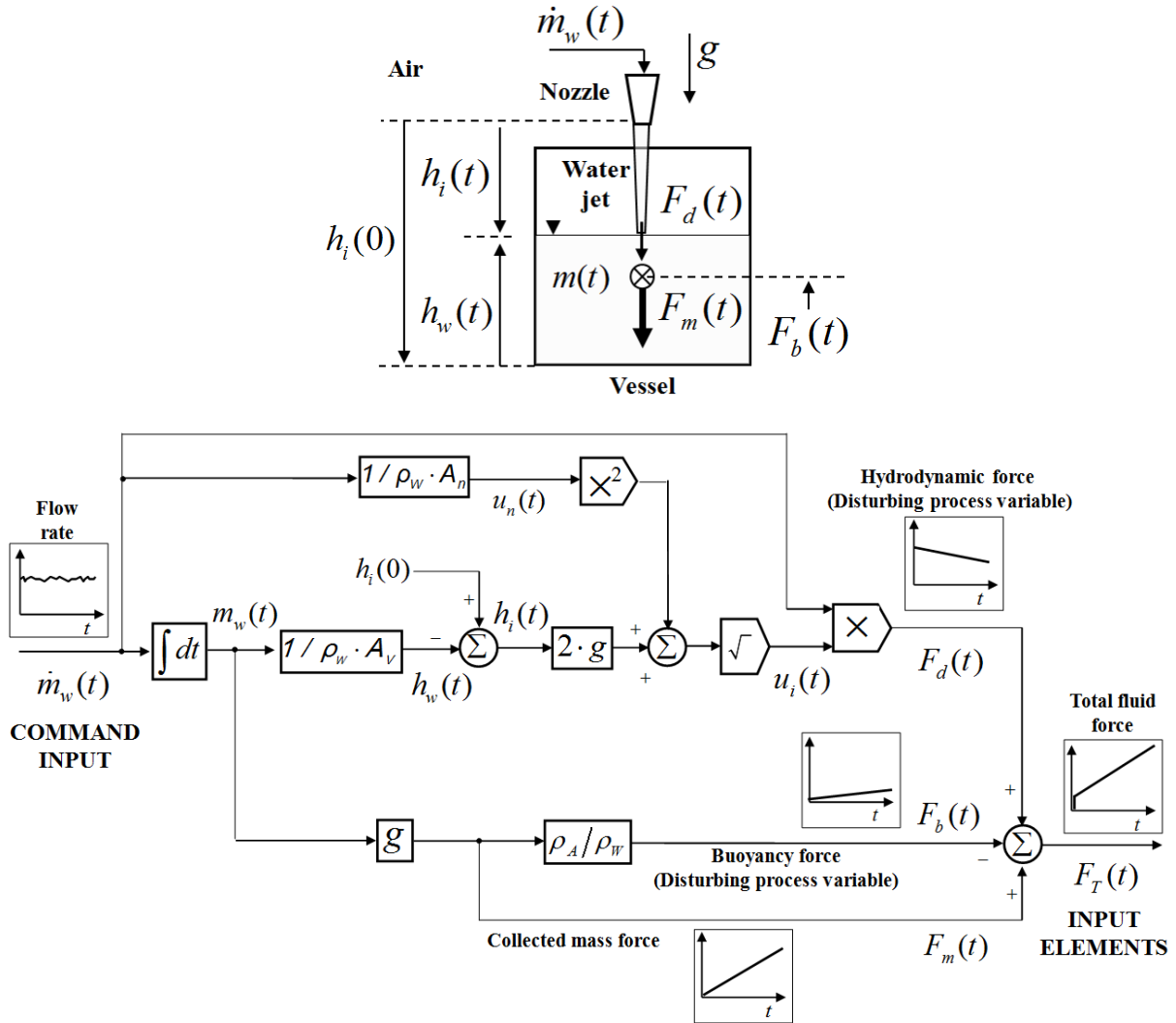


Fig. 3.3 Block diagram of the total fluid force representing the input signal of the 1-Degree-of-freedom weighing system [7]

3.2 The weighing system and its numerical representation

In general, it is understood that a balance is designed only to reproduce the unit of mass. In principle this statement is correct, based on the fact that the weighing system manufacturers provide an internal scale factor to convert the gravitational force exerted by a weighing object into mass [8]. However, during the dynamic process of fluid mass collection, the utilization of such a scale factor is not longer applicable, since the weighing system is unable to distinguish

between the acting force attributed to the collected water mass (desired magnitude), and the buoyancy, fluid motion and reacting system response forces [9]. Therefore, after this brief explanation, it is understood that a weighing system is indeed a force measuring device, which has to be re-characterized, in order to deliver a magnitude in Newtons.

For this research work, an Electromagnetic Force Compensation balance (EFC) is in use, and in which its operational principle consists in inducing an electromagnetic force that can compensate and equal the acting force exerted upon its weighing platform [10]. As illustrated in **Fig. 3.4**, the EFC balance features an electric circuit comprising an inductive positioning sensor as well as an oscillator and resistors R to provide a certain constant voltage V [11]. When the filling process takes place, the fluid force causes the parallel levers to deflect or to move from its equilibrium position. As this happens, the high-resolution inductive positioning sensor registers the current z-axis beam location, and hence it generates a potential difference Δv .

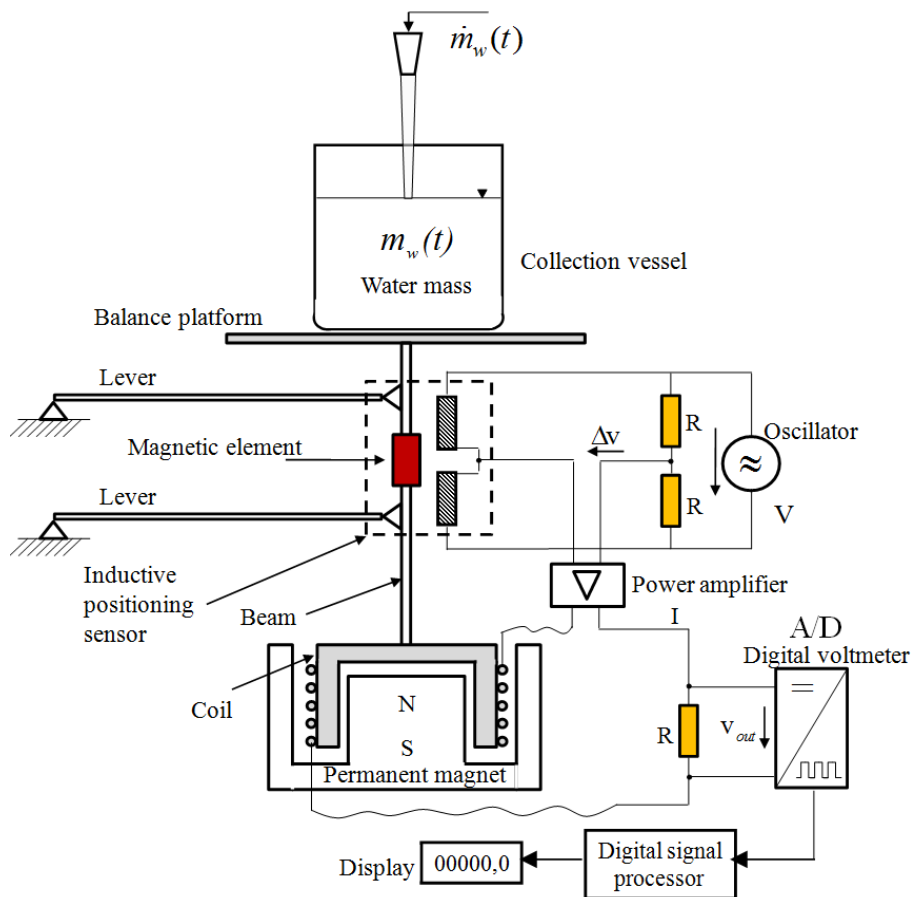


Fig. 3.4 Working principle of an Electromagnetic Force Compensation (EFC) cell used as a weighing system [11]

Then, the potential difference magnitude is increased by a power amplifier, which delivers an amount of current I to the coil (inserted into a permanent magnet), in order to immediately return the beam into its zero position by changing the force of the electromagnetic field. Thereafter, an A/D digital voltmeter acquires the voltage output signal v_{out} , which is then filtered out by an internal signal processing algorithm, scaled as a mass unit, and displayed.

Now, the main task in this section is to have a numerical representation of the recalled system, which will allow a better understanding of why and how the balance responds in a certain way to the given fluid-mechanical process conditions, and to identify the magnitude of some sources of measurement noise. On the other hand, this model-based approach can be only valid if the theoretical basis of the process (input, system, process model, and measurand as illustrated in **Fig. 3.1**) shows a satisfactory level of agreement with the real measurement process, as demonstrated in **Chapter 5** and **Chapter 6**.

The proposed numerical model of the weighing system is based on Newton's third law [12], and it is restricted to a 1-Degree-of-Freedom (1-DoF), which is the normal axis of weighing (z axis). Such a law states that the acting fluid forces involved in the process (**Eq. 3.11**), will generate an equal but opposite response to the mechanical forces $\sum F_{Mech}(t)$ exerted by the weighing system's elastic elements and its mass (**Eq. 3.12**). In other words, **Eq. 3.12** says that the system struggles at all times for an equilibrium position, due to the continuous alternation of upward and downward forces in the process.

$$F_T(t) = \sum F_{Mech}(t) \quad (3.12)$$

In this instance, the balance will be represented as a system with a time-varying increasing mass, and by two analogous elements, a damper and a spring, which simulate in a general basis the sensing element of the balance (cell).

3.2.1 Spring force

As mentioned, one of the elastic elements employed to simulate the balance is defined by a spring, in which its reacting force denoted by $F_{Bal}(t)$ is equal to the product of the characterized

balance stiffness coefficient k_{Bal} , and the displacement z undergone by the balance along the measurement run (**Eq. 3.13**). This element can be also seen as the component dealing with the storage of potential energy in the balance [13].

$$F_{Bal}(t) = k_{Bal} \cdot z \quad (3.13)$$

3.2.2 Inertial force and system total mass

The second element of the system deals with its mass, and it is agreed to be equal to the summation of: the collection vessel mass (m_v), the weighing platform mass (m_p), the initial amount of water mass ($m_w(0)$), and the time-varying collected water mass ($m_w(t)$). As a remark, the mass element constitutes the main mechanism of kinetic energy storage in the balance [14], and as described by **Eq. 3.14**, it will turn out to be larger in magnitude as the filling process goes on (**Fig. 3.5**).

$$m_T(t) = m_v + m_p + m_w(0) + m_w(t) \quad (3.14)$$

where $m_T(t)$ constitutes the total mass held by the balance elastic elements.

When a dynamic weighing liquid flow measurement is taking place, the continuous alternation of acting fluid forces and reacting mechanical forces causes the system's total mass $m_T(t)$ to accelerate in an oscillatory form \ddot{z} . Therefore, the result of this dynamic condition is an inertial force $F_{Inertial}(t)$ exerted upon the system, and it is described by **Eq. 3.15** [15].

$$F_{Inertial}(t) = m_T(t) \cdot \ddot{z} \quad (3.15)$$

Here, it is important to underline, that such an inertial force is present in great part due to the hydrodynamic force, which causes the balance to move. If the hydrodynamic force were not present, the acceleration component in **Eq. 3.15** will be zero, so that no inertial force would take part in the process. In other words, the system would be considered as static. Furthermore, in the

measurement process, the inertial force is subjected to decrease as the hydrodynamic force diminishes.

3.2.3 Damping force

The third element of the weighing system model is related with the inherent characteristic of a system to dampen (or to reduce) the oscillatory force amplitude. Or in other words, it is the element responsible for the gradual dissipation of energy from the system [13]. In this case, the damping force $F_c(t)$ can be determined as a product of the system z-axis velocity during a measurement run, and the corresponding damping coefficient of the system $c_{Bal}(t)$ (**Eq. 3.16**). Subsequently, the system's damping coefficient shown in **Eq. 3.17** is agreed to be a function dependent of the critical damping fraction ζ (**Eq. 3.18**), the current system's natural angular frequency $\omega_n(t)$ (**Eq. 3.19**), and its total mass $m_T(t)$ [13].

$$F_c(t) = c_{Bal}(t) \cdot \dot{z} \quad (3.16)$$

$$c_{Bal}(t) = 2 \cdot \zeta \cdot m_T(t) \cdot \omega_n(t) \quad (3.17)$$

$$\zeta = \left[1 - \left(\frac{\omega_d}{\omega_n(t)} \right)^2 \right]^{1/2} \quad (3.18)$$

$$\omega_n(t) = \sqrt{\frac{k_{Bal}}{m_T(t)}} \quad (3.19)$$

As **Eq. 3.18** and **Eq. 3.19** suggest, the system damping coefficient can be alternatively expressed in terms of the characterized spring coefficient $k_{Bal}(t)$, its mass $m_T(t)$, and the damped angular frequency of the balance ω_d , which is obtained (or characterized) as a function of the system total mass $m_T(t)$ via experimentation, then $\omega_d(m_T(t))$ (see **Chapter 5**). Hence,

$$c_{Bal}(t) = 2 \cdot \left(1 - \left(\frac{\omega_d(m_T(t))}{\sqrt{\frac{k_{Bal}}{m_T(t)}}} \right)^2 \right)^{1/2} \cdot m_T(t) \cdot \sqrt{\frac{k_{Bal}}{m_T(t)}} \quad (3.20)$$

And after some algebraic simplifications in **Eq. 3.20**, the damping coefficient takes the following form:

$$c_{Bal}(t) = 2 \cdot \left(k_{Bal} \cdot m_T(t) - \omega_d^2(m_T(t)) \cdot m_T^2(t) \right)^{1/2} \quad (3.21)$$

3.2.4 1-Degree-of-Freedom motion equation of the weighing system

Now, at this point, the number of reacting mechanical forces of the weighing system $\sum F_{Mech}(t)$ (right side of **Eq. 3.12**) can be represented as the summation of:

$$\sum F_{Mech}(t) = F_{Inertial}(t) + F_c(t) + F_{Bal}(t) \quad (3.22)$$

Then, **Eq. 3.22** can be substituted into the into the Newton's third law equation (**Eq. 3.12**), in order to yield the system's 1-Degree of Freedom motion equation shown in **Eq. 3.23**.

$$F_m(t) + F_d(t) - F_b(t) = F_{Inertial}(t) + F_c(t) + F_{Bal}(t) \quad (3.23)$$

Likewise, the recalled system's 1-Degree of Freedom (1-DoF) motion equation can be written in an extended form (**Eq. 3.24**), with the aim to see how the motion characteristics of the balance (\ddot{z} , \dot{z} , and z), the acting fluid forces, its elastic properties, its mass, and its damped angular frequency are related into a single mathematical expression.

$$F_m(t) + F_d(t) - F_b(t) = m_T(t) \cdot \ddot{z} + c_{Bal}(t) \cdot \dot{z} + k_{Bal} \cdot z \quad (3.24)$$

or

$$F_m(t) + F_d(t) - F_b(t) = m_T(t) \cdot \ddot{z} + \left[2 \cdot \left(k_{Bal} \cdot m_T(t) - \omega_d^2(m_T(t)) \cdot m_T^2(t) \right)^{1/2} \right] \cdot \dot{z} + k_{Bal} \cdot z \quad (3.25)$$

The sketch shown in **Fig. 3.5** illustrates the meaning of **Eq. 3.25**, stating that the balance can be treated as a dynamic fluid-mechanical system. This analogous system comprises a collection vessel of mass m_v , enclosing a time-varying water column of mass $m_w(t)$, in addition to a possible amount of collected water before the measurement run $m_w(0)$, and it is being supported by a platform of mass m_p . Such a platform is mounted on two parallel elastic elements of stiffness coefficient k_{Bal} , and damping coefficient $c_{Bal}(t)$, respectively. The upper end of the water column is agreed to be limited by a free surface at a constant atmospheric pressure, and the effect of the local acceleration of gravity g . Additionally, the fluid and mechanical forces in this measurement process are limited to take place along the weighing axis, therefore, the system is subjected to have 1-DoF. In relation to its source of motion, this is assumed to come from the command input, mass flow [16].

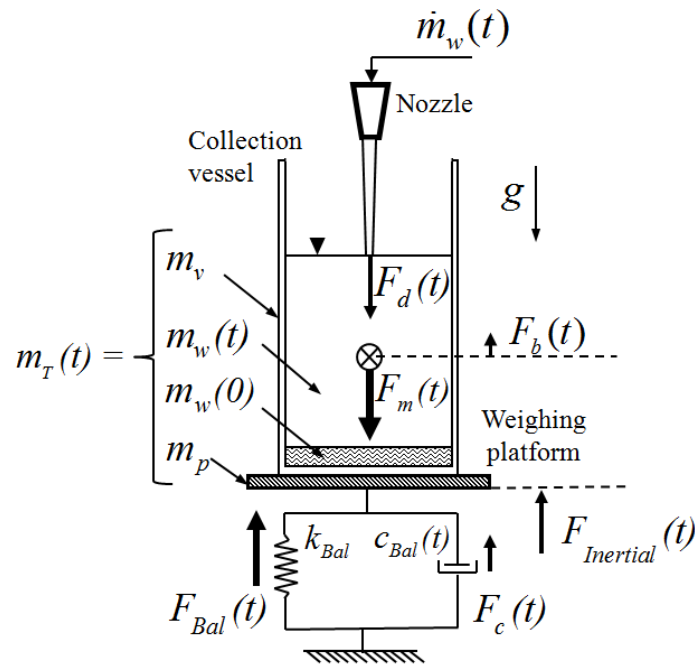


Fig. 3.5 Free body diagram describing the water mass and elastic elements of the system as well as the fluid (acting) and mechanical (reacting) forces involved in the process

Alternatively, the weighing system can be also represented in **Fig. 3.6** as a block diagram, with the purpose to graphically describe the motion equation shown in **Eq. 3.25**. According to the block diagram, the input signal is the total fluid force $F_r(t)$, and it acts upon the weighing system. In practice, there are some additional fluid forces acting upon the weighing system, such as the vortex axial force inside the collection vessel as well as the water wave oscillatory forces

(denoted by $F_q(t)$). These forces, which despite not being treated in the current analysis, they have to be mentioned and depicted in **Fig. 3.6**, as a reminder that they must be investigated and included in a future model. From the numerical analysis perspective (**Chapter 5**), the effect of $F_q(t)$ upon the measurand will be overlooked, because none descriptive equation has been derived, and added into the input signal subsystem. On the other hand, the results of experimental tests (**Chapter 6**) will be limited to state that the error in calculating the measurand is in part, due to the lack of information to quantify $F_q(t)$. Hence, $F_q(t)$ will be assumed in the experimental analysis as a process noise variable.

As a result of such a fluid impact force, the current system with mass $m_T(t)$, brakes its static condition, and accelerates with a certain magnitude \ddot{z} . Then, the acceleration is time-integrated in order to describe the system's motion in terms of velocity \dot{z} and displacement z . In this instance, the system velocity is related with the damping coefficient of the balance sensing element, in order to yield the so called reacting damping force $F_c(t)$. Whereas, the product of the system displacement, and its stiffness coefficient will be equal to the reacting balance force response $F_{Bal}(t)$. The behavior of these reacting forces is seen in the block diagram as a feedback response.

In this case, $F_{Bal}(t)$ is representing the balance force response (output signal) because it is the variable that summarizes in its magnitude: the acting fluid forces (input), the damping force effect of balance sensing element, and the unwanted inertial force the system is subjected during a dynamic process.

3.2.5 Technical considerations in regards to the modeling of the weighing system

The numerical model considered in this chapter is an analogous representation of the weighing system, wherein its dynamic response is simulated by coupling these basic mechanical elements, known as: damper, spring, and masses. One must be aware that during the characterization of the weighing system, the obtained elastic properties (k_{Bal} and $c_{Bal}(t)$) and the mass magnitude used for the numerical model, might slightly differ from the real system. This is due to the fact, that even high-accurate weighing systems are not absolutely linear, but quasi-linear in their response [13]. Furthermore, the numerical model is described as a 1 DoF system, in which its motion is restricted to the normal axis of the balance z (weighing axis). However, in the reality, the weighing system responds in a multi-axis direction (angular and translational motion), so that a set of partial differential motion equations (including the feedback positioning control loop of the balance) would get closer to the real system response. The multi-axis system modeling is a concept that should be kept in mind, in order to achieve a more thorough analysis of the system and its measurement accuracy. Nonetheless, as demonstrated in **Chapter 5** and **Chapter 6**, the numerical and experimental results of a 1-DoF approach turned out to be accurate enough, meaning that the most relevant system parameters and their magnitudes are taking place at the weighing axis.

The following remarks describe some system's aspects that must be taken into account, in order to avoid some misinterpretation of data when the numerical model and the real process are compared.

- The characterization of the spring coefficient k_{Bal} cannot be perfect, because the real system may present slight non-linear force-displacement characteristics and even some hysteresis [17] in its response. The consequence of this mechanical condition in the numerical model is a balance force response, that might differ at some degree from the real response,

- In mechanical terms, the magnitude of the characterized system mass $m_T(t)$ is not absolute, because in reality, there are some additional small balance components (i.e. bolts, nuts, levers, etc), which cannot be taken apart and weighed, and therefore are disregarded. As a consequence, the effect of overlooking this mass will generate a slight difference in the inertial force magnitude, in comparison with the real system when looking at its related variable, the acceleration \ddot{z} ,
- The characterized damping coefficient $c_{Bal}(t)$ used in the numerical model is not exact but approximately equal to the real system magnitude, because the natural angular frequency is a dependent function of two other characterized system elements, k_{Bal} and $m_T(t)$ (**Eq. 3.19**). Furthermore, another reason that makes slightly different the numerical model from its counterpart is, that the damping force is not merely produced by k_{Bal} and $m_T(t)$, but also by the some small friction between balance components [13].

3.2.6 General representation of the weighing system internal filter and the discrete time representation of its output signal

Most of commercial weighing systems used in the industry feature an internal filter, which is responsible for minimizing the unwanted amplitude of the balance oscillatory force response, or the inertial force as it has been discussed in the previous section. Such a type of filter can be described in a general basis as a first-order low pass filter [18], which its aim is to allow passing any oscillatory force response that is below to an established cutoff frequency (pass band). And conversely, the low pass filter will eventually attenuate the amplitude of those oscillatory forces, which are larger than the cutoff frequency (stop band).

Fig. 3.7 summarizes the low pass filter concept by presenting it in a Bode plot, in which the pass band comprises any spectrum within a frequency ($f_d = \omega_d/2\pi$) lower than the cutoff frequency, f_{LPF} . On the other hand, as soon as the system oscillatory force equals the cutoff frequency, this will start undergoing an attenuation in the order of -3 dB. Furthermore, if the system frequency response is larger than the cutoff frequency, the amplitude will be reduced at a rate of 20 dB per decade [19].

In the practice, the internal filter of an industrial weighing system is more complex than a first-order low pass filter. Nevertheless, due to the lack of information from the balance manufacturers in regards to their established filter algorithms, it is in this case feasible to proceed with a basis algorithm, which can yield a general but valid representation of what a pass/stop frequency internal filter does.

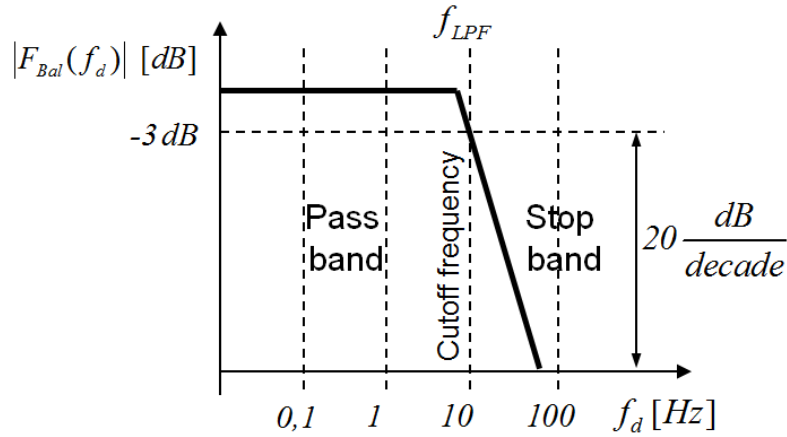


Fig. 3.7 Bode plot representing the internal low pass filter used in the numerical model

According to **Eq. 3.26**, the first-order low pass filter can be simply expressed as the ratio of the filtered output signal $F_{Bal_LPF}(f_d)$ to the input signal $F_{Bal}(t)$, which is equal to the level of attenuation that the balance output signal will undergo after passing the filter. This magnitude is known as gain factor $G_{LPF}(f_d)$.

$$\frac{|F_{Bal_LPF}(f_d)|}{|F_{Bal}(f_d)|} = G_{LPF}(f_d) \quad (3.26)$$

Commonly, the gain factor of the low pass filter is expressed in complex terms (Left side of **Eq. 3.27**), because its operation is based on a frequency domain [18]. However, it is possible to obtain its magnitude and phase shift $\theta_{LPF}(t)$ if the complex number is represented in a polar form as shown in **Eq. 3.27**. Thus,

$$G_{LPF}(\omega) = \frac{1}{1 + i \cdot \left(\frac{\omega_d(m_T(\omega))}{\omega_{LPF}} \right)} \rightarrow G_{LPF}(t) = \left[\sqrt{1 + \left(\frac{\omega_d(m_T(t))}{\omega_{LPF}} \right)^2} \right]^{-1} \quad \angle \theta_{LPF}(t) = \tan^{-1} \left(\frac{\omega_d(m_T(t))}{\omega_{LPF}} \right) \quad (3.27)$$

Eq. 3.27 indicates that in practical terms, it is possible to apply the first-order low pass filter because the cutoff frequency ω_{LPF} information is mostly provided by the balance manufacturers, and the oscillatory frequency of the system $\omega_d(m_T(t))$ can be experimentally obtained by characterizing the oscillatory mechanical response of the balance.

Fig. 3.8 illustrates in a block diagram, the implementation of low pass filter (**Eq. 3.26** and **Eq. 3.27**), depicting that the continuous-time response of the balance $F_{Bal}(t)$ stands for the input signal of the internal filter. On the other hand, the block diagram describes the current frequency of the oscillatory weighing system $\omega_d(m_T(t))$, and the cutoff frequency ω_{LPF} as the responsible variables for tuning the gain of the filter. Finally, $F_{Bal_{LPF}}(t)$ and $\theta_{LPF}(t)$ denote respectively, the balance response after attenuating its oscillatory magnitude and phase shift.

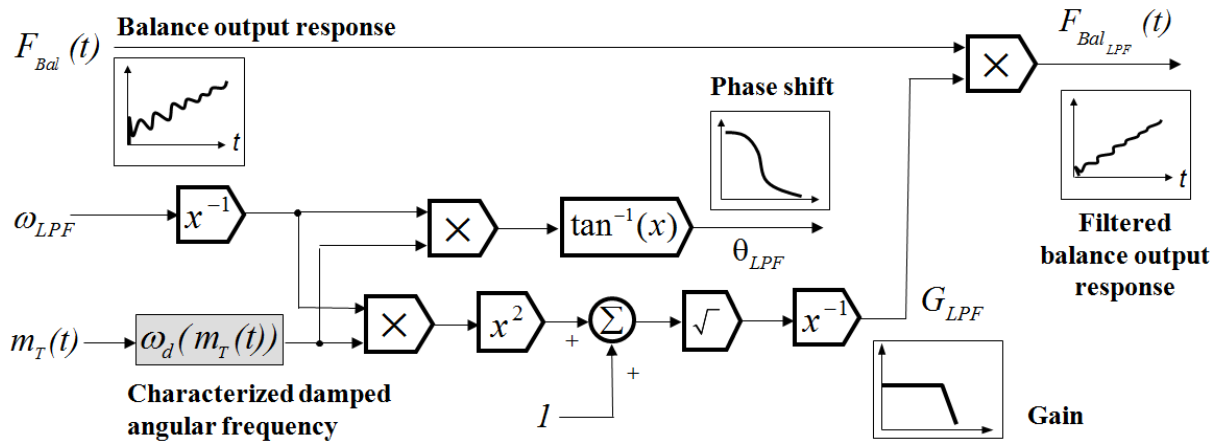


Fig. 3.8 First-order low pass filter in a 1-Degree-of-Freedom weighing system model

At this stage of the process, the balance response signal has been presented in terms of a numerical model, and its output signal is agreed to be attenuated in a continuous-time form by a low pass filter. However, for an appropriate comparison and analysis of the weighing system, it

is still required to represent the balance output signal response in a discrete-time form, as it is delivered by the physical system.

Such a discrete-time conversion shown in **Eq. 3.28** is carried out by first defining the continuous-time output signal, which is $F_{Bal_{LPF}}(t)$. The second part of the equation comprises a series of Dirac impulses, that acquire data only at constant time intervals along the measurement. The impulse function for this application is described as the difference between a given time t within the measurement, and the product of the data sampling number N and the system's data sampling time t_s . In other words, $\delta(t - N \cdot t_s)$ [18].

$$F_{Bal}(t_n) = F_{Bal_{LPF}}(t) \cdot \sum_{N=0}^{\infty} \delta(t - N \cdot t_s) \quad (3.28)$$

Fig. 3.9 describes the continuous-discrete time conversion in **Eq. 3.28** as a block diagram, and it illustrates the expansion of its cumulative sum in a cascade form.

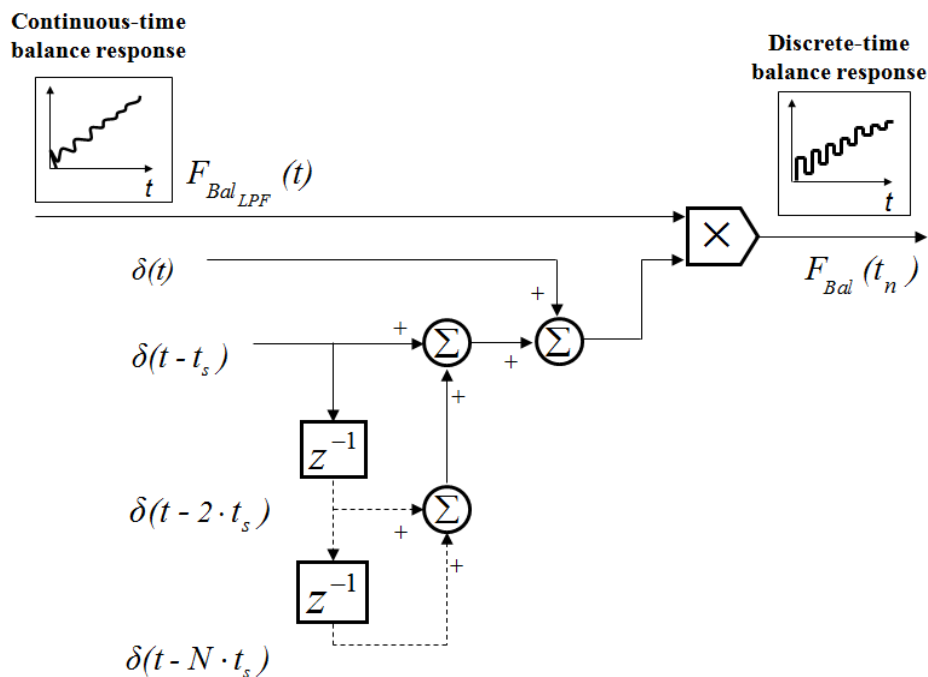


Fig. 3.9 Continuous/discrete time conversion of the balance output response

3.3 The connecting volume effect in liquid flow measurements

For the sake of explanation, the definition of mass and volumetric flow in a closed conduit system was presented in **Chapter 2** in terms of a simplified form of the continuity equation (**Eq. 2.1**). However, in practice, if such a simplified equation were intended to be used in a liquid flow primary standard, the expected result would be a mass flow rate calculation with reduced measurement accuracy, as it neglects the storage effect from the connecting volume (pipeline between the flowmeter under calibration and the weighing system). In other words, this effect indicates that in a real system, the eventual temperature changes of the fluid and the pipeline material will cause the fluid mass inside the connecting volume (CV) to change during the measuring time, and as a consequence, the mass flow circulating through the installed flowmeter will differ in some degree from the mass flow being discharged into the collection vessel and measured by the liquid flow primary standard (**Fig. 3.10**).

In this instance, the general continuity equation shown in **Eq. 3.29** is the basis equation employed in flow calibration facilities to quantify the connecting volume effect in the measurement [20]. The following equations and text below describe the background of this equation. As written in **Eq. 3.29**, the continuity equation establishes that the summation of the rate of change of mass inside a selected connecting volume V_{CV} (first term), plus the mass flow rate passing through an arbitrary area of the connecting volume A_{CV} (second term) has to be equal to zero, in order to comply with the law of mass conservation [20].

$$\frac{d}{dt} \int_{V_{CV}} \rho_{w_{CV}} \cdot dV + \int_{A_{CV}} \rho_{w_{CV}} \cdot u(t) \cdot dA = 0 \quad (3.29)$$

Here, $\rho_{w_{CV}}$ and $u(t)$ denote respectively the water density in the connecting volume (CV), and the mean velocity of the fluid at an arbitrary region across the CV.

Now, for the purpose of applying the general continuity equation, **Eq. 3.29** has to be derived in terms of the boundary conditions of the liquid flow primary standard. First, since there is no mass flow passing through the walls of the pipeline, it is inferred that the product $u(t) \cdot dA$ of the integral for this portion of surface is equal to zero. On the other hand, the mass is indeed flowing

in a normal direction to the cross section area of the flowmeter A_{Meter} (inlet section) as well as the cross section area of the nozzle outlet A_n (outlet section). Therefore, in accordance to the given statements, **Eq. 3.29** can be written for this specific case as [21]:

$$\frac{d}{dt} \int_{V_{CV}} \rho_{w_{CV}} \cdot dV + \left[- \int_{A_{Meter}} \rho_{w_{Meter}} \cdot u_{Meter}(t) \cdot dA + \int_{A_n} \rho_{w_n} \cdot u_n(t) \cdot dA \right] = 0 \quad (3.30)$$

In **Eq. 3.30**, $\rho_{w_{Meter}}$ and ρ_{w_n} stand for the water density at the flowmeter and the nozzle outlet location. Furthermore, the terms $u_{Meter}(t)$ and $u_n(t)$ represent the mean normal velocity of the fluid at the flowmeter and nozzle outlet location. Moreover, the second and third term of **Eq. 3.30** correspond respectively to the inlet and outlet mass flow of the control volume. Note that the minus sign at the inlet surface term is given, because the flow direction is opposite to the pressure force direction exerted by the water enclosed in the connecting volume [22].

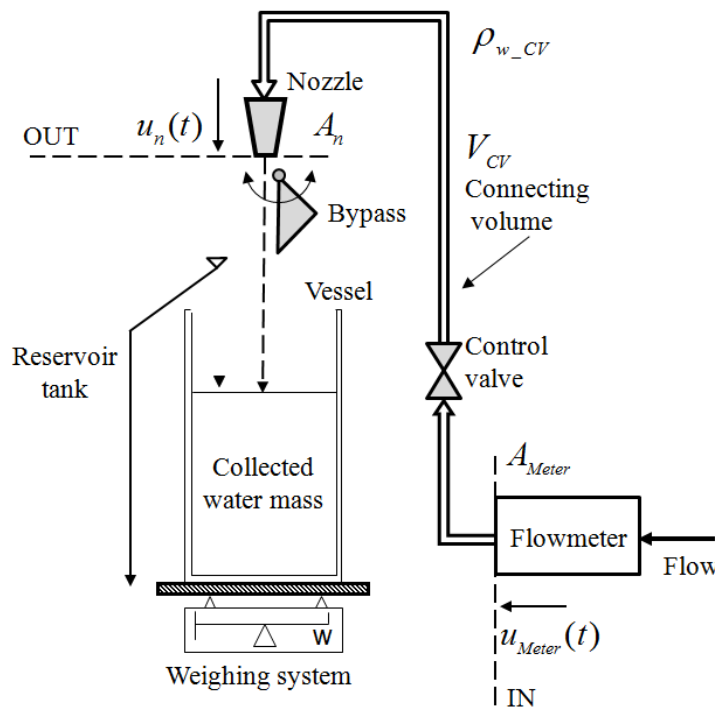


Fig. 3.10 The connecting volume of a liquid flow primary standard

Moreover, in accordance to the law of mass conservation, it can be stated that the mass outflow of the control volume (third term of **Eq. 3.30**) is equal to the mass flow rate delivered to the dynamic weighing liquid flow standard $\hat{m}_w(t_n)$, as illustrated in **Fig. 3.10**. Likewise, the same statement applies for the mass flow rate passing through the inlet section of the CV (second term of **Eq. 3.30**), which in practical terms turns out to be equal to the mass flow rate measured by the flowmeter $\dot{m}_{Meter}(t_n)$. Thus,

$$\frac{d}{dt} \int_{V_{CV}} \rho_{w_CV} \cdot dV + \left[-\dot{m}_{Meter}(t_n) + \hat{m}_w(t_n) \right] = 0 \quad (3.31)$$

In a more thorough description, **Eq. 3.32** points out the two physical effects that cause the fluid mass to change in the CV (first term of **Eq. 3.31**). One is originated by the pipeline volume change due to the thermal expansion or contraction of its material in a certain time, and the second effect is regarded to the fluid density variations inside the CV with respect to time.

$$\begin{aligned} \frac{d}{dt} \int_{V_{CV}} \rho_{w_CV} \cdot dV &= \frac{d(\rho_{w_CV} \cdot V_{CV})}{dt} \\ &= \rho_{w_CV} \cdot \frac{d(V_{CV})}{dt} + V_{CV} \cdot \frac{d(\rho_{w_CV})}{dt} \end{aligned} \quad (3.32)$$

Then, in order to find out the practical-oriented solution to this analysis, the rate of mass change depicted in **Eq. 3.31** has to be represented as the limit of the nominal change of water mass within a time interval Δt that approaches to zero. Hence,

$$\frac{d}{dt} \int_{V_{CV}} \rho_{w_CV} \cdot dV = \rho_{w_CV} \cdot \lim_{\Delta t \rightarrow 0} \frac{\Delta V_{CV}}{\Delta t} + V_{CV} \cdot \lim_{\Delta t \rightarrow 0} \frac{\Delta \rho_{w_CV}}{\Delta t} \quad (3.33)$$

where the time interval is defined as:

$$\Delta t = t_n - t_{n-1} = t_s \quad (3.34)$$

Therefore, due to a small temperature changes in the CV, and the thermal expansion properties of the fluid and pipeline material, the nominal change of fluid density and CV volume are assumed to be [23]:

$$\Delta\rho_{w_CV} = -\rho_{w_CV} \cdot \beta_w \cdot \Delta\vartheta_{w_CV} \quad (3.35)$$

$$\Delta V_{CV} = V_{CV} \cdot 3 \cdot \alpha_{CV} \cdot \Delta\vartheta_{CV} \quad (3.36)$$

As for the equations above, β_w denotes the volumetric thermal expansion coefficient of water ($207 \cdot 10^{-6} / K$), and α_{CV} is the linear expansion coefficient for the connecting pipe ($17,3 \cdot 10^{-6} / K$) [24]. Meanwhile, the variables $\Delta\vartheta_{w_CV}$ and $\Delta\vartheta_{CV}$ described in **Eq. 3.35** and **Eq. 3.36**, correspond to the undergone temperature difference of water (**Eq. 3.37**) and pipeline material (**Eq. 3.38**) between the time step t_{n-1} and t_n . Hence,

$$\Delta\vartheta_{w_CV} = \vartheta_{w_CV}(t_n) - \vartheta_{w_CV}(t_{n-1}) \quad (3.37)$$

$$\Delta\vartheta_{CV} = \vartheta_{CV}(t_n) - \vartheta_{CV}(t_{n-1}) \quad (3.38)$$

Thus, after substituting **Eq. 3.34**, **Eq. 3.35** and **Eq. 3.36** into **Eq. 3.33**, the rate of change of mass in the CV (connecting volume effect) can be determined by the following expression [23]:

$$\begin{aligned} \frac{d}{dt} \int_{V_{CV}} \rho_{w_CV} \cdot dV &= \left(\rho_{w_CV} \cdot 3 \cdot V_{CV} \cdot \alpha_{CV} \cdot \Delta\vartheta_{CV} - V_{CV} \cdot \rho_{w_CV} \cdot \beta_w \cdot \Delta\vartheta_{w_CV} \right) / \Delta t \\ &= \left[\rho_{w_CV} \cdot V_{CV} \cdot \left(3 \cdot \alpha_{CV} \cdot \Delta\vartheta_{CV} - \beta_w \cdot \Delta\vartheta_{w_CV} \right) \right] / t_s \end{aligned} \quad (3.39)$$

Finally, **Eq. 3.39** can be substituted into **Eq. 3.31**, in order to yield a practical form of the continuity equation (**Eq. 3.40**), which helps to correct the measurement error caused by the storage effect of the connecting volume, and thus it allows comparing both measurement approaches.

$$\hat{m}_w(t_n) = \dot{m}_{Meter}(t_n) - \frac{\rho_{w_CV} \cdot V_{CV} \cdot (3 \cdot \alpha_{CV} \cdot \Delta \vartheta_{CV} - \beta_w \cdot \Delta \vartheta_{w_CV})}{t_s} \quad (3.40)$$

3.3.1 Accuracy considerations in relation to the connecting volume effect in dynamic weighing liquid flow measurements

The significance of the discussed connecting volume effect upon the flow measurement accuracy can depend not only on the fluid and pipeline material temperature, but also on the type of primary standard in use. The following calculation examples shown in this section are made with the purpose to illustrate the impact of the connecting volume effect in the measurand, when this parameter is neglected either in a static weighing or in a dynamic weighing mass flow measurement.

The first calculation is based on a measurement run performed by the liquid flow primary standard, assuming this operates in a static-weighing mode at an average mass flow rate \bar{m}_w of 8 kg/min, with a collection time of 60s in a 10-L vessel. In this instance, the fluid and connecting volume temperature variations during the collection time are respectively 50 mK and 200 mK, based on data observations from a liquid flow primary standard. Additionally, the water density is agreed to be 998,2 kg/m³ at 20°C [25], and with a nominal connecting volume of 0,7 L. Thus, in accordance to **Eq. 3.39**, the magnitude of the connecting volume effect in a static-weighing mode (for this example) is:

$$\begin{aligned} \left[\int_{V_{CV}} \rho_{w_CV} \cdot dV \right]_{Static} &= \frac{998,2 \frac{kg}{m^3} \cdot 0,0007 m^3 \cdot \left(3 \cdot 17,3 \cdot 10^{-6} \frac{1}{K} \cdot 0,2K - 207 \cdot 10^{-6} \frac{1}{K} \cdot 0,05K \right)}{60s \cdot \left(\frac{1min}{60s} \right)} \quad (3.41) \\ &= 2,096 \cdot 10^{-8} \frac{kg}{min} \end{aligned}$$

Or in terms of its relative uncertainty:

$$\begin{aligned} [U_{CV}]_{Static} &= \pm \frac{\left[\int_{V_{CV}} \rho_{w_CV} \cdot dV \right]_{Static}}{\bar{m}_w} \cdot 100\% \quad (3.42) \\ &= \pm 2,62 \times 10^{-7} \% \end{aligned}$$

For the case of a dynamic weighing liquid flow measurement, the situation is rather different, because the measuring time can be in the order of milliseconds. That condition implies that during such a small period of time, only very small temperature variations of approximately ± 1 or 2 mK could take place (worst case scenario). On the other hand, it is important to mention that in a real process, these variations can be basically equal to the uncertainty attributed to a temperature sensor [26]. This means, that the recalled magnitude of temperature change could not be entirely attributed to the heat exchange through the fluid and the pipeline material, but also due to another factors, such as: temperature influence upon the measurement bridge resistors, different temperature gradients along the sensor stem, sensor hysteresis, the internal algorithm used to scale the electric output signal of the sensor into temperature units, and so on [26]. Therefore, for the example of a sampling time of 4ms at 8 kg/min, the magnitude of the connecting volume effect is:

$$\left[\int_{V_{CV}} \rho_{w_{CV}} \cdot dV \right]_{Dynamic} = \frac{998,2 \frac{kg}{m^3} \cdot 0,0007m^3 \cdot \left(3 \cdot 17,3 \cdot 10^{-6} \frac{1}{K} \cdot 0,002K - 207 \cdot 10^{-6} \frac{1}{K} \cdot 0,001K \right)}{0,004s \cdot \left(\frac{1min}{60s} \right)}$$

$$= -1,08 \cdot 10^{-3} \frac{kg}{min}$$
(3.43)

$$[U_{CV}]_{Dynamic} = \pm \frac{\left[\int_{V_{CV}} \rho_{w_{CV}} \cdot dV \right]_{Dynamic}}{\dot{m}_{TS}} \cdot 100\%$$

$$= \pm 0,0135\%$$
(3.44)

When looking at the result of the connecting volume effect in a dynamic weighing liquid flow primary standard (**Eq. 3.43 and Eq. 3.44**), it turns out to be that its magnitude becomes larger. The explanation to this quite significant increment is that despite the small temperature increments, the measuring time is thousands of times smaller than the total collection time in a static weighing primary standard, whereby the quotient gets larger. Eventually, the designated measuring time can be increased, for instance to 25ms, which results in a lower relative uncertainty of about 0,002%, but at the expense of most likely increasing the measurement uncertainty when overlooking and extrapolating measurement data. In conclusion, the storage effect of the connecting volume cannot be simply disregarded from a dynamic weighing primary

standard. As suggested by these examples and in the following **Chapter 5** and **Chapter 6**, this effect can be considered as the third main uncertainty contributor in the measurement process after the mass flow calculation model, and the process and measurement noise (**Table 3.1**). According to reference [27] the connecting volume effect stands as the fifth uncertainty contributor for static weighing calibration systems.

| No | STATIC WEIGHING APPROACH | DYNAMIC WEIGHING APPROACH |
|----|---|-----------------------------------|
| 1 | Timing error of the bypass valve (also known as diverter valve) | Mass flow calculation model |
| 2 | Flow stability | The measurement and process noise |
| 3 | Water density | Connecting volume effect |
| 4 | Mass determination | |
| 5 | Connecting volume | |

Table 3.1 Main uncertainty contributors of the static [27] and dynamic weighing liquid flow primary standards

4. Filtering techniques for the determination and accuracy of mass flow rate (Process model)

In this chapter, a series of filters are presented with the aim of processing the acquired data from the weighing system output signal $F_{Bal}(t_n)$, and thus, delivering an estimate of the desired measurand, mass flow rate.

The block diagram sketched in **Fig. 4.1** stands for the recalled three main subsystems of the dynamic weighing liquid flow primary standard. In **Chapter 3**, a description of the command input as well the first two subsystems (Fluid force and weighing system) were presented. Now, **Chapter 4** will address with the third subsystem known as *Process model*, which has to be expressed in a discrete-time form t_n , due to the time constant of the balance output signal, and data acquisition system involved in the real measurement process.

As seen in **Fig. 4.1**, the process model subsystem is divided into two subsystems called respectively: *Hydrodynamic force filter* and *Measurement noise filter*. The Hydrodynamic force filter has the task to analytically quantify and eliminate (or drastically reduce) the magnitude of the disturbing state variables from the measurement process; so the measurand $\hat{m}_{HF}(t_n)$ can be dynamically estimated with a higher accuracy [1]. As mentioned in **Chapter 3**, such disturbing process variables are described as: the hydrodynamic force $F_d(t_n)$ driven by the impacting water jet, and in a minor degree, the upward air buoyancy force $F_b(t_n)$ that causes an apparent loss of collected mass force [2]. The latter occurs either under dynamic or static measurement conditions.

The second subsystem known as measurement noise filter comprises a signal filter algorithm, which deals with the identification and attenuation of the measurement noise [3], and it is originated in great part by the reacting inertial force $F_{Inertial}(t_n)$ of the weighing system. The task of this filter is to make the estimate measurements $\hat{m}_w(t_n)$ more precise [4], and to re-enhance their accuracy.

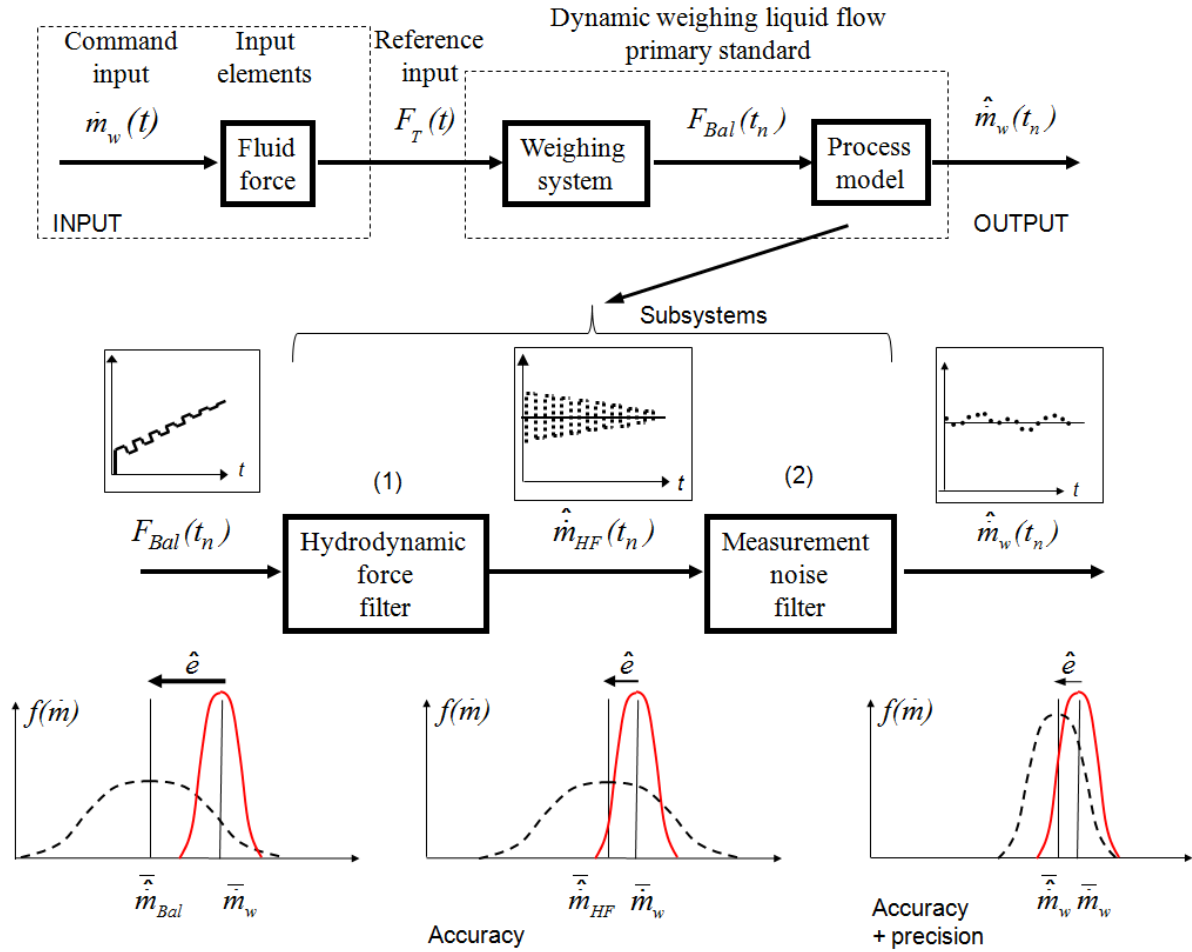


Fig. 4.1 General block diagram representation of the process model, its two subsystems, and the treatment of the measurement data to estimate the mass flow rate

As shown in **Fig. 4.1**, \hat{e} denotes the estimated error, $\dot{m}_w(t_n)$ is the true measurand value, $f(\dot{m})$ stands for the probability distribution of \dot{m} [5], and $\hat{m}_{Bal}(t_n)$, which is the estimate value of mass flow rate given by the direct response of the balance (**Eq. 4.1**). As a remark, it is important to note that $\hat{m}_{Bal}(t_n)$ is indeed an estimate measurand value, but it has not been treated by the influence of the hydrodynamic and buoyancy forces, in addition to the measurement noise induced by the dynamic response of the weighing system.

$$\hat{m}_{Bal}(t_n) = \frac{F_{Bal}(t_n) - F_{Bal}(t_0)}{g \cdot (t_n - t_0)} \quad (4.1)$$

4.1 Derivation of a filter for the attenuation of the hydrodynamic force effect upon the balance output response and determination of mass flow rate

One form to derive an algorithm that can filter out the presence of the discrete-time hydrodynamic and buoyancy force from balance output signal, consists in analyzing the 1-degree-of-Freedom motion equation derived in **Chapter 3 (Eq. 4.2)**, because it is the equation that relates the recalled unwanted fluid state variables, with the response of the balance used in the process.

$$F_{Inertial}(t_n) + F_c(t_n) + F_{Bal}(t_n) = F_m(t_n) + F_d(t_n) - F_b(t_n) \quad (4.2)$$

As mentioned in **Chapter 3**, it is agreed that $F_{Bal}(t_n)$ denotes the balance response because is indeed the variable that summarizes in its magnitude: the acting fluid forces, the damping force effect of the balance sensing element, and the inertial force the system is subjected during the dynamic process (**Section 3.2.4**). Hence, the equation of motion can be expressed as $F_{Bal}(t_n)$, equal to the summation of all involved acting-reacting forces (**Eq. 4.3**)

$$F_{Bal}(t_n) = F_m(t_n) + F_d(t_n) - F_b(t_n) - F_{Inertial}(t_n) - F_c(t_n) \quad (4.3)$$

In the real measurement process, the balance is unable to measure each of the fluid force variables independently, but their summation represented by the variable called $F_T(t_n)$, in addition to the mechanical reacting forces of inertia and damping, as shown in **Eq. 4.4**.

$$F_{Bal}(t_n) = F_T(t_n) - F_{Inertial}(t_n) - F_c(t_n) \quad (4.4)$$

Now, for the sake of obtaining a practical equation for the determination of mass flow rate, it is necessary to simplify **Eq. 4.4** based on the physical fact, that the balance force response $F_{Bal}(t_n)$, and the acting fluid forces are *estimated to be equal* (**Eq. 4.5**) [6]. The explanation for this assumption is the following.

$$F_{Bal}(t_n) \triangleq F_T(t_n) \quad (4.5)$$

Firstly, consider the Force-time graph shown in **Fig. 4.2(a)**, wherein $F_T(t_n)$ is split into its three components: collecting mass, hydrodynamic, and buoyancy force. On other hand, take a look to **Fig. 4.2(b)**, in which the path of a ramp-like response of $F_T(t_n)$ and $F_{Bal}(t_n)$ are basically overlapping all along the filling process. In other words, the average slope magnitude is agreed to be the same in both cases. However, the relatively small difference still remaining between these two state variables $F_T(t_n)$ and $F_{Bal}(t_n)$ is due to the inertial force $F_{Inertial}(t_n)$, damping force $F_c(t_n)$, in addition to the balance time response, the effect of the continuous-discrete time conversion, and low pass filter upon the balance output signal. These signal-conditioned unwanted state variables will be treated in the following section, regarding the measurement noise filter and its application. Summarizing, **Eq. 4.6** gathers the above statements in an expression, describing that the balance output response can be equal to the summation of estimated fluid force variables, denoted by a hat symbol “ $\hat{}$ ”.

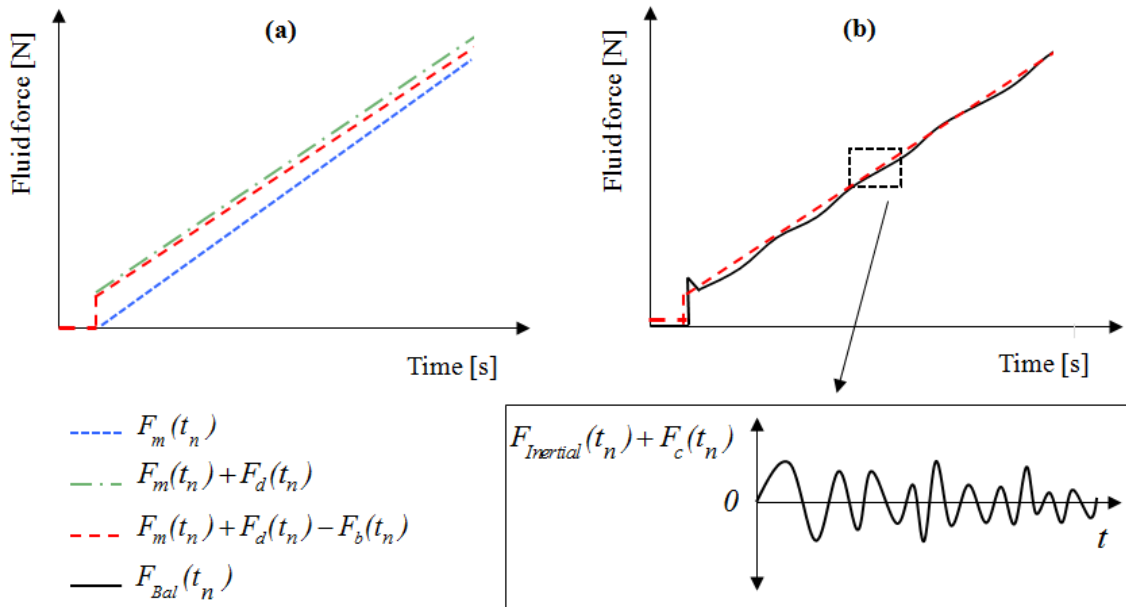


Fig. 4.2 Graphical representation of (a) acting fluid forces and (b) balance force response during the filling process

$$F_{Bal}(t_n) = \hat{F}_m(t_n) + \hat{F}_d(t_n) - \hat{F}_b(t_n) \quad (4.6)$$

After writing **Eq. 4.6** as a function of mass flow rate in terms of the discrete time form t_n , the equation takes the following form:

$$\begin{aligned}
F_{Bal}(t_n) &= \hat{m}_{HF}(t_n) \cdot g \cdot t_n + \hat{m}_{HF}(t_n) \cdot \hat{u}_i(t_n) - \hat{m}_{HF}(t_n) \cdot g \cdot \left(\frac{\rho_A}{\rho_w} \right) \cdot t_n \\
&= \hat{m}_{HF}(t_n) \cdot \left[g \cdot \left(1 - \frac{\rho_A}{\rho_w} \right) \cdot t_n + \hat{u}_i(t_n) \right]
\end{aligned} \tag{4.7}$$

where the subindex *HF* stands for the mass flow rate estimate after applying the hydrodynamic force filter, g is the local acceleration of gravity (9,8125 m/s²), and $\hat{u}_i(t_n)$ is the water jet impact velocity.

Then, after substituting the hydrodynamic force equation (**Eq. 3.8**) in a discrete-time form into **Eq. 4.7**, such an equation becomes:

$$F_{Bal}(t_n) = \hat{m}_{HF}(t_n) \cdot \left[g \cdot \left(1 - \frac{\rho_A}{\rho_w} \right) \cdot t_n + \underbrace{\left\{ \frac{\left(\frac{\hat{m}_{HF}(t_n)}{\rho_w \cdot A_n} \right)^2}{\hat{u}_n(t_n)} + 2 \cdot g \cdot \left(h_i(0) - \left[\frac{\hat{m}_{HF}(t_n) \cdot t_n}{\rho_w \cdot A_v} \right] \right) \right\}^{1/2}}_{\hat{h}_i(t_n)} \right] \tag{4.8}$$

As a remark, it is important to underline that in **Eq. 4.8**, the local acceleration of gravity g is considered as a constant, due to the fact that the changing center of gravity of the water mass during the filling process, and the effect it has upon the g value is relatively small [7]. Now, in order to carry on with the equation to estimate the measurand $\hat{m}_{HF}(t_n)$, it is necessary to express **Eq. 4.8** in a form that the square root of the impact velocity can be cancelled out, and thus making the factorization easier. Hence,

$$\begin{aligned}
&\left\{ F_{Bal}(t_n) - \hat{m}_{HF}(t_n) \cdot g \cdot \left(1 - \frac{\rho_A}{\rho_w} \right) \cdot t_n \right\}^2 = \\
&\left\{ \hat{m}_{HF}(t_n) \cdot \left[\left(\frac{\hat{m}_{HF}(t_n)}{\rho_w \cdot A_n} \right)^2 + 2 \cdot g \cdot \left(h_i(0) - \left[\frac{\hat{m}_{HF}(t_n) \cdot t_n}{\rho_w \cdot A_v} \right] \right) \right]^{1/2} \right\}^2
\end{aligned} \tag{4.9}$$

And after some algebraic steps in **Eq. 4.9**, it turns out to be that the hydrodynamic force filter equation is a polynomial equation of fourth order, and it is described in the following canonical form:

$$\begin{aligned} & \left[\frac{I}{\rho_w^2 \cdot A_n^2} \right] \cdot \hat{m}_{HF}^4(t_n) - \left[\frac{2 \cdot g \cdot t_n}{\rho_w \cdot A_v} \right] \cdot \hat{m}_{HF}^3(t_n) + \left[2 \cdot g \cdot h_i(0) - g^2 \cdot \left(1 - \frac{\rho_A}{\rho_w} \right)^2 \cdot t_n^2 \right] \cdot \hat{m}_{HF}^2(t_n) + \dots \\ & \dots + \left[2 \cdot F_{Bal}(t_n) \cdot g \cdot \left(1 - \frac{\rho_A}{\rho_w} \right) \cdot t_n \right] \cdot \hat{m}_{HF}(t_n) - F_{Bal}^2(t_n) = 0 \end{aligned} \quad (4.10)$$

As **Eq. 4.10** indicates, the determination of the measurand $\hat{m}_{HF}(t_n)$ cannot be obtained by simply substituting the variables into the equation, as that occurs in a second-order equation, wherein its two roots (not necessarily distinct) are obtained by simply using the so called Quadratic formula [8]. One practical way to accurately solve **Eq. 4.10** consists in implementing a numerical method that can calculate the eigenvalues (or roots) of such a polynomial equation. In this instance, **Eq. 4.11** shows the characteristic time-varying matrix \mathbf{E}_n [9] of the fourth order equation, wherein its coefficients are contained.

$$\mathbf{E}_n = \begin{bmatrix} -b(t_n)/a(t_n) & -c(t_n)/a(t_n) & -d(t_n)/a(t_n) & -e(t_n)/a(t_n) \\ 1 & 0 & 0 & 0 \\ 0 & 1 & 0 & 0 \\ 0 & 0 & 1 & 0 \end{bmatrix} \quad (4.11)$$

where the order of these coefficients in relation to **Eq. 4.10** as well as its variable is written as:

$$p(\lambda(t_n)) = a(t_n) \cdot \lambda^4(t_n) + b(t_n) \cdot \lambda^3(t_n) + c(t_n) \cdot \lambda^2(t_n) + d(t_n) \cdot \lambda(t_n) + e(t_n) = 0 \quad (4.12)$$

In order to find out the eigenvalues of **Eq. 4.10** for each time step t_n , such an equation has to be represented in an equivalent form, in which the determinant of its characteristic matrix \mathbf{E}_n minus the dot product of the scalar values $\lambda(t_n)$ and the identity matrix \mathbf{I} is equal to zero, as shown in **Eq. 4.13**. Likewise, this polynomial equation can be written in a factorial form, in order to describe more clearly the eigenvalues \mathbf{E}_n .

$$\begin{aligned}
p(\lambda(t_n)) &= \det(\mathbf{E}_n - \lambda(t_n) \cdot \mathbf{I}) \\
&= (\lambda(t_n) - \lambda_1(t_n)) \cdot (\lambda(t_n) - \lambda_2(t_n)) \cdot (\lambda(t_n) - \lambda_3(t_n)) \cdot (\lambda(t_n) - \lambda_4(t_n)) = 0
\end{aligned}
\tag{4.13}$$

In this instance, **Eq. 4.13** is solved by a robust numerical method called QR algorithm [10 and 11], which is available in some technical computing software, such as MatLab®, and it allows a fast and an effective iterative method to calculate the eigenvalues of the characteristic matrix \mathbf{E}_n .

Furthermore, it is important to note that in **Eq. 4.12** and **Eq. 4.13**, the scalar $\lambda(t_n)$ is intentionally used to represent the main variable of the polynomial equation $p(\lambda)$, instead of the measurand $\hat{m}_{HF}(t_n)$ shown in **Eq. 4.10**. The reason is that after solving the determinant, the four eigenvalues found $\lambda_1(t_n)$, $\lambda_2(t_n)$, $\lambda_3(t_n)$ and $\lambda_4(t_n)$ can be either equal or distinct among each other (**Eq. 4.14**). In this case, only the real part of the complex number eigenvalue is taken into account, and the selected eigenvalue is the one that gets closer to the average estimate mass flow rate $\bar{\hat{m}}_{Bal}(t_n)$ yield by **Eq. 4.1**.

$$\hat{m}_{HF}(t_n) = \lambda_1(t_n) \wedge \vee \lambda_2(t_n) \wedge \vee \lambda_3(t_n) \wedge \vee \lambda_4(t_n)
\tag{4.14}$$

where the symbols “ \wedge ” and “ \vee ” stand respectively for the logical operators “and” and “or”.

As for the experimental determination of mass flow rate $\hat{m}_{HF}(t_n)$, this follows in principle the same methodology used for the numerical approach. Nevertheless, in the real process, additional considerations have to be taken into account, because the water and air temperature (\mathcal{G}_w and \mathcal{G}_A) and consequently their densities, can change during the measurement run. Hence, the water and air density variables are agreed to be temperature-depended variables denoted as $\rho_w(\mathcal{G}_w)$ and $\rho_A(\mathcal{G}_A)$.

Another consideration to make during the experimentation is that the estimate impact height component $\hat{h}_i(t_n)$ described in **Eq. 4.8** can yield to some calculation errors, due to the fact that the cross section area of the collection vessel A_v can significantly vary from its nominal value at

different locations, especially at the vessel bottom. Therefore, in order to attain a better estimate value of the impact height, a characterization will be carried out to get an equation that can relate the changes of the water surface level h_w , with the imminent displacement of the balance platform z when the mass increases. In other words, the impact height will be experimentally defined as a function of the balance platform displacement denoted as $\hat{h}_i(z)$.

It is worth to mention that an impact height equation via a characterized cross section area of the vessel A_v is also possible. However, it can be a quite challenging and time-consuming task in terms of (i.e. cylindrical vessel) [12]: mounting a length standard inside the vessel, moving the length standard not only in a translational but also in a rotational form, so the vessel diameter can be characterized at different lengths and locations. In addition to the above mentioned issues, the roundness errors can be also rather significant, for the fact that most vessels are designed and manufactured as containers. Nevertheless, if the vessel were a high-accurate rounded-shape cylinder, the characterization of A_v would result in a better approach for calculating $\hat{h}_i(t_n)$, from the point of view of reducing the number of process variables as well as the number of measurement uncertainty contributors.

The details of the impact height characterization procedure via balance platform displacement are described in **Chapter 6**, regarding the experimental setup of the prototype used as a dynamic weighing liquid flow primary standard.

Hence, after considering the above statements, the experimental equation for the estimation of the water mass flow rate can be written as follows:

$$\begin{aligned} & \left[\frac{I}{\rho_w^2(\vartheta_w) \cdot A_n^2} \right] \cdot \hat{m}_{HF}^4(t_n) + \left[2 \cdot g \cdot \hat{h}_i(z) - g^2 \cdot \left(1 - \frac{\rho_A(\vartheta_A)}{\rho_w(\vartheta_w)} \right)^2 \cdot t_n^2 \right] \cdot \hat{m}_{HF}^2(t_n) + \dots \\ & \dots + \left[2 \cdot F_{Bal}(t_n) \cdot g \cdot \left(1 - \frac{\rho_A(\vartheta_A)}{\rho_w(\vartheta_w)} \right) \cdot t_n \right] \cdot \hat{m}_{HF}(t_n) - F_{Bal}^2(t_n) = 0 \end{aligned} \quad (4.15)$$

As a remark, the eigenvalue method used to iteratively solve the numerical approach is also employed to obtain the experimental estimate collected mass and flow rate from **Eq. 4.15**.

4.2 Proposed filter algorithms for an improved mass flow rate calculation based on the identification and reduction of measurement noise

So far, the hydrodynamic force filter (first process model subsystem) enables to represent some physical phenomena that are implicit in the process, as well as depicting a mathematical model that can help to separate, or at least to attenuate the unwanted process variables from the measurand. Now, the second process model subsystem, known as Measurement noise filter is dealing with one particular issue: The weighing system do not provide the exact desired quantity $\dot{m}_w(t_n)$, because it introduces its own system dynamic response into the output signal $\hat{m}_{HF}(t_n)$, which adds in a major or a minor degree measurement noise $v(t_n)$ (**Eq. 4.16**).

$$\hat{m}_{HF}(t_n) = \dot{m}_w(t_n) + v(t_n) \quad (4.16)$$

For the treatment of the measurement noise in the liquid flow primary standard, three different filter algorithms are proposed, with the aim to realize, which one delivers the most precise and accurate estimate value (**Fig. 4.3**). These filters are:

- 1) Central moving average filter [13], which aims to smooth out the trend of the measurand by creating a plot line of connected data subset averages, defined by a certain number of measurement data before and after the current time step t_n ,
- 2) Least-Mean-Square adaptive filter, which adapts to the input signal by iteratively tuning its parameters (i.e. curve-fitting), in order to deliver an estimate value with a minimized signal error [14 and 15], and
- 3) Linear Kalman filter algorithm that combines all available measurement data, plus prior knowledge of the weighing system, in order to produce an estimate measurand, wherein its error is statistically minimized, and it does not require to store and reprocess large amounts of previous measurement data to deliver its output [16].

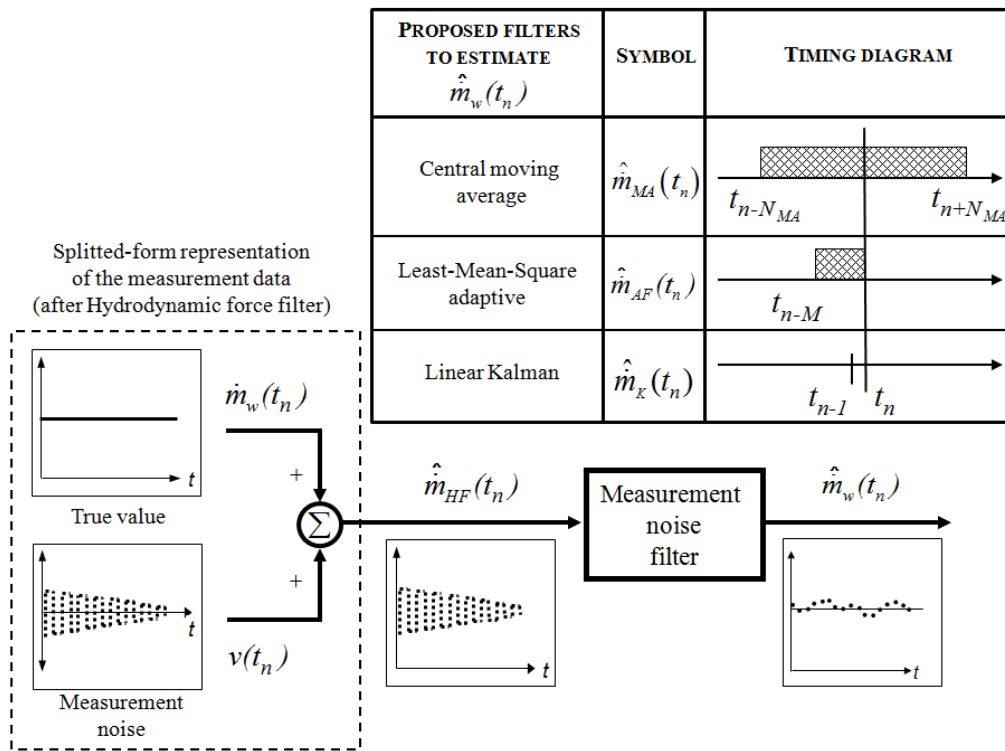


Fig. 4.3 The measurement noise filter and the three selected filters for the analysis

4.2.1 Central moving average filter

The central moving average is a type of filter that estimates the value of the measurand by averaging several values from a number of data subsets, and thus repeats the same procedure for the whole measuring time of the process.

The moving average is the first filter considered in this work, due to its simplicity for its implementation, but also because of its ability to drastically decrease the amplitude of measurement noise from the input signal $\hat{m}_{HF}(t_n)$, while keeping a sharp step response to changes in the measurand [17]. As an important remark, the central moving average filter in use is indeed a data smoothing algorithm. This means, an algorithm that can prevent a large erroneous shifting of the estimate values by not only considering the measurement data before the reference time t_n (as it is the case of an ordinary moving average) but also the data after t_n [18]. As illustrated in **Fig. 4.4**, this algorithm can be also represented as a combination of two filters. In this instance, one of the filters averages all the *a priori* data to time t_n to produce an estimate $\hat{m}_{MA}^+(t_n)$. This can be recalled as a forward filter. Meanwhile, the second filter (backward filter) averages all the *a posteriori* data to time t_n , and gets the second

estimate $\hat{m}_{MA}^-(t_n)$. Then, by putting together these two filters, a more accurate estimate $\hat{m}_{MA}(t_n)$ of the measurand can be achieved (Eq. 4.17), when analyzing two different trends of mass flow rate between time t_n [19].

$$\hat{m}_{MA}(t_n) = \frac{1}{2} \cdot \left(\overbrace{\frac{1}{(N_{MA}/2)} \cdot \sum_{i=n-(N_{MA}/2)}^n \hat{m}_{HF}(t_i)}^{\hat{m}_{MA}^+(t_n)} + \overbrace{\frac{1}{(N_{MA}/2)} \cdot \sum_{i=n+1}^{n+(N_{MA}/2)} \hat{m}_{HF}(t_i)}^{\hat{m}_{MA}^-(t_n)} \right) \quad (4.17)$$

$$= \frac{1}{N_{MA}} \cdot \sum_{i=n-(N_{MA}/2)}^{n+(N_{MA}/2)} \hat{m}_{HF}(t_i)$$

According to Eq. 4.17, N_{MA} denotes the number of data samples to average by the filter, and n stands for the measurement sample to be smoothed out. Furthermore, one must be aware about the appropriate designation of N_{MA} , due to the fact that an excessive number of samples can eventually produce a stiff filter output response, leading to a possible misinterpretation of the measurand [19].

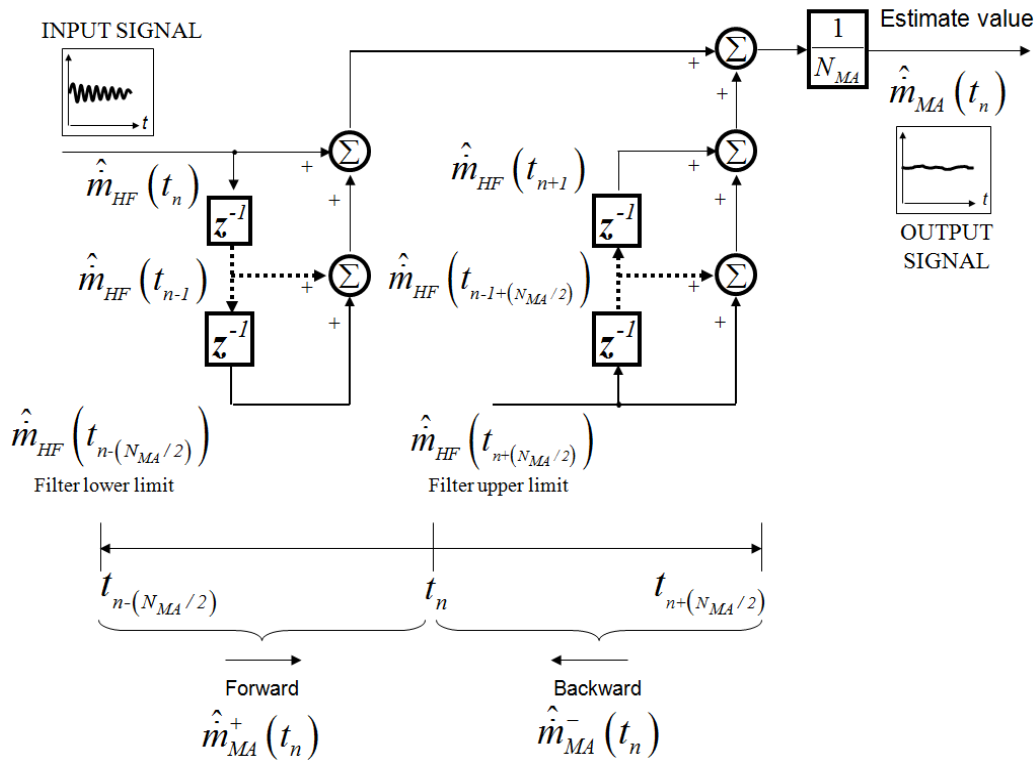


Fig. 4.4 Block diagram representing the central moving average filter algorithm [14]

4.2.2 Least-Mean-Square adaptive filter

As the name suggests, this type of filter adapts to the performance of the input signal delivered by the previous hydrodynamic force filter $\hat{m}_{HF}(t_n)$, with the aim to learn how to distinguish between the measurement noise caused by the oscillatory motion of the balance, and the true measurand. Then, such information is used to proceed with the removal (or high attenuation) of the noise from its input signal, and thus, yielding an estimate of the measurand [15]. The general concept about how this type of filter operates is graphically depicted in **Fig. 4.5**. Firstly, the scheme in **Fig. 4.5** refers to an input signal, wherein the true measurand value is corrupted with a time-varying noise amplitude [20].

Secondly, making reference to **Fig. 4.5**, the filter incorporates in its structure a decorrelation delay, followed by the basis Least-Mean-Square (LMS) algorithm of the adaptive filter. The decorrelation delay is in this instance a useful statistical tool, which helps to identify the measurand from the noisy input signal by comparing a version of the input signal $\hat{m}_{HF}(t_n)$ with a second version that has been delayed D intervals $\hat{m}_{HF}(t_{n-D})$. The *decorrelation delay* D is not a number that can be given arbitrarily. On the contrary, it must be chosen so that the signal value $\hat{m}_{HF}(t_n)$ will not correlate either with $\hat{m}_{HF}(t_{n-D})$ or with respect to $v(t_n)$. In other words, none similarities or repeating patterns must appear between them [21].

The basic working principle of the LMS adaptive filter algorithm exemplified in **Fig. 4.5** consists in applying an iterative approximation technique, where its outcome $\hat{m}_{AF}(t_n)$ is given by the summation of convoluted filter coefficients $h(k)$, and the decorrelated input data (**Eq. 4.18**).

$$\hat{m}_{AF}(t_n) = \sum_{k=0}^{M-1} h(k) \cdot \hat{m}_{HF}(t_{n-D-k}) \quad (4.18)$$

where M denotes the number of filter coefficients, and $\hat{m}_{AF}(t_n)$ is the estimate measurand yield by the adaptive filter (output signal).

The filter coefficients recalled in **Eq. 4.18** have the task to approach the measurand value by attenuating the input signal amplitude (this means, narrowing the spread of the measurement noise), and in this manner, making the estimates more accurate along the measuring time. As a remark, the level of accuracy and convergence of the adaptive filter depends in many cases of the number of filter coefficients used in the algorithm [22].

In regards to the iterative part of the LMS adaptive filter, this is based on the ongoing renewal of its coefficients $h(k)$, so the measurand can be better estimated after each step [23]. As depicted in **Fig. 4.5**, the numerical process of updating the filter coefficients consists firstly in using the values of the previous step filter coefficients as current values called $h_c(k)$. Thereafter, such current filter coefficient values are sum up with the product of the feedback error signal value $e_{AF}(t_n)$, the filter step size Δ_{AF} , and the decorrelated delay input signal value $m\hat{m}_{HF}(t_{n-D-k})$, in order to yield a set of updated filter coefficients, $h_{up}(k)$ (**Eq. 4.19**).

$$h_{up}(k) = h_c(k) + \Delta_{AF} \cdot e_{AF}(t_n) \cdot \hat{m}_{HF}(t_{n-k-D}) \quad (4.19)$$

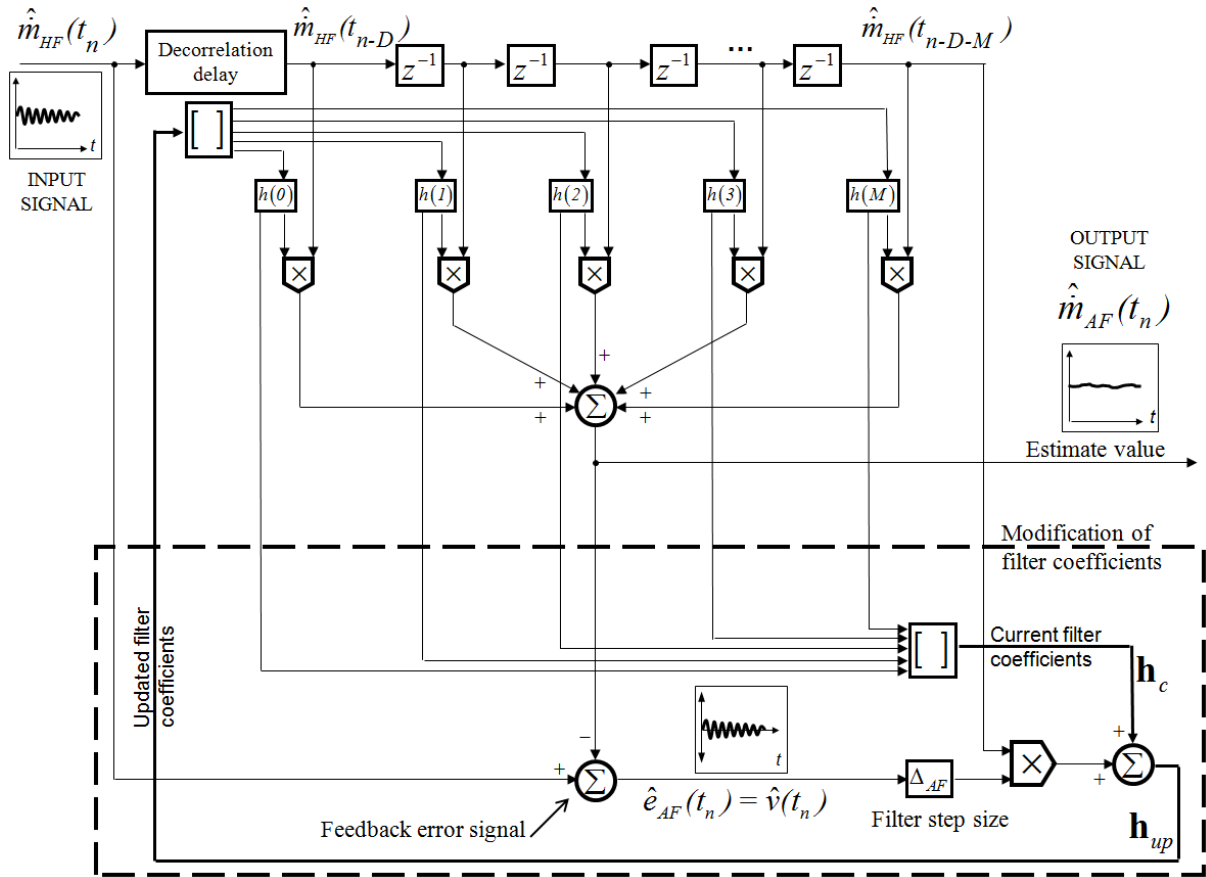


Fig. 4.5 Block diagram of a delayed input Least-Mean-Square adaptive filter for noise removal [20]

As observed in Eq. 4.20, Fig. 4.5, and Fig. 4.6, the feedback estimate error signal $e_{AF}(t_n)$ reveals a particular feature of this filter, which unlike the adaptive filters for system identification (see reference [24]), it seeks for the minimization of error by comparing the difference between the estimate value $\hat{m}_{AF}(t_n)$, and the measurement input signal $\hat{m}_{HF}(t_n)$ [21]. In other words, $e_{AF}(t_n)$ can be referred as the estimate version of the measurement noise $\hat{v}(t_n)$, due to the fact that $\hat{m}_{AF}(t_n)$ is also an estimate value of the true measurand value $\dot{m}_w(t_n)$.

$$\begin{aligned} \hat{e}_{AF}(t_n) &= \hat{m}_{HF}(t_n) - \hat{m}_{AF}(t_n) \\ &= \hat{v}(t_n) \end{aligned} \tag{4.20}$$

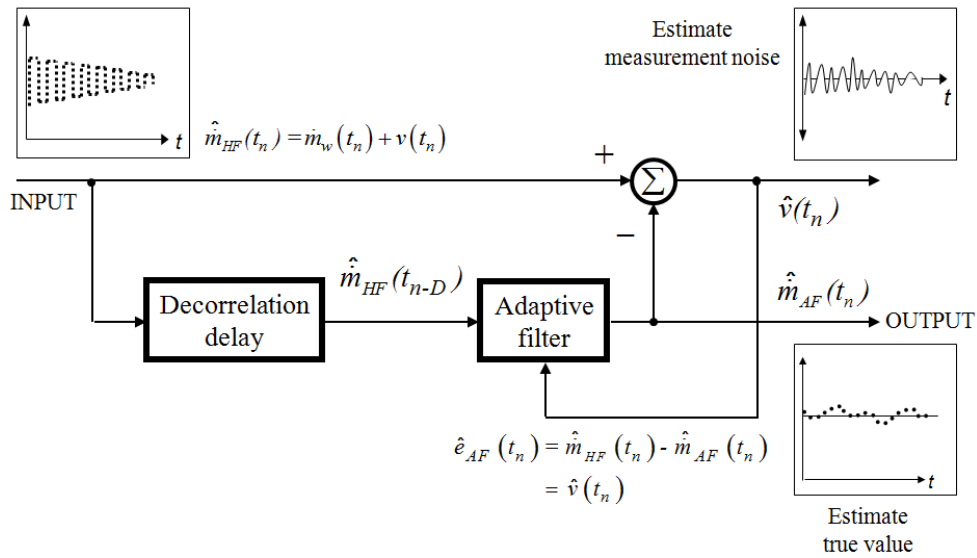


Fig. 4.6 Graphical explanation of the estimate error signal feedback [21]

The determination of filter step size Δ_{AF} (Eq. 4.21) is another crucial task for the successful implementation of the algorithm into the measurement process. Such a variable is responsible for determining the amount of correction to be applied as the filter adapts from one iteration to the next. In order to choose the appropriate step size, it is necessary to take into account the following considerations [25 and 26]:

- 1) If the step size is too small, the time of convergence (based also on the number of filter coefficients) can be too long, so that the estimate value might never reach an accurate enough value,
- 2) If the step size is too large, that might cause the adaptive filter to diverge, and becoming unstable.

Therefore, in order to ensure satisfactory convergence and stability in the filter, the step size Δ_{AF} must be within a recommended range [21]:

$$0 < \Delta_{AF} < \frac{1}{10 \cdot M \cdot P_{AF}} \quad (4.21)$$

where M is the number of filter coefficients, and P_{AF} is the average power of the input signal data set, and it is described as:

$$P_{AF} = \frac{I}{N_{AF} + I} \cdot \sum_{n=0}^{N_{AF}} \hat{m}_{HF}^2(t_n) \quad (4.22)$$

Here, N_{AF} represents the number of input signal data.

As a remark, it is recommended to start with small step sizes, so that the estimate values of the filter can be more reliable in terms of its accuracy level, but at the expense of the taking some additional time to adapt the filter into the measurand [23].

The delayed input signal LMS adaptive filter algorithm is not the only method employed by adaptive filtering theory to remove noise. For instance, the Normalized Least-Mean-Square adaptive filter (NLMS) can converge more quickly than the LMS due to its time-varying step size that minimizes the instantaneous estimate error [23 and 27]. Moreover, the Recursive Least-Square (RLS) [28] exhibits an even faster convergence speed than the LMS or NLMS, because its time-varying estimate error uses a statistical factor, the Kalman filter will be described, with the aim to analyze the effectiveness of such recursive filtering techniques in this particular process [29]. Furthermore, despite the recalled enhanced performance of the NLMS and RLS in relation to LMS, the LMS has three significant characteristics that makes it quite feasible for its implementation. One is the fact that the LMS algorithm does not require high computational resource as the RLS demands [30]. The second characteristic and advantage (in some cases) is that the RLS the input signal is considered deterministic, while in the LMS it is considered stochastic. This means, if the designated model of the RLS does not approach the true value, the filter output might experience a poor tracking performance. The third relevant characteristic of the LMS over the NLMS is that despite the fast convergence attributed to NLMS time-varying estimate error, this sometimes presents problems to adjust its output signal with the measurand [21, 23 and 25].

4.2.3 Linear Kalman filter

The Kalman filter [31] is a computational algorithm that combines all available measurement data $\hat{m}_{HF}(t_n)$, with the knowledge of the system, the statistical description of measurement noise, and the initial conditions of the measurand, in order to estimate the mass flow rate variable $\hat{m}_K(t_n)$. Another characteristic of the this filter is that, unlike other data processing algorithms, the Kalman filter does not require all previous data to be kept in storage, and to reprocess them every time step a new measurement is taken. This recursive approach [14] is also seen as a remarkable advantage, especially when the large amount of processing data can significantly increase the numerical complexity of a filter algorithm, or in the worst case, it makes the filter unstable.

For the aim to estimate the magnitude of the measurand from the measurement data $\hat{m}_{HF}(t_n)$, it is necessary first, to have a model depicting the general behavior of the mass flow rate \dot{m}_K , and the measurement noise $v_K(t_n)$, as shown in **Eq. 4.23**.

$$\hat{m}_{HF}(t_n) = \dot{m}_K + v_K(t_n) \quad (4.23)$$

In this instance, it is possible to agree that the measurand of the Kalman filter \dot{m}_K can be equal to the average mass flow rate from hydrodynamic force filter, because this measurement process is carried out at a quasi-steady flow condition. Furthermore, the given average or expected value (**Eq. 4.24**) among the noisy measurement signal does not imply the true magnitude of the measurand. Nonetheless, the average value has a much higher probability of getting closer to the true measurand value [32 and 33], in comparison to the spread measurement data enclosed in a broadband.

$$\dot{m}_K = \frac{1}{N} \cdot \sum_{n=1}^N \hat{m}_{HF}(t_n) \quad (4.24)$$

In regards to the measurement noise $v_K(t_n)$, it can be described in practical terms as a variable with N number of data, that approaches to a normal probability distribution $p(v_K)$, with a zero

mean value, and a variance σ_K^2 shown in **Eq. 4.25** [34]. The variance is an important aspect in this data processing algorithm, because it tells how dispersed the measurements are from the expected value [35].

$$p(v_k) \sim N(0, \sigma_K^2) \quad (4.25)$$

$$\sigma_K^2 = \sqrt{\frac{1}{N-1} \cdot \sum_{n=1}^N (v_K(t_n) - \theta)^2} \quad (4.26)$$

In practice, the true measurement noise variance cannot be exactly (or directly) determined, however it can be fairly estimated by calculating the variance σ_{HF}^2 (**Eq. 4.27**) of the filter input data $\hat{m}_{HF}(t_n)$. The reason for stating an experimental estimation of the measurement noise variance (and not an equality) is based on the fact that, σ_K^2 is a direct function of the measurement noise data (**Eq. 4.26**), and σ_{HF}^2 is a function of the measurement data and its average value, which stands within or near the narrowband probability distribution of the true measurand values buried in the measurement data (**Eq. 4.28**).

$$\sigma_{HF}^2 = \sqrt{\frac{1}{N-1} \cdot \sum_{n=1}^N (\hat{m}_{HF}(t_n) - \bar{m}_K)^2} \quad (4.27)$$

$$\sigma_K^2 \triangleq \sigma_{HF}^2 \quad (4.28)$$

Filter algorithm

As illustrated in **Fig. 4.7**, the Kalman filter resembles a feedback loop structure, in which the filter estimates the measurand at some time step t_n , and on the other hand it obtains a feedback signal in the form of a noisy measurement. For its implementation, the Kalman filter algorithm is divided into two sets of matricial equations that make possible its recursive feature [14]. The first set known as *Time update equations* is in charge for projecting forward (in time) the current estimate $\hat{\mathbf{x}}_n^-$ (**Eq. 4.29**) and the predicted estimate error covariance \mathbf{P}_n^- (**Eq. 4.30**), so an *a priori measurand estimate* can be obtained for the next time step. On the other hand, the second set known as *Measurement update equations* (**Eq. 4.31**, **Eq. 4.32** and **Eq. 4.33**) is responsible for correcting the predicted measurand estimate. **Eq. 4.31** is in this case not only the main equation

of the measurement update equations but also for the Kalman filter algorithm, because it handles the three mechanisms of recursive signal filtering [29 and 36]. These are:

- The *measurement residual* $(\mathbf{y}_n - \mathbf{H} \hat{\mathbf{x}}_n^-)$, which reflects the difference between the current measurement vector \mathbf{y}_n , and the predicted measurement estimate $\hat{\mathbf{x}}_n^-$,
- The *Kalman gain matrix* \mathbf{K}_n (Eq. 4.32) is defined as a time-varying optimal weighting value [16 and 32] based on the predicted error covariance (Eq. 4.30) and the *measurement noise covariance* \mathbf{R} , which helps to improve the *a posteriori measurand* estimate as well as minimizing the *a posteriori error covariance* [36] (Eq. 4.33), and
- The *corrected state estimate value* $\hat{\mathbf{x}}_n$ equal to the summation of the predicted t_{n-1} step estimate $\hat{\mathbf{x}}_n^-$ and its corresponding estimate correction $\mathbf{K}_n \cdot (\mathbf{y}_n - \mathbf{H} \cdot \hat{\mathbf{x}}_n^-)$.

Time update equations (predictor):

$$\hat{\mathbf{x}}_n^- = \mathbf{A} \hat{\mathbf{x}}_{n-1} \quad (4.29)$$

$$\mathbf{P}_n^- = \mathbf{A} \mathbf{P}_{n-1} \mathbf{A}^T \quad (4.30)$$

Here, \mathbf{A} is the so called *transition matrix*, which relates the state variables at the previous time step t_{n-1} to the current time step t_n [37]. On the other hand, $\hat{\mathbf{x}}_n^-$ and $\hat{\mathbf{x}}_{n-1}$ are the vectors denoting the predicted state variable at the time step t_n and the current state variable estimate at t_{n-1} respectively.

Measurement update equations (corrector):

$$\hat{\mathbf{x}}_n = \hat{\mathbf{x}}_n^- + \mathbf{K}_n (\mathbf{y}_n - \mathbf{H} \hat{\mathbf{x}}_n^-) \quad (4.31)$$

$$\mathbf{K}_n = \mathbf{P}_n^- \mathbf{H}^T (\mathbf{H} \mathbf{P}_n^- \mathbf{H}^T + \mathbf{R})^{-1} \quad (4.32)$$

$$\mathbf{P}_n = (\mathbf{I} - \mathbf{K}_n \mathbf{H}) \mathbf{P}_n^- \quad (4.33)$$

Where \mathbf{H} stands for the *measurement matrix* that relates the state variables to the measurement \mathbf{y}_n . Note that the upper character “^T” denotes a transposed matrix.

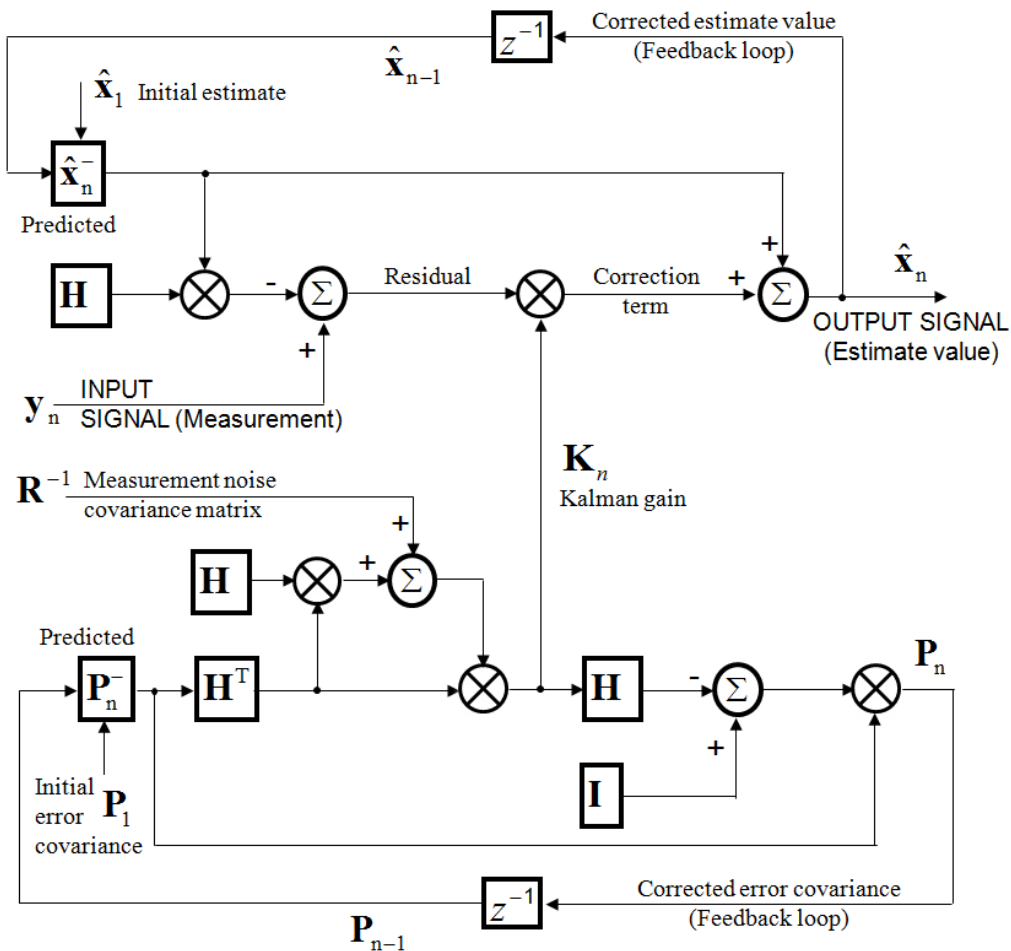


Fig. 4.7 The Kalman filter cycle known also as Predictor-corrector algorithm [14 and 29]

Estimating the measurand

In the following pages, the Kalman filter is derived as a second order algorithm, due to the fact that such a measurement process features two state variables, known as: collected mass (primary), and mass flow rate (secondary). The primary variable is an important element in the estimation process, because in order to deliver an accurate estimate of mass flow rate, it is necessary first to accomplish the same condition for the collected mass. In terms of the algorithm, the Kalman filter has to designate an estimate error covariance matrix, with the aim to optimize the estimation of both state variables [37, 38].

First, it is necessary to define the estimate errors corresponding to each of the two state variables of the measurement process. In this instance, the error denoted as \hat{e} is defined as the difference between the estimate values (\hat{m}_K and \hat{m}_K), and the current state values (\hat{m}_{HF} and \hat{m}_{HF}). Note

that the term *estimate error* is used instead *error*, to underline the fact that there is no absolute certainty in the true measurand value. Therefore,

$$\hat{e}_m = \hat{m}_K - \hat{m}_{HF} \quad (4.34)$$

$$\hat{e}_f = \hat{\dot{m}}_K - \hat{\dot{m}}_{HF} \quad (4.35)$$

As the Kalman filter algorithm implies matricial operations, the estimate error is represented as:

$$\hat{\mathbf{e}} = \begin{bmatrix} \hat{e}_m \\ \hat{e}_f \end{bmatrix} \quad (4.36)$$

Now, in order to use the knowledge of the state variable estimate errors for the accurate estimation of the measurand, the Kalman filter uses the covariance matrix as a statistical measure to realize the degree in which these two state variables change or vary together. From the covariance analysis, three important statistical assumptions of state variable association can be made [39]:

- 1) If the covariance turns out to be positive, then it is inferred that both state variables vary together in the same direction relative to their expected values,
- 2) The covariance is negative, if one of the state variables tends to be above its expected value, meanwhile the second state variable is below its expected value, and
- 3) If the covariance is zero, then the variables are said to be statistically independent.

Hence, the covariance of the two state variables is represented in a matricial form by **Eq. 4.37**, wherein the diagonal of the matrix represents the variance of collected mass and mass flow rate.

$$\mathbf{P} = \begin{bmatrix} \hat{\mathbf{e}} \cdot \hat{\mathbf{e}}^T \\ \hat{e}_m^2 & \hat{e}_m \cdot \hat{e}_f \\ \hat{e}_f \cdot \hat{e}_m & \hat{e}_f^2 \end{bmatrix} \quad (4.37)$$

As for the initial estimate error covariance matrix, this can be obtained by substituting the collected mass $\hat{m}_{HF}(t_1) \cdot t_1$, mass flow rate $\hat{m}_{HF}(t_1)$ at the time step $t_1 > 0$, in addition to reference values m_K and \dot{m}_K , into the estimate errors shown in **Eq. 4.34** and **Eq. 4.35**. On the other hand, at the initial stage of the filtering process, the covariance terms of the matrix are set to 0. The latter is due to the lack of information to set an accurate correlation level at this particular time, as well as giving a more conservative assumption of little or no correlation between the state variables [40]. This is preferred to designating a relatively high covariance, that in return could significantly delay the filter convergence. In any case, the Kalman filter algorithm will predict and correct the variance and covariance terms of the matrix within the following iterations.

$$\mathbf{P}_1 = \begin{bmatrix} \hat{e}_m^2(t_1) & 0 \\ 0 & \hat{e}_f^2(t_1) \end{bmatrix} \quad (4.38)$$

The initial estimate of the primary state (water mass) could be agreed to be equal to zero, assuming that the collection vessel is empty. However, in order to keep the mathematical consistency in terms of the second variable derivative, it is preferred to assignate a small value, such as $\dot{m}_K \cdot t_1$. For the second state variable, it is possible to designate an arbitrary value for the initial mass flow rate. Nevertheless, the usage of the average mass flow rate value given by hydrodynamic force filter (**Eq. 4.24**) turns out to be a good initialization.

$$\hat{x}(t_1) = \dot{m}_K \cdot t_1 \quad (4.39)$$

$$\hat{\dot{x}}(t_1) = \dot{m}_K \quad (4.40)$$

Then, according to **Eq. 4.29**, the predicted (a priori) state estimate can be described as:

$$\begin{aligned} \hat{\mathbf{x}}_n^- &= \mathbf{A} \hat{\mathbf{x}}_{n-1} \\ &= \begin{bmatrix} 1 & t_S \\ 0 & 1 \end{bmatrix} \begin{bmatrix} \hat{m}_K(t_{n-1}) \\ \hat{\dot{m}}_K(t_{n-1}) \end{bmatrix} = \begin{bmatrix} \hat{m}_K(t_{n-1}) + \hat{\dot{m}}_K(t_{n-1}) \cdot t_S \\ \hat{\dot{m}}_K(t_{n-1}) \end{bmatrix} \end{aligned} \quad (4.41)$$

In the current implementation of the Kalman filter, the measurement noise covariance \mathbf{R} (Eq. 4.42) is possible to be estimated, because the user is able to analyze the variance (Eq. 4.43, Eq. 4.44 and Eq. 4.27) from data sets once the measurements are completed (off-line) [36 and 40]. Alternatively, such a standard deviation can be expanded in terms of its measurement confidence interval [41], with the aim to increase the certainty in the estimate values.

$$\mathbf{R} = \begin{bmatrix} \sigma_m^2 \\ \sigma_f^2 \end{bmatrix} \quad (4.42)$$

$$\sigma_m^2 = \sqrt{\frac{1}{N-1} \cdot \sum_{n=1}^N \left(\hat{m}_{HF}(t_n) \cdot t_n - \dot{m}_K \cdot t_n \right)^2} \quad (4.43)$$

$$\sigma_f^2 = \sigma_{HF}^2 \quad (4.44)$$

Now with all the necessary information gathered, it is possible to derive the predicted covariance equation shown in Eq. 4.30 as well as the corrected measurement equations (Eq. 4.31, Eq. 4.32, and Eq. 4.33). Fig. 4.8 illustrates in a scalar form, the estimation process of mass flow rate via Kalman filter. Hence:

Therefore, the *a priori* state error covariance matrix is:

$$\begin{aligned} \mathbf{P}_n &= (\mathbf{A} \mathbf{P}_{n-1} \mathbf{A}^T) = \\ &= \begin{bmatrix} \left(p_{n-1,22} \cdot t_s^2 + (p_{n-1,21} + p_{n-1,12}) \cdot t_s + p_{n-1,11} \right) & \left(p_{n-1,22} \cdot t_s + p_{n-1,12} \right) \\ \left(p_{n-1,22} \cdot t_s + p_{n-1,12} \right) & \left(p_{n-1,22} \right) \end{bmatrix} \\ &= \begin{bmatrix} \bar{p}_{n,11} & \bar{p}_{n,12} \\ \bar{p}_{n,21} & \bar{p}_{n,22} \end{bmatrix} \end{aligned} \quad (4.45)$$

The Kalman gain factor that is defined as:

$$\begin{aligned} \mathbf{K}_n &= \mathbf{P}_n \mathbf{H}^T \left(\mathbf{H} \mathbf{P}_n \mathbf{H}^T + \mathbf{R} \right)^{-1} \\ &= \begin{bmatrix} \bar{p}_{n,11} \cdot \left(\bar{p}_{n,11} + \sigma_m^2 \right)^{-1} \\ \bar{p}_{n,21} \cdot \left(\bar{p}_{n,11} + \sigma_f^2 \right)^{-1} \end{bmatrix} = \begin{bmatrix} k_{n,11} \\ k_{n,21} \end{bmatrix} \end{aligned} \quad (4.46)$$

The posteriori state error covariance matrix:

$$\begin{aligned} \mathbf{P}_n &= (\mathbf{I} - \mathbf{K}_n \mathbf{H}) \mathbf{P}_n^- \\ &= \begin{bmatrix} (1 - k_{n11}) \cdot p_{n11}^- & (1 - k_{n11}) \cdot p_{n12}^- \\ (p_{n21}^- - k_{n21} \cdot p_{n11}^-) & (p_{n22}^- - k_{n21} \cdot p_{n12}^-) \end{bmatrix} \end{aligned} \quad (4.47)$$

And the *a posteriori* state estimate is then:

$$\begin{aligned} \hat{\mathbf{x}}_n &= \hat{\mathbf{x}}_n^- + \mathbf{K}_n (\mathbf{y}_n - \mathbf{H} \hat{\mathbf{x}}_n^-) \\ &= \begin{bmatrix} \hat{m}_K(t_{n-1}) \\ \hat{m}_K(t_{n-1}) \end{bmatrix} + \begin{bmatrix} k_{n11} \\ k_{n21} \end{bmatrix} \left(\hat{m}_{HF}(t_n) - [1 \ 0] \begin{bmatrix} \hat{m}_K(t_{n-1}) \\ \hat{m}_K(t_{n-1}) \end{bmatrix} \right) \\ &= \begin{bmatrix} \hat{m}_K(t_{n-1}) + k_{n11} \cdot (\hat{m}_{HF}(t_n) - \hat{m}_K(t_{n-1})) \\ \hat{m}_K(t_{n-1}) + k_{n21} \cdot (\hat{m}_{HF}(t_n) - \hat{m}_K(t_{n-1})) \end{bmatrix} \end{aligned} \quad (4.48)$$

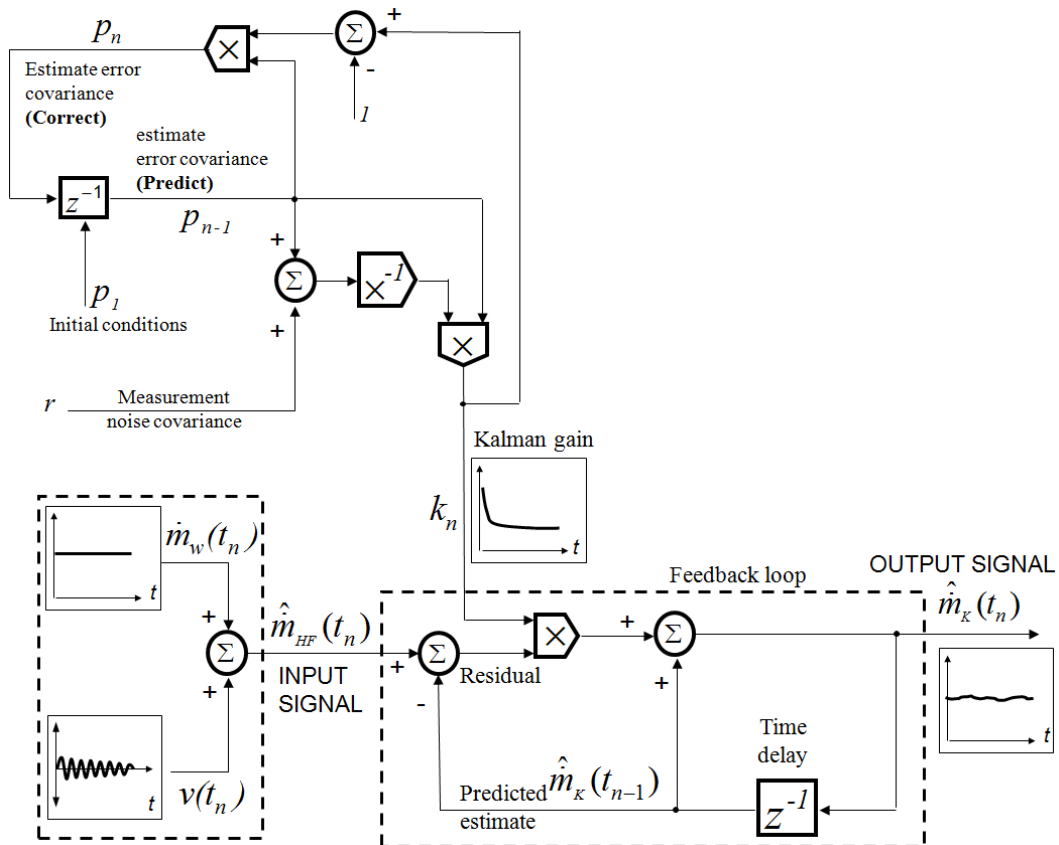


Fig. 4.8 Block diagram describing the estimation of mass flow rate via Kalman filter (scalar form representation)

4.3 Summary

In this chapter, an inverse-problem approach with two algorithms has been presented, in order to estimate the time-varying mass flow rate. The first algorithm is in charge of filtering out the negative influence of the hydrodynamic and the buoyancy force variables have upon the measurand. In order to do this, the filter uses the balance signal response as input signal, in addition to an analytical model to estimate the magnitude of such unwanted forces, based on the physical properties of the fluid, the geometry and dimensions of the system, and time. The second algorithm is a filter, which attenuates the measurement noise still embedded in the signal coming from the first filter. In this research work, the measurement noise is assumed to be greatly caused (but not entirely) by the fluid force-induced oscillatory motion of the weighing system. In this case, three data processing algorithms (central moving average filter, least-mean-Square adaptive filter, and linear Kalman filter) have been proposed for the treatment of corrupted signal. The central moving average filter that smoothes out the trend of the measurand by using a series of data subsets averages, which are defined by a number of measurement data before and after the current time step t_n . The Least-Mean-Square adaptive filter adapts to the input signal by iteratively tuning its parameters (filter coefficients), in order to deliver an estimate measurand value with a minimized feedback error signal. The linear Kalman filter combines the knowledge of the weighing system output signal (i.e. variance) and its recursive method to produce a mass flow rate estimate value. In the following **Chapter 5**, the performance of the proposed measurement noise filters will be numerically assessed in terms of their stabilization time, accuracy, precision, and their ability of reproducing consistent results at different stationary and quasi-steady mass flow rates.

5. Numerical determination of mass flow rate and the response of the dynamic weighing liquid flow standard

The dynamic simulation of the weighing system is the basis for understanding or exemplifying, which fluid and mechanical phenomena are taking place, finding out the sources of measurement noise, the unwanted variables involved, and realizing which variables are the most relevant in the measuring process. Furthermore, a comparison between the numerical and the real process measurements is carried out, with the aim to validate the theoretical background of the measurement process model as well as the mass flow rate calculation via dynamic-weighing.

The numerical analysis shown in this document firstly evaluates the system's input signal, and its frequency response. The next step comprises the simulation of the continuous time system response (**Chapter 3**), followed by the oscillatory signal attenuation of the low pass filter, and the discrete time representation of the output signal. The latter is compared with the balance readout, in order to see the level of agreement. Afterwards, the effectiveness of the hydrodynamic force filter is numerically evaluated, so then its contribution to the measurement accuracy can be quantified.

The second part concerning to data processing techniques, addresses the performance of three proposed measurement noise filters. The assessment is focused on their capabilities to enhance the measurement accuracy and precision as well. Finally, the numerical analysis evaluates the role that the data sampling frequency as well as the low-pass-filter cutoff frequency, play upon the measurand estimates; and it suggests a possible way to re-enhance the accuracy. **Fig. 5.1** summarizes in a block diagram all the recalled steps for the estimation of the mass flow rate via dynamic weighing. As a reminder (**Chapter 3**), $F_q(t)$ denotes the fluid forces caused by the vortex axial force inside the collection vessel and the oscillatory force of the water waves. In this numerical analysis, $F_q(t)$ is not taken into account, because none equation has been derived to describe their behavior. Nevertheless, it is reminder that such forces have to be considered in subsequent investigations, so that a more thorough system model can be achieved.

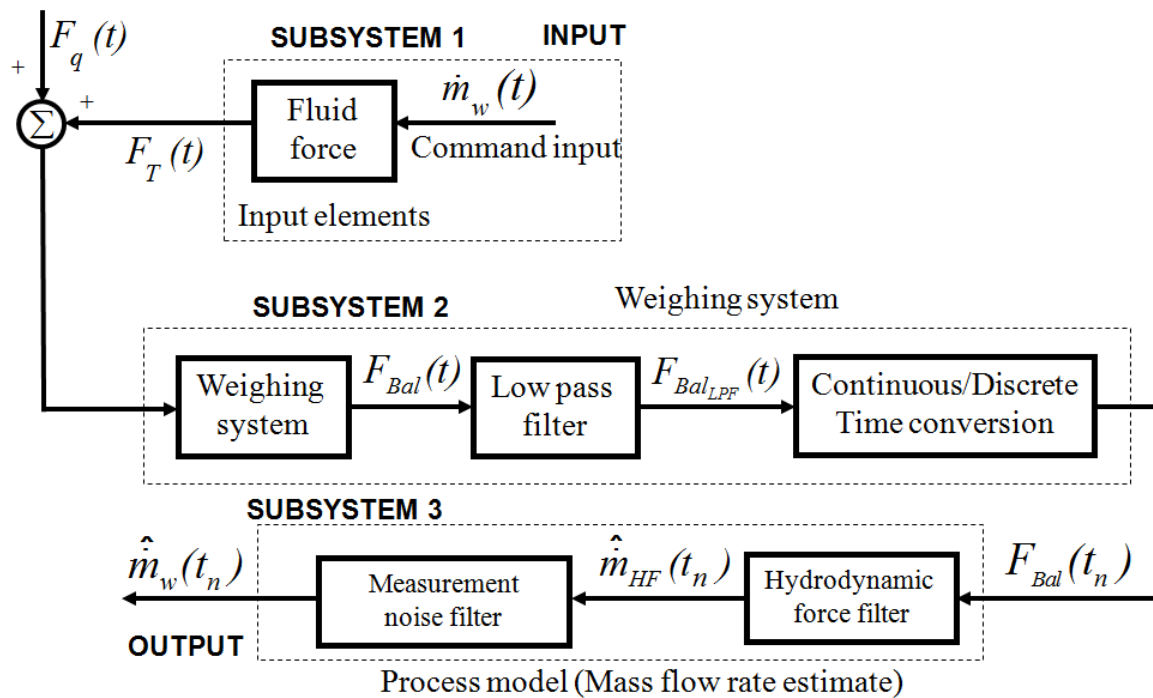


Fig. 5.1 Block diagram describing the steps made for the simulation of the mass flow rate estimate via dynamic weighing

5.1 Fluid forces acting upon the weighing system (input signal)

As recalled, the input signal of the measurement process does not comprise a single physical variable, but a summation of three predominant forces, which in part, dictate the dynamic behavior of the system. In this instance, the simulations of time-varying fluid force magnitudes are exemplified at the lowest and highest flow rates attained by the dynamic weighing liquid flow primary standard prototype (**Fig. 5.2**), which is described in full detail in **Chapter 6**. Additionally, the vessel is assumed to be empty, whereby the initial collected water mass is zero.

In regards to the hydrodynamic force $F_d(t)$ shown in **Fig. 5.2**, this exhibits a proportional increment in its magnitude in relation to the operational mass flow rate, and an inverse response to the level rise of the collected water.

As for the collected water mass force $F_m(t)$, it can be described as a ramp-function like variable, wherein its magnitude is the product of its slope (the current mass flow rate), the time t of the measurement, and its initial value agreed to be zero. As a remark, the level of filling in these simulations is carried out at 80% of the vessel nominal capacity (8 L).

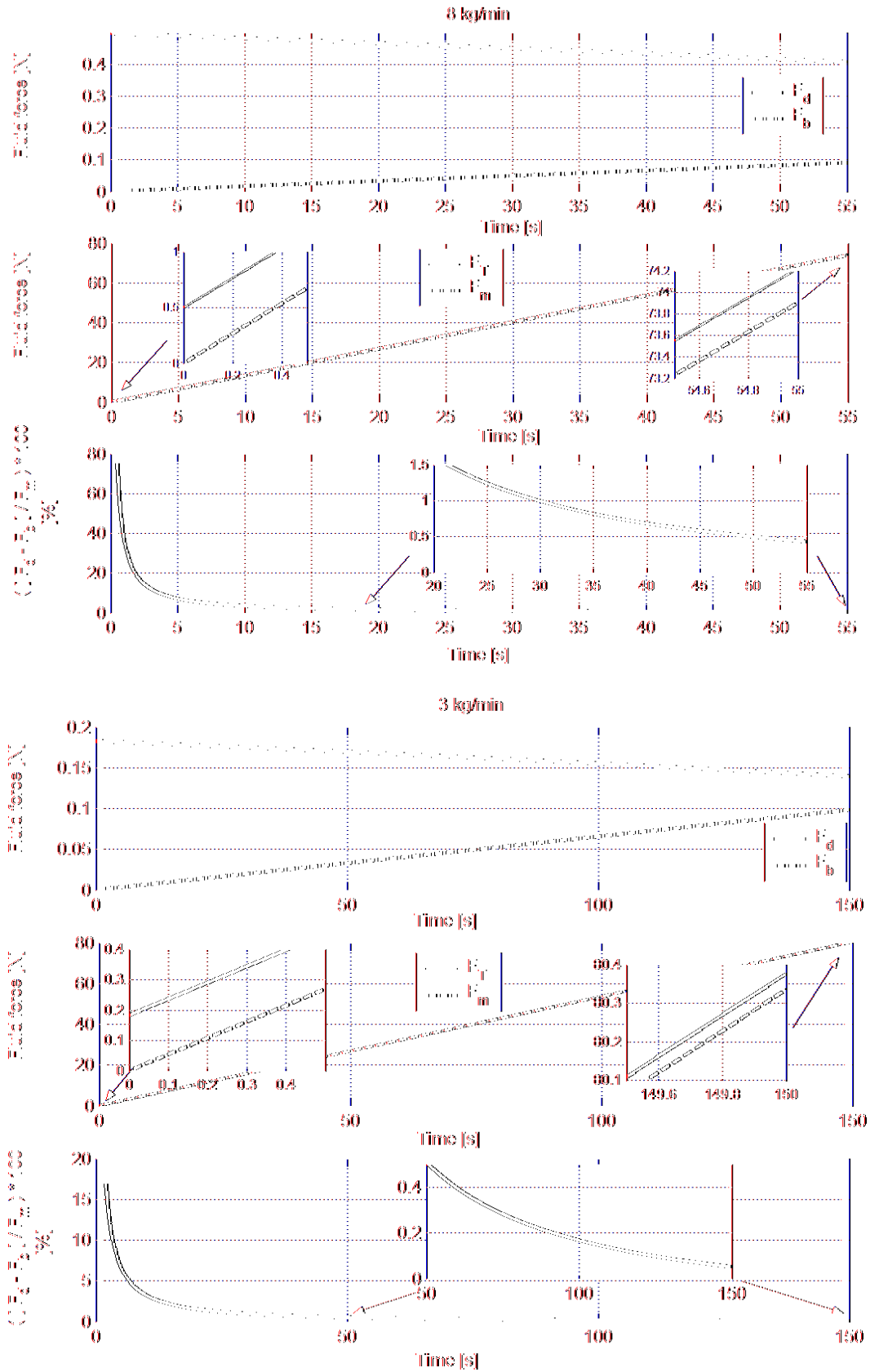


Fig. 5.2 Fluid forces acting upon the weighing system (Input signals)

It is worth to highlight that, the time-varying mass flow rate data used to carry out all simulations are extracted from the experimental data given by a flowmeter used as a reference standard. This is intentionally done, with the aim to approximate the real conditions undergone by the physical system (**Chapter 6**).

Concerning to the buoyancy force $F_b(t)$, this acts as a function of the water mass and in an upward direction, therefore its response is seen in **Fig. 5.2** as a positive slope. Furthermore, in a dynamic weighing condition, the buoyancy force is by no means influenced by the inertial mass force, but only by the air density, water density, the local acceleration of gravity, and the increasing collected water mass. For the sake of simplification, the density of air and water is assumed to be constant at a reference temperature of 20°C.

The summation of these forces yields what is called, the total fluid force $F_T(t)$. In **Fig. 5.2**, such a variable is intentionally compared with the collected mass force, in order to show their difference in terms of magnitude. As expected, the magnitude difference (or slope shift) between $F_T(t)$ and $F_m(t)$ becomes more significant as the mass flow rate increases.

The two lower graphs at 3 kg/min and 8 kg/min in **Fig. 5.2** also illustrate the magnitude ratio between the hydrodynamic force - buoyancy force ($F_d(t) - F_b(t)$), and the collected mass force, $F_m(t)$. Such a ratio helps to visualize the considerable systematic error involved, when simply considering the balance output response as an estimate mass to calculate the current flow rate. Additionally, **Fig. 5.2** shows that the influence of $F_d(t)$ and $F_b(t)$ are quite strong during the first 1/3 of the filling process, and especially at the highest flow rate. Thereafter, such a ratio curve exhibits an exponential decay of the hydrodynamic and buoyancy force influence upon the measurement process, which can be as low as 0,1% at 3 kg/min.

5.2 Frequency response of the weighing system

The aim of this task is to apply a Fast Fourier Transform (FFT) in order to find out the balance frequency response upon its weighing axis (z axis), and how this behaves along the measuring time. This kind of information is important to be known because in practice, the weighing system features a low pass filter, which uses such frequency information, in order to define the attenuation level of the output signal. As understood, the low pass filter is an algorithm, which

balance manufacturers commonly use, with the purpose to diminish the amplitude of the system oscillatory force from the output signal. The latter is an unwanted signal considered as measurement noise. In the simulation work, the characterized balance oscillatory frequency will be used by the low pass filter of the numerical model (**Chapter 3**), as an attempt to reproduce the real attenuated output signal displayed by the balance readout.

The balance frequency characterization consists of applying a non-contact laser displacement sensor (LDS) [1] to measure the oscillatory displacement of the balance platform at two different planes, as depicted in **Fig. 5.3**. The reason for measuring at two different planes (XZ and YZ) is in order to characterize the eigenfrequencies generated by the translational and angular motion of the balance platform during the measurement process, and thus, to identify which one corresponds to the z axis oscillatory motion [2]. Note that, if this eigenfrequency characterization were carried out at one plane, the result might possibly lead to an overlooking of an eigenfrequency, including the one belonging to the z axis, which could be only detected at one particular plane. In addition to the non-contact laser displacement sensor, an accelerometer is also mounted upon the balance platform and oriented along the z axis, with the goal to corroborate the results from the first method (LDS), regarding the weighing axis frequency identification.

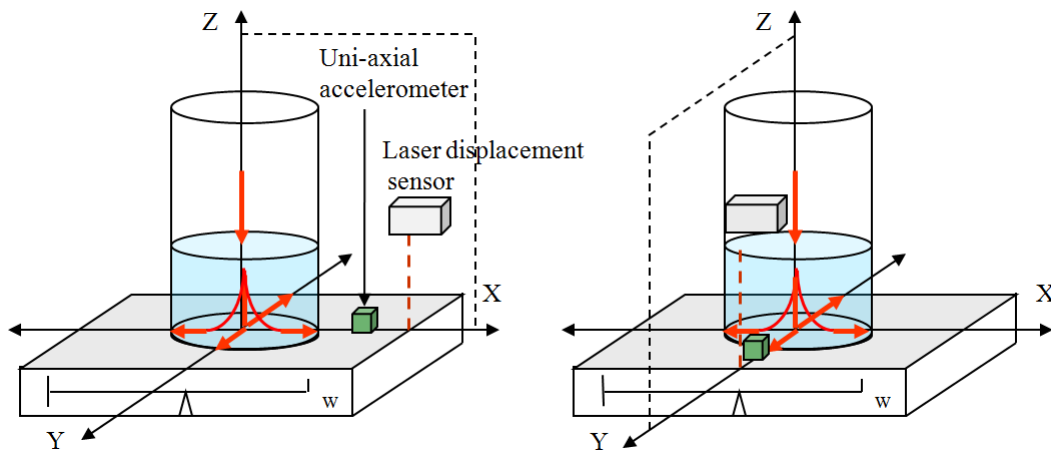


Fig. 5.3 Setup of the weighing system frequency characterization test

After carrying out the experimental tests, the results revealed three frequency spectra that are present in a bandwidth of 24 Hz, wherein the lower and upper limits are respectively, 9 Hz and 33 Hz. The explanation to the frequency response decay and magnitude observed in **Fig. 5.4**

(regardless the motion axis) is predominantly based upon the stiffness coefficient of the weighing system, and the continuous increment of the system mass caused by the collected water.

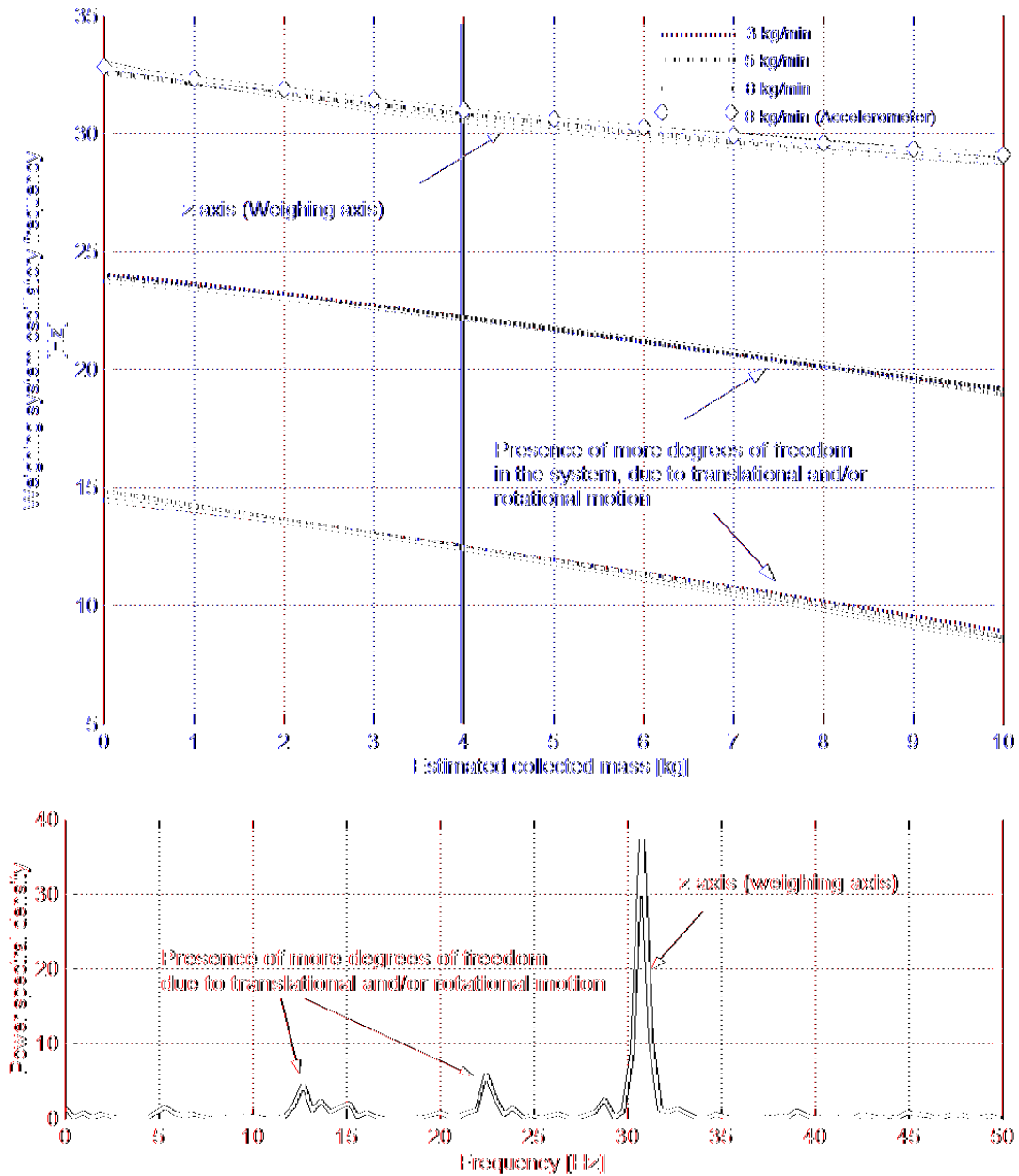


Fig. 5.4 Three frequency spectra taking place during the filling process at 3, 5 and 8 kg/min and their power spectral density at an estimated collected mass of 4 kg

As depicted in Fig. 5.4, such a frequency response is agreed to behave nearly in the same manner, even if the weighing system operates at a low, medium, or large mass flow rate.

Moreover, after comparing the results obtained by the non-contact displacement sensor and the uniaxial accelerometer (**Fig. 5.4**), it points out that the eigenfrequency of the weighing axis (z axis) is ranging between 33 Hz and 29 Hz, because of the near overlapping between the two different measurement approaches. As a remark, the z axis eigenfrequency was detected at both planes (XZ and YZ), and with a relatively higher amplitude of its spectrum, in comparison to the other two eigenfrequencies (**Fig. 5.4**).

Note that the term *estimated collected water mass* in **Fig. 5.4** is used, because the system frequency characterization was carried out dynamically [3]. This means, that the eigenfrequencies were tracked during the collection process, and the mass had to be calculated as an estimate by using **Eq. 5.1** (see **Chapter 4**) and **Eq. 5.2**.

$$\left[\frac{I}{\rho_w^2(\vartheta_w) \cdot A_n^2} \right] \cdot \hat{m}_{HF}^4(t_n) + \left[2 \cdot g \cdot \hat{h}_i(z) - g^2 \cdot \left(1 - \frac{\rho_A(\vartheta_A)}{\rho_w(\vartheta_w)} \right)^2 \cdot t_n^2 \right] \cdot \hat{m}_{HF}^2(t_n) + \dots \quad (5.1)$$

$$\dots + \left[2 \cdot F_{Bal}(t_n) \cdot g \cdot \left(1 - \frac{\rho_A(\vartheta_A)}{\rho_w(\vartheta_w)} \right) \cdot t_n \right] \cdot \hat{m}_{HF}(t_n) - F_{Bal}^2(t_n) = 0$$

$$\hat{m}_{HF}(t_n) = \hat{m}_{HF}(t_n) \cdot t_n \quad (5.2)$$

Another important conclusion made after analyzing the system's mechanical frequency response is the presence of the oscillatory transverse forces upon the x axis and y axis (**Fig. 5.3** and **Fig. 5.4**), produced by the radial spread of the submerged water jet [4]. This would indicate that the system is subjected to move in more than one degree of freedom (rotational and/or translational), and that not only the system's mass but also the system's moment of inertia around the x and y axes, play a role in the dynamic response of the balance.

An additional assumption extracted from the results in **Fig. 5.4** is the fact that at least two oscillatory transverse forces are superimposed in the balance output signal [5]. Eventually, their magnitudes are in principle much smaller, because as illustrated in **Fig. 5.3** and **Fig. 5.4**, the main driven force is acting upon the normal axis (z axis). On the other hand, from the point of view of the balance sensing element, this will be able to measure exclusively (theoretically) the force oriented upon the weighing axis (z axis). However, due to its inherent transverse sensitivity [6], a small residual force (even negligible in some cases) from the flow-induced radial forces

will be measured and displayed. The impact of the transverse sensitivity upon the balance readout is mainly a function of the particular mechanical design of a weighing sensing element (cell), the mechanical coupling between balance weighing platform and its cell, the magnitude of the radial fluid forces, the balance positioning control system [7], the internal low pass filter and the data sampling rate of the output signal. This characteristic of the system can be named as a *mechanical crosstalk effect*, due to the fact that an unwanted signal(s), in the case of radial forces, can be superimposed in the balance readout.

In this research work, one of the main goals was to find out the main phenomena (mechanical and fluid aspects) that greatly affect the system, and an accurate estimation of mass flow rate. For this reason, the system is analyzed with respect to the axis, wherein the main acting fluid force and balance dynamic response is taking place, the z axis. Nevertheless, the mechanical cross talk effect is intentionally mentioned in this chapter, as a hint for a future investigation related to a more thorough understanding and accuracy enhancement of a dynamic weighing liquid flow primary standard (Multi-axis weighing system model). Eventually, this further investigation will have to include the identification task of the other two eigenfrequencies (**Fig. 5.4**), with their corresponding system's degrees of freedom.

5.3 Continuous time and discrete time response of the balance

Fig. 5.5 shows the balance simulated response during the filling process. As shown in the upper graph of **Fig. 5.5**, the balance output response is depicted in its continuous time form. According to the numerical calculations, the output signal follows the path of the total fluid force, in addition to an oscillatory signal caused by the balance reacting dynamic response. The graphs depict a nominal undesired oscillatory signal of 33 Hz (at the initial stage of the process), and with a maximum amplitude of $\pm 0,5$ N at 8 kg/min, and $\pm 0,2$ N at 3 kg/min.

According to the weighing system signal conditioning, the continuous time balance response must undergo a decrement in its oscillatory amplitude. Hence, a low pass filter uses the frequency response upon the z axis to define the attenuation level of the signal [8]. In this instance, the eigenfrequency ranging from 33 Hz to 29 Hz is out of the low pass filter pass band, which features a cutoff frequency of 10 Hz [8].

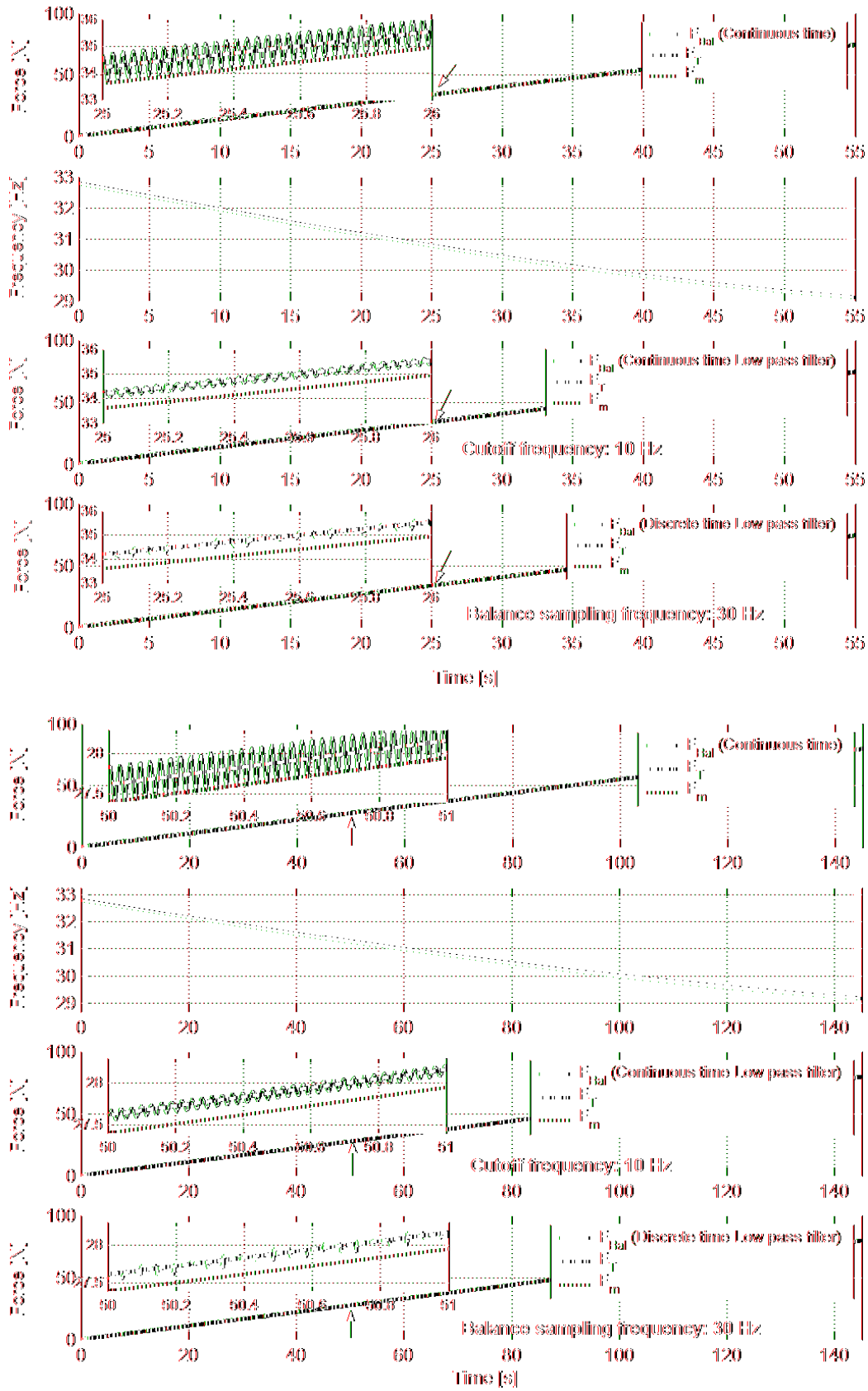


Fig. 5.5 Simulation of the continuous and discrete time dynamic response of the balance at 8 kg/min (upper graph) and 3 kg/min (lower graph)

Moreover, the numerical outcome given by the low pass filter depicts a continuous time signal that has been attenuated from -11 db to -9 db, due to the eigenfrequency decrement along the filling process, and with a signal phase shift between 73° and 71° , as shown in **Fig. 5.6**. Herein, the simulated original signal has continuously changed, not only in terms of its oscillatory amplitude, but also in relation to its frequency and phase [9].

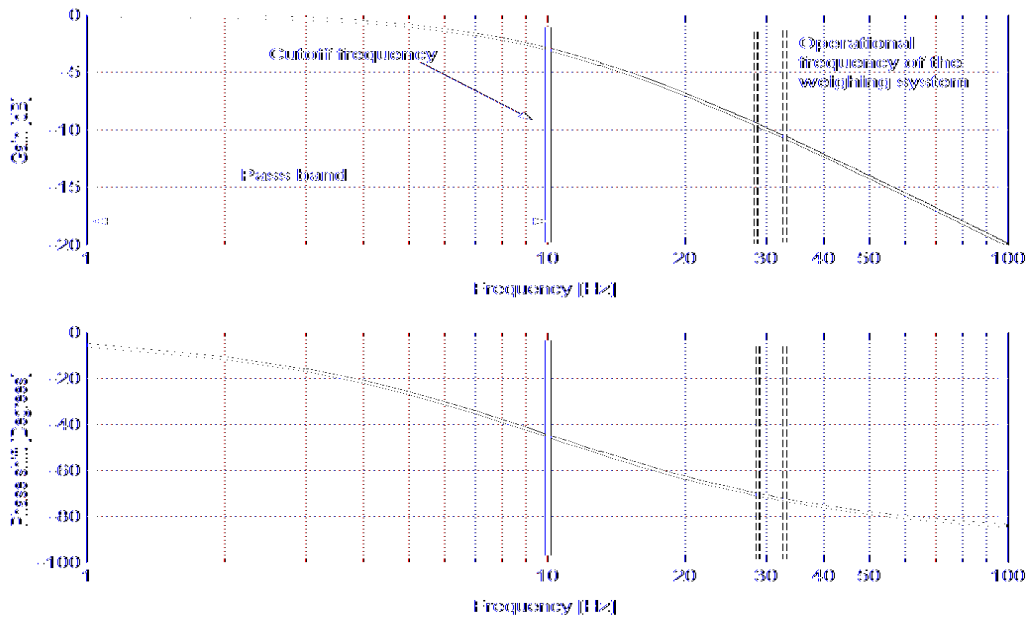


Fig. 5.6 Low pass filter gain and phase shift of the weighing system model

The last step before displaying the measured reacting force is to convert it into a discrete time form. In this case, the designated data sampling frequency of the balance is 30 Hz [8] observed in **Fig. 5.5**, the original continuous time balance output signal has experienced a serious aliasing effect [10] after passing through the low pass filter, and the discrete time conversion. Nevertheless, the signal is still valuable because it continues following the path (or slope change) of the total fluid force $F_T(t)$. As mentioned in **Chapter 4**, the total fluid force is one of the key variables used in the process model (Hydrodynamic force filter) to calculate the mass flow rate estimates.

Finally, the simulated output response of the weighing system is compared with its experimental counterpart, the balance readout. For instance, **Fig. 5.7** shows the start point of the measurement process at 8 kg/min, wherein the experimental data depict an initial signal overshoot, greatly

caused by the first shock of the water jet upon the vessel [11]. This overshoot response depicted in **Fig. 5.7** was not replicated by the simulation, nevertheless, the initial step and the subsequent ramp response agree with the experimental part. Furthermore, the simulated signal in both mass flow rates (8 kg/min and 3 kg/min) yields a discrete-time oscillatory response, which is fairly similar in magnitude, with the one measured experimentally.

As mentioned, the numerical model uses the mass flow data provided by the PTB traceable transfer standard (flowmeter), with the aim to replicate as close as possible the quasi-steady and quasi-uniform mass flow rate.

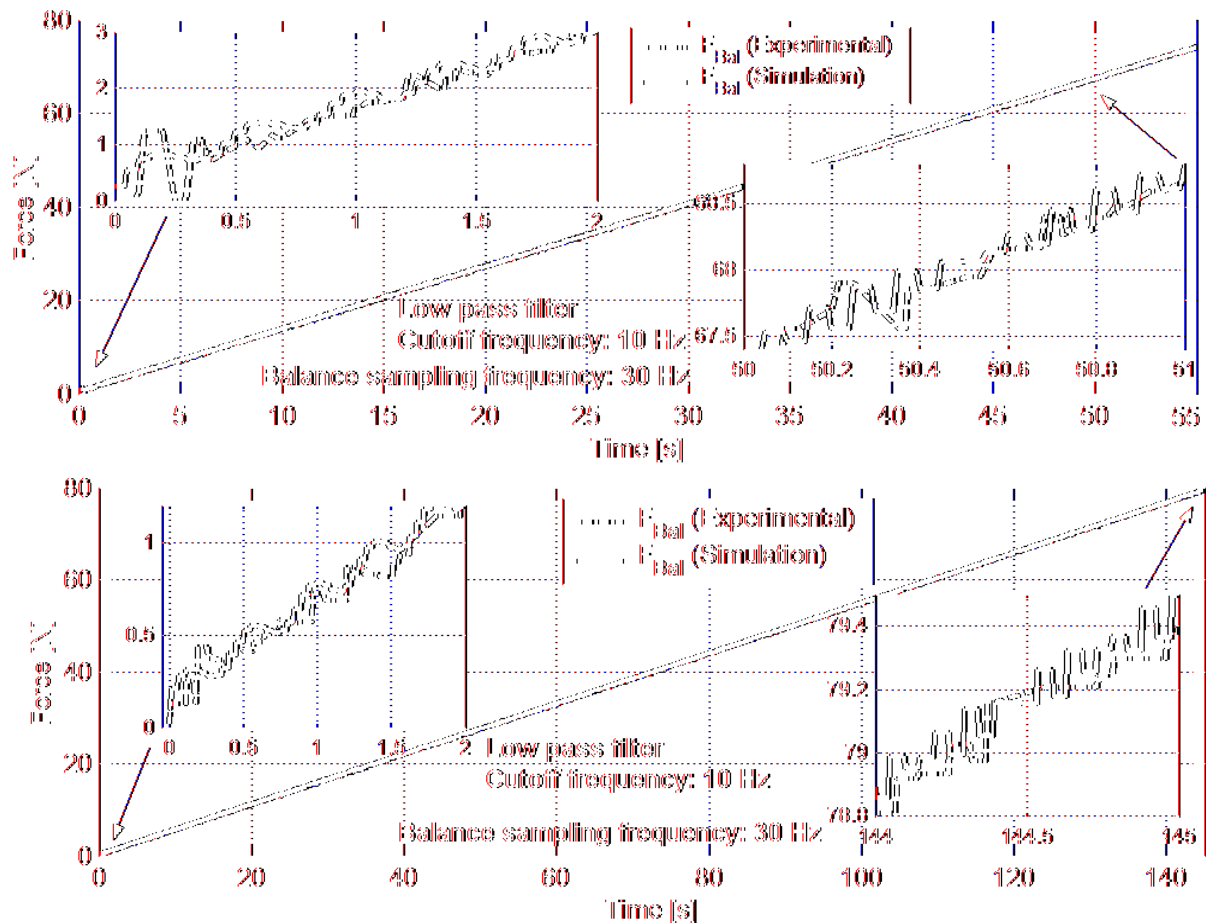


Fig. 5.7 Numerical and experimental comparison of the balance weighing axis eigenfrequency and its discrete-time output signal response at 8 kg/min (upper graph) and 3 kg/min (lower graph)

5.4 Hydrodynamic force filter

In this instance, the hydrodynamic force filter is applied at three different mass flow rates, with the goal to see its effectiveness in approximating to the average value of the true measurand, or in other words, improving the measurement accuracy.

At 8 kg/min, two different calculation approaches are compared. One is the mass flow rate obtained by directly using the force measurements given by balance readout, time, and the local acceleration of gravity (**Eq. 4.1**). The result from this estimation method delivers a series of measurements that are quite spread along its average value ($\pm 0,2$ kg/min at 5s, or a maximum relative error of $\pm 2,43\%$ with respect to its average value), but they gradually decrease until $\pm 0,25\%$ at 55s. As illustrated in **Fig. 5.8**, the difference between the average value obtained by this approach and the average reference mass flow rate is 0,24%.

The second approach depicted in **Fig. 5.8** is the outcome given by the Hydrodynamic force filter, already described in **Chapter 4**. In regards to its performance, the data spread is similar to the first approach (Balance readout), due to the fact that such a filter treats only the accuracy of the whole measurement data, but not their precision. That is exactly the task of the measurement noise filter, in which their numerical results are presented in the next section. According to the attained results, the average value of hydrodynamic force filter output signal is able to get really closer to the true measurand. The percent relative error found at this flow rate was 0,01%.

A similar output signal response takes place at the mid flow (5 kg/min), wherein the scattered data at the initial stage of the measurement (10s) exhibit a percent relative error of 1,35%. As demonstrated from the highest and mid flow rate, the degree of data scattering is proportional to the operational mass flow rate. On the other hand, when comparing the outcome given by the two measurement approaches, it is clear that the hydrodynamic force filter enhances the accuracy of the mass flow rate estimate values about 5 times in relation to its counterpart.

The results at the lowest flow rate can be seen as an affirmation of the two filters response, wherein the dispersion of data is lower (i.e. 0,67% relative error at 20s) as the mass flow rate decreases. For a detailed explanation of this process condition, see **Section 5.1** (specifically **Fig. 5.2**), regarding to the fluid forces acting upon the weighing system.

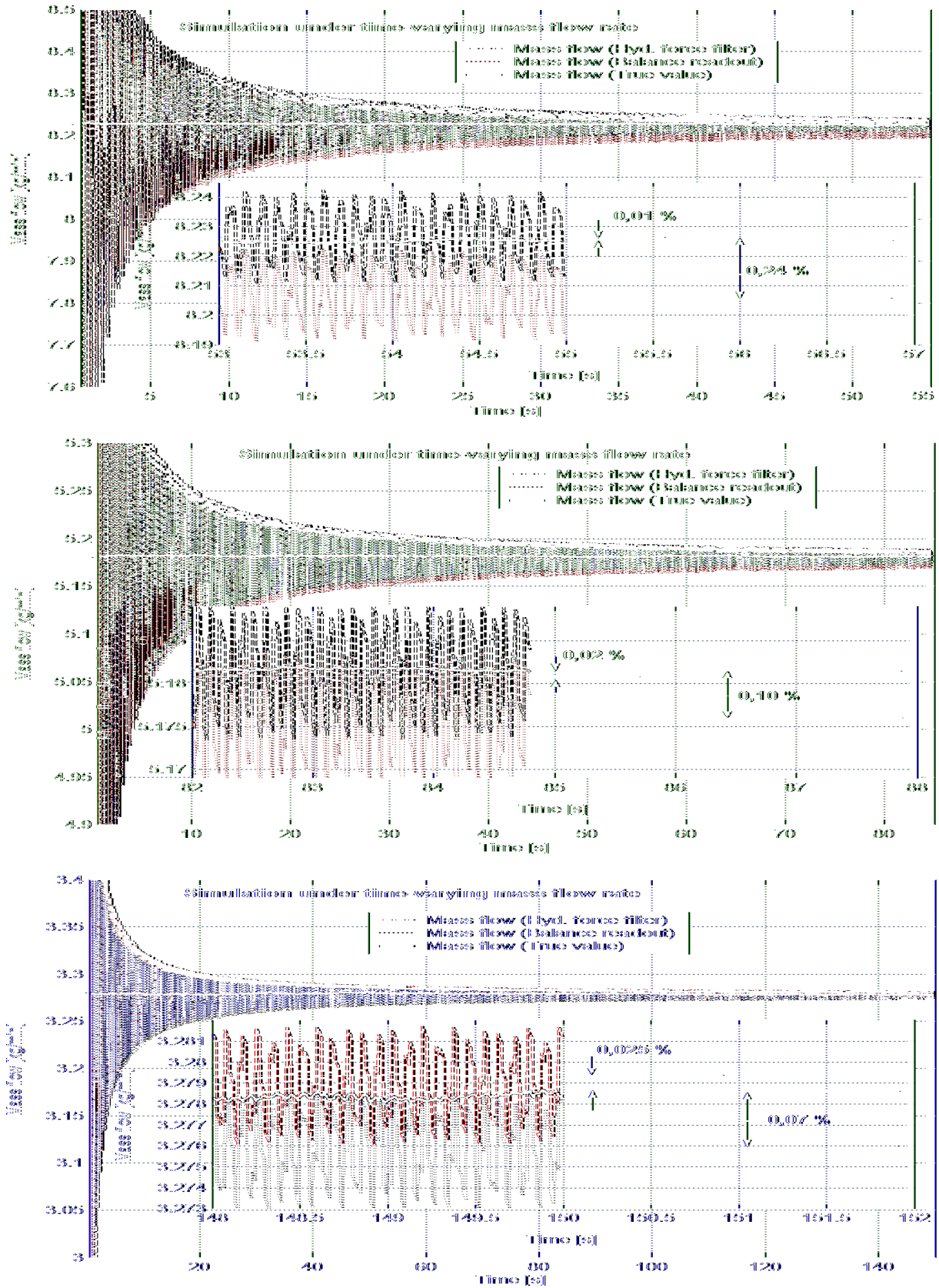


Fig. 5.8 Response of hydrodynamic force filter and its effect upon the measurement accuracy enhancement at 8, 5 and 3 kg/min

5.5 Proposed measurement noise filters

5.5.1 Central moving average filter

Fig. 5.9 shows the measurand tracking performance of the central moving average filter at the highest mass flow rate (8 kg/min). In this figure, the results show that 23 of 28 estimating values are moving along the average mass flow rate value (8,227 kg/min), and overlapping several times the true time-varying mass flow rate. As a remark, the number of samples used to calculate each of the estimate points was 490 samples.

A particular behavior observed from this filter output is that the estimate values are barely following the path of the true mass flow rate, especially at the second half of the collection time. However, this apparent limitation is compensated by the fact that the error band of the estimate values with respect to the true measurand is in the order of $\pm 0,025\%$.

At 5 kg/min, the central moving average filter converges after 12.5s, wherein 25 of 30 estimate values are within an error band of $\pm 0,02\%$, with relation to the true time-varying mass flow rate. In this instance, the central moving average filter is able to only coincide with the average of the measurand, but also to carry out a better tracking of the transient flow response.

With regard to the lowest mass flow rate, the central moving average took about 1/10 of the measurement time to stabilize, and thus getting 54 of 58 estimate values within an error band of $\pm 0,03\%$. Furthermore, it is worth to observe in **Fig. 5.9**, that despite the non-exact estimation of the central moving average, it follows the ascending and descending path of the time-varying mass flow rate.

One common characteristic found out after analyzing the response of the central moving average (at three different mass flow rates) is: the overshoot response appearing at the initial stage of the filter estimation process, which seems to have a strong correlation with the large measurement variance (Hydrodynamic force filter output signal), originated by the dynamic mechanical response of the weighing system. Moreover, the settling time of 12.5s was consistently repeated at the three different flow rates, suggesting that this behavior might be independent of the measurement data, but related to the filter algorithm and its parameters.

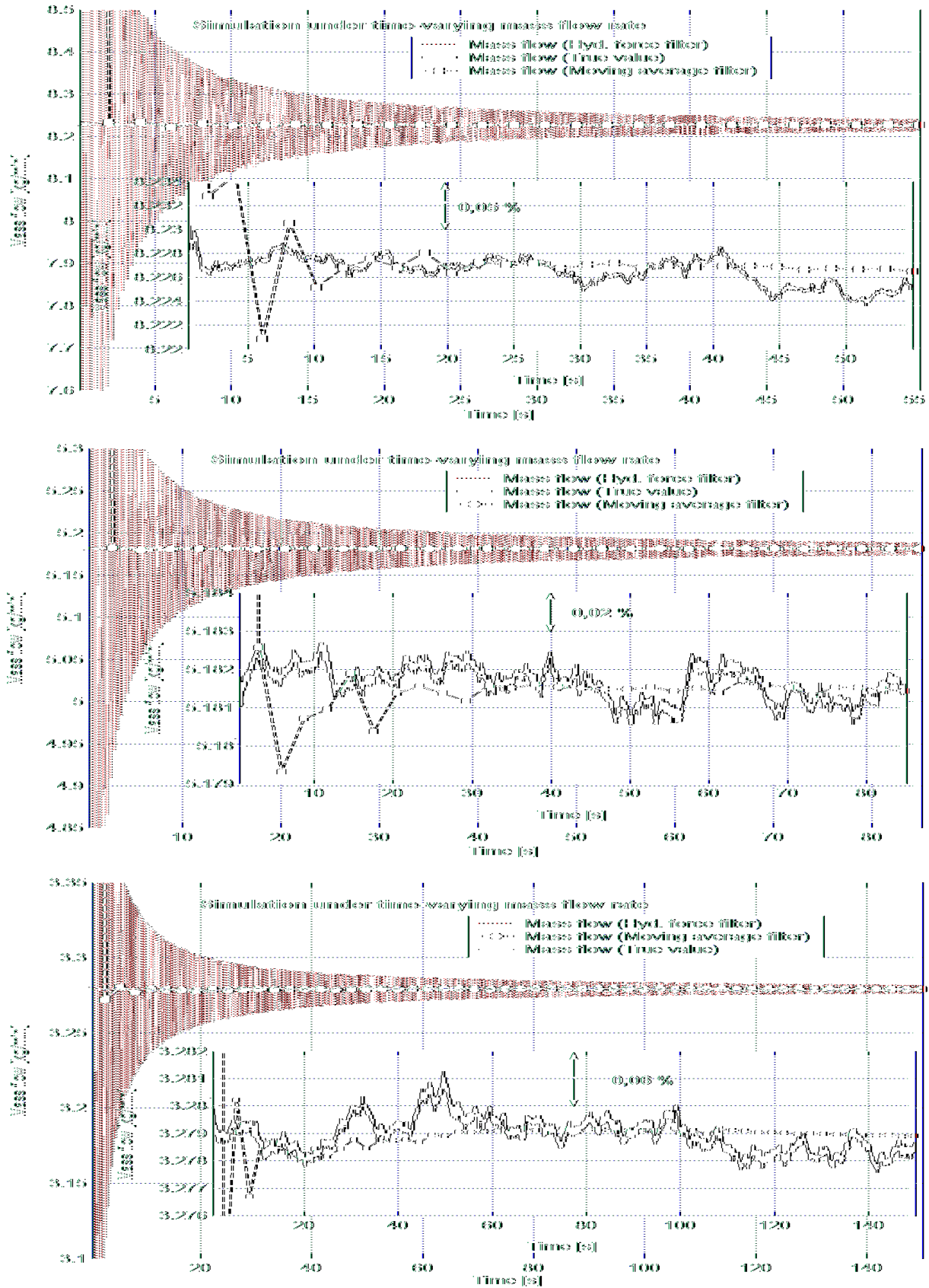


Fig. 5.9 Performance of the central moving average filter at 8, 5 and 3 kg/min

5.5.2 Least-Mean-Square adaptive filter

At the highest flow (8 kg/min), the adaptive filter presents an initial response delay of 2,5s (**Fig. 5.10**), caused by the decorrelation of its input signal (**Chapter 4, Section 4.2.2**), and the number of filter coefficients (500) used to minimize the measurement noise. On the other hand, the adaptive filter uses as an initial estimate, the average mass flow rate magnitude yield by the hydrodynamic force filter, which according to **Fig. 5.10** turns out to have an accuracy of approximately 0,01%.

During the estimation process, the filter takes approximately 1/3 of the total measuring time (20s) to smoothly reach an estimate within $\pm 0,05\%$. As shown in **Fig. 5.10**, the non-overshoot convergence response of the filter denotes a stable and reliable estimation process, which is associated with the number of filter coefficients in use, and the designated stability fraction of the signal error (**Chapter 4, Section 4.2.2**). Finally, the outcome given by the adaptive filter at 8 kg/min yields a set of 8750 estimate values.

As for the measurements carried out at 5 kg/min, the adaptive filter takes also 1/3 of the nominal measuring time to converge, within $\pm 0,04\%$, in relation to the average mass flow rate (5.1815 kg/min). After the second half of the filling process, some of the estimate values are overlapping and keeping a good tracking of the true measurand; especially between the time 50s and 80s. According to the obtained results, the number of estimates after the filter stabilizes is approximately 13750.

Concerning to the lowest flow, **Fig. 5.10** points out that the adaptive filter required about 1/4 of the total measuring time to stabilize with a non-overshoot response. After the first half of the process time, the adaptive filter was able to obtain about 25000 estimates that mostly follow the average mass flow rate of 3,279 kg/min, within a band of $\pm 0,03\%$.

The adaptive filter as well as the moving average (**Fig. 5.9** and **Fig. 5.10**) seems to be affected by the influence of the relatively large measurement noise taking place at the first 1/3 of the process time. One main reason of such a common behavior is that both algorithms utilize a weighted sum, in order to determine their estimate values. In other words, the estimates at the initial part of the process are subjected to deliver more inaccurate values, because of the large measurement variance, and the low magnitude of its statistical weight (reliability).

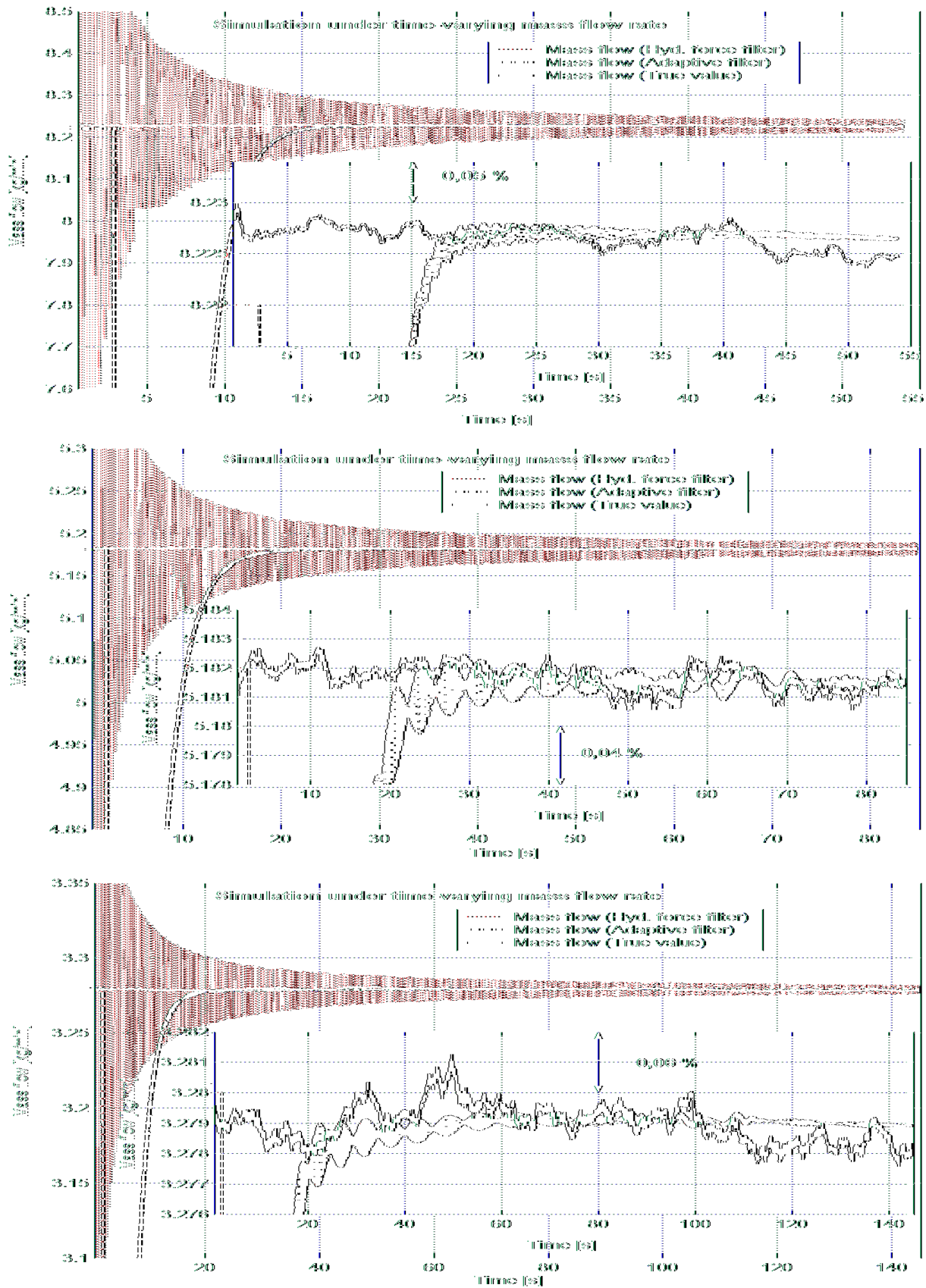


Fig. 5.10 Performance of the Least-Mean-Square adaptive filter at 8, 5 and 3 kg/min

5.5.3 Linear Kalman filter

At 8 kg/min, the Kalman filter rapidly approaches to the true time-varying mass flow rate. The largest difference found between both measurement data was 0,1% during the first second of the estimation process (Fig. 5.11). A particular characteristic observed in the Kalman filter response is that besides following the quasi-steady mass flow rate, its scattered data serve as a band that covers the measurand all along the measuring time. The same type of response occurs for the two following flow rates at 5 kg/min and 3 kg/min. From this numerical test, the Kalman filter was able to perform an approximate of 11250 accurate estimates after 10s.

In relation to the mid flow, the estimate values as well as the true value were very relative more uniform through the measuring time than the outcome data at 8 kg/min and 3 kg/min. In this instance, the estimate data are spread in a range of $\pm 0,02\%$ after 30s. Moreover, as shown in this graph and the one at 3 kg/min, the Kalman filter demonstrates its ability to rapidly minimize the variance in its estimate error, as well as attenuating the large amplitude measurement noise during the initialization phase.

At 3 kg/min, the reference measurements exhibit a clear decrement of 0,03% with respect to its initial value. However, this process condition does not represent a major problem to the Kalman filter algorithm, as it is capable to follow the same flow trend with a maximum relative difference of only 0,02% at 50s.

The average mass flow rate (hydrodynamic force filter output signal) was used not only by the adaptive filter algorithm, but also by the Kalman filter to set its initial estimate. Hence, as a result, the estimate values can converge the reference data with less number of iterations. As recalled, the last statement is applicable, because the process is intended to be performed at a steady flow condition. Furthermore, when comparing the performance of the three proposed filter, it is concluded that the Kalman filter delivers the largest number of estimate data with the lowest relative error.

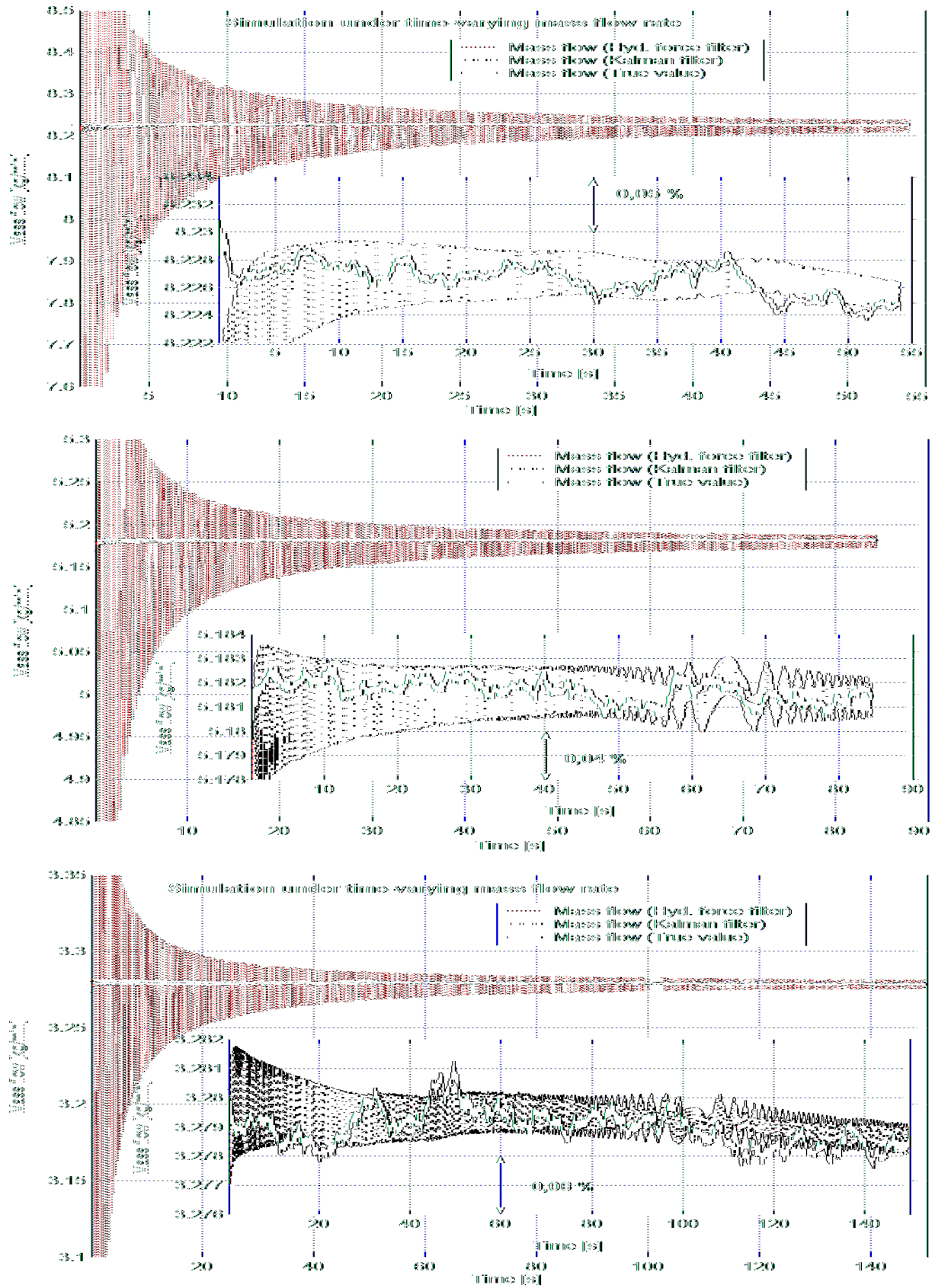


Fig. 5.11 Performance of the Linear Kalman filter at 8, 5 and 3 kg/min

A remarkable feature of the linear Kalman filter is its covariance matrix, which turns out to be an effective way in minimizing the error in knowledge (model) of the system, and therefore it can be used as a tool to statistically measure the uncertainty of the state variables [12, 13]. In this case, the covariance term $E[\hat{e}_m, \hat{e}_f]$ in the matrix (**Eq. 4.47**) describes the degree of association between the two state variables. On the other hand, it is more convenient to present the covariance results in terms of their correlation coefficients (**Eq. 5.3**), so that the degree of association can be assessed in a -1 to 1 scale. For instance, the correlation coefficient of 0,75 at 8 kg/min indicates a positive strong association between the state variables, meaning that both follow the same incremental path (**Fig. 5.12**). A weak correlation coefficient of 0,2 was only observed at the first 5s, assuming that this could be in part caused by the overshoot response of the weighing system during the first water jet impact. As for the other two flow rates (5 and 3 kg/min), they show a moderate positive correlation coefficient of 0,58 and 0,52 respectively. A possible explanation for the decrement of the correlation coefficient in comparison to the upper flow can be attributed to relatively large standard deviations of the estimated collected mass and flow error, σ_m and σ_f .

$$\rho(\hat{e}_m, \hat{e}_f) = \frac{E[\hat{e}_m, \hat{e}_f]}{\sigma_m \cdot \sigma_f} \quad (5.3)$$

As shown in **Fig. 5.12**, the linear Kalman filter offers the possibility of simultaneously evaluating the error from the states variables of the measurement process. However, in order to keep the same line of analysis with the above mentioned filters, only the mass flow state variable is discussed. Then, according to the covariance matrix results shown in **Fig. 5.12**, the linear Kalman filter's estimate error in calculating the time-varying mass flow rate is as follows:

| Average mass flow rate | Estimate error | Relative error |
|------------------------|----------------|----------------|
| [kg/min] | [kg/min] | [%] |
| 8,226 | 0,004 | 0,05 |
| 5,181 | 0,004 | 0,08 |
| 3,279 | 0,004 | 0,12 |

Table 5.1 Mass flow rate estimate error

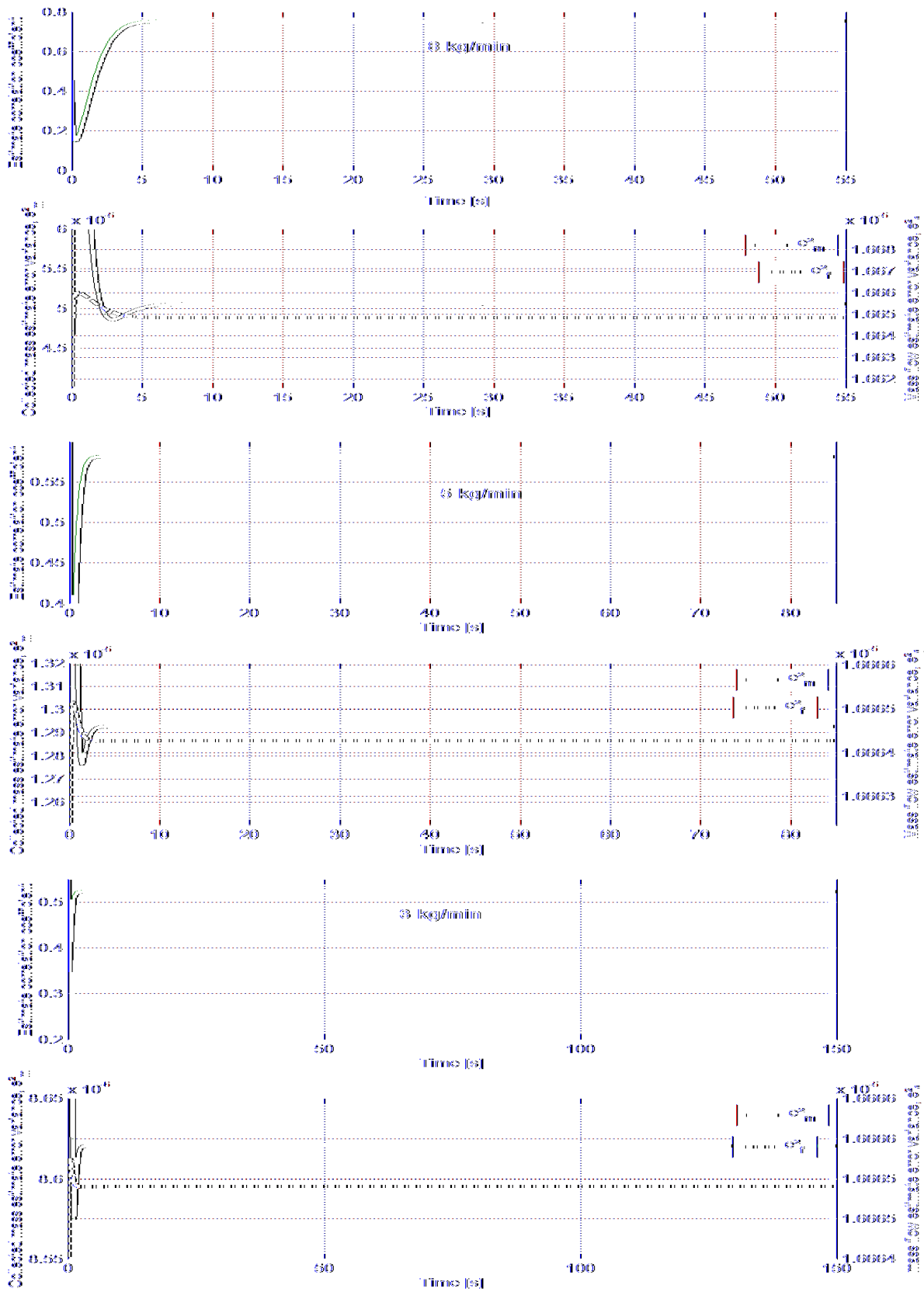


Fig. 5.12 Linear Kalman filter estimate error variance and correlation coefficient at 8, 5 and 3 kg/min

5.5.4 Summary

Central moving average

- The highly corrupted measurement noise present in one or more samples enclosed in a data set increases the measurement variance, and as a consequence, considerably affects the accuracy of the central moving average calculation,
- The central moving average filter shows an initial overshoot, which is later overcome by a smoother and more accurate estimation response,
- The moving average estimation process yields a limited number of estimate values in relation to its counterparts, the LMS adaptive and the linear Kalman filter. However, such a number can be sufficient or even larger, if compared with the number of data samples (usually from 5 to 10 measurement points) required in a regular calibration task [14].

LMS Adaptive filter

- As noted in the series of simulations, the adaptive filter features neither an overshoot nor an unstable system response. This is achieved at the expense of a considerable time taken in order to converge the reference values,
- The LMS adaptive filter as well as the moving average filter seem to be affected by the influence of the relatively large measurement noise taking place at the first 1/4 of the process time. One main reason of such a common behavior is that both algorithms utilize a weighted average (with their corresponding filter coefficients) in order to determine their estimate values. In other words, the estimates at the initial part of the process are subjected to deliver more inaccurate values because of the large measurement variance, and hence a lower statistical weight (reliability) [15].

Linear Kalman filter

- As shown in the simulation results, the Kalman filter benefits from its recursive property with no need of storing past measurements for the purpose of computing its present estimate (but only its previous step). This feature makes possible the rapid minimization of the variance in its estimation error, a less stiff response to sudden changes of the measurand, and ultimately, more time-varying accurate estimates,
- The usage of the average mass flow rate magnitude (coming from the Hydrodynamic force filter) as a basis for the measurand estimation is a key parameter the Kalman filter employs to obtain a reliable estimate response in less iterative cycles. The last statement is applicable because the process is intended to be performed at a quasi-steady and stationary flow condition.

5.6 The influence of the data sampling frequency and the low pass filter cutoff frequency upon the mass flow rate estimate values and its measurement accuracy enhancement

When dynamic weighing mass flow measurements are performed experimentally, the outcome is at some degree limited by the manufacturer design specifications. In this instance, it is referred to the maximum data sampling frequency the balance readout can deliver, and the internal filter algorithm (low pass filter) used to attenuate the undesired oscillatory response of the balance. The following section analyzes numerically the effects of the data sampling frequency as well as the low pass filter upon the measurand, by changing their parameters. The main goal of comparing these results is to have some understanding about the factors that negatively contribute in the determination of the measurand, and what can be done in practice, in order to bring more accurate and precise mass flow rate measurements.

In principle, any of the recalled measurement noise filters could be used to evaluate the measurand response under the different measurement parameters previously mentioned. However, it is more appropriate to select in this case the Kalman filter, because according to the numerical and experimental (**Chapter 6**) results, it is the one that stabilizes faster, it is accurate in its response, and in general, it is capable to follow more effectively the time-varying mass flow rate.

The numerical analysis is divided into three aspects:

- The measurand response is evaluated at two different mass flow rates, at three different data sampling frequencies, and at a low pass filter cutoff frequency of 10 Hz, which is equal to the value set up in the balance (**Fig. 5.13**),
- The measurand response is assessed at two different data sampling frequencies, and at three different low pass filter cutoff frequencies (**Fig. 5.14** and **Fig. 5.15**), and
- To analyze the characteristics of a mass flow rate measurement at two different data sampling frequencies, with the absence of a low pass filter (**Fig. 5.16**).

In **Fig. 5.13**, the results of the mass flow rate estimate values are presented at 8 kg/min and 3 kg/min, with a data sampling frequency of 10 Hz, and a low pass filter cutoff frequency of 10 Hz (see upper graphs). In this example, both flow rates present a measurand response, which lasted about 1/3 of the process time to converge the true mass flow rate value. The maximum relative errors between the estimated values, and the true values at the first stage of the process were in the order of 0,085% at 8 kg/min, and 0,092% at 3 kg/min. Remember, that the term true value is valid (at least numerically), because it is a known input quantity introduced in the model. This is a clear example of how not only the fluctuating flow but also a limited data sampling frequency can affect the ability of a filter to estimate the measurand. This is especially a concern in the regions where the amplitude measurement noise is relatively high.

The two mid graphs at 8 kg/min and 3 kg/min in **Fig. 5.13** show the estimate values at a low pass filter cutoff frequency of 10 Hz, and an increased data sampling frequency of 30 Hz. The 30 Hz magnitude of the data sampling frequency is intentionally assessed in order to try to reproduce the response of the system at its current set up. The graphs clearly describe a prompt convergence of the estimate values, despite the larger data spread at the beginning of the process. This initial behavior can be associated with the influence of the large measurement noise.

The two simulations carried out at a data sampling frequency of 90 Hz show a particular behavior in terms of the fast stabilization time and the spread of the estimated data, which turn out to be very homogeneous along the time (0,01%).

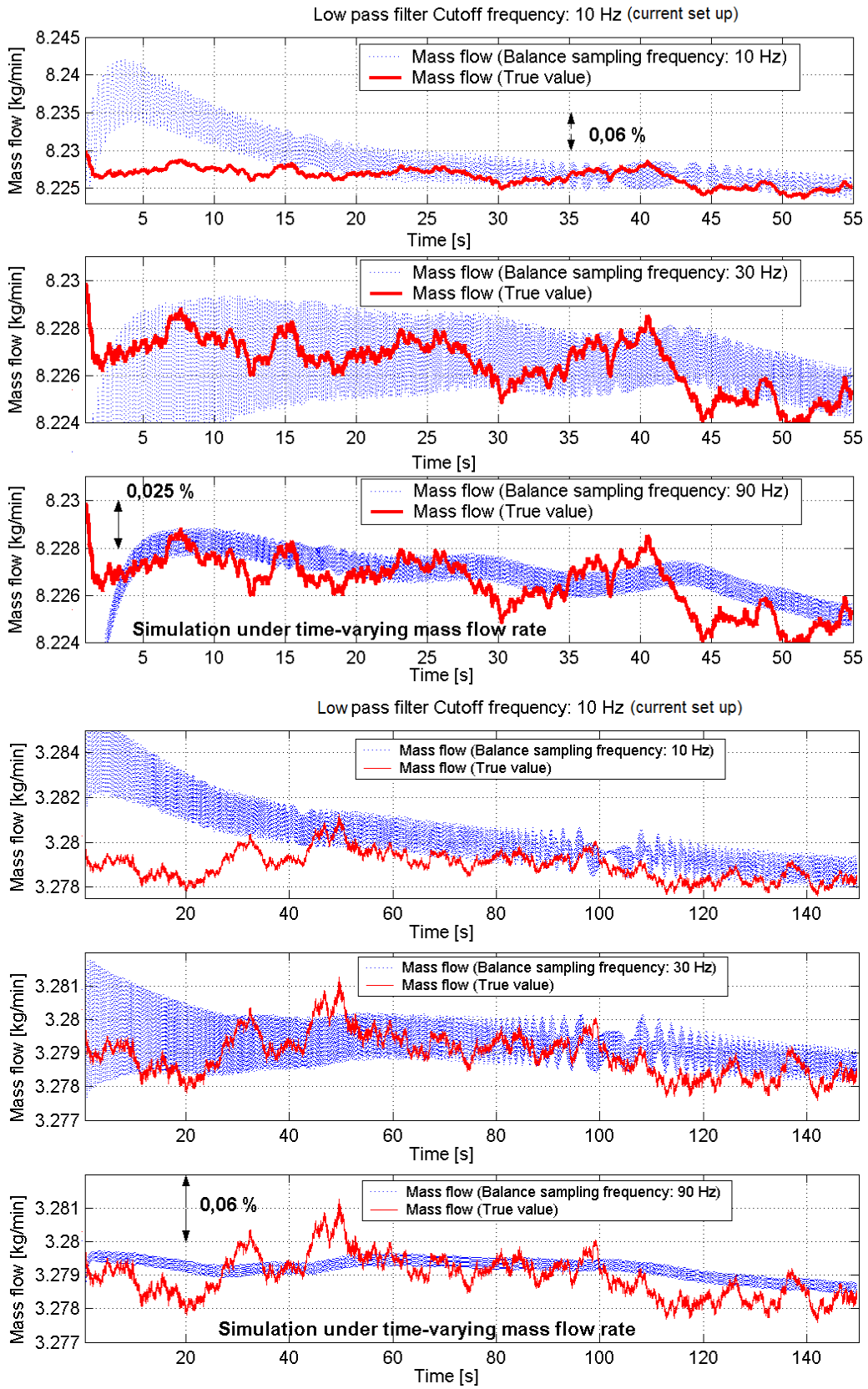


Fig. 5.13 Simulation of the balance output signal response (8 kg/min and 3 kg/min) at a data sampling frequency of 10 Hz, 30 Hz and 90 Hz, and a fix low pass filter cutoff frequency of 10 Hz

As seen in **Fig. 5.13**, the response of the estimation process describes a quite similar behavior regardless of the mass flow rate. Therefore, the analysis can be dedicated to one mass flow rate.

Fig. 5.14 summarizes the performance of the estimation task at three different low pass filter cutoff frequencies (5 Hz, 10 Hz and 20 Hz) at 30 Hz in relation to its data sampling frequency. The measurements performed at three different cutoff frequencies present a common response in terms of estimation path. On the other hand, **Fig. 5.14** also indicates that the level of coverage from the estimate values (seen as data spread) is proportional to the cutoff frequency. This can be expected, because the low pass filter yields higher attenuation levels at small cutoff frequencies, as happens, for instance, at 5 Hz.

Fig. 5.15 describes the simulated response of the Kalman filter to estimate the mass flow rate when the balance sampling frequency is significantly higher (90 Hz), and at three different cutoff frequencies. The outcome indicates that the influence of the measurement noise is minimal in all cases because the larger number of data samples allows the filter to reduce, in less iterations, the measurement variance. The upper graph (at 5 Hz) in **Fig. 5.15** underlines an important fact that besides attenuating the unwanted balance oscillatory force, the low pass filter takes part of the measurand data. The overriding of measurand data is clearly seen when comparing the different cutoff frequencies of the system. The wider the low pass filter's pass band, the more accurate the estimation.

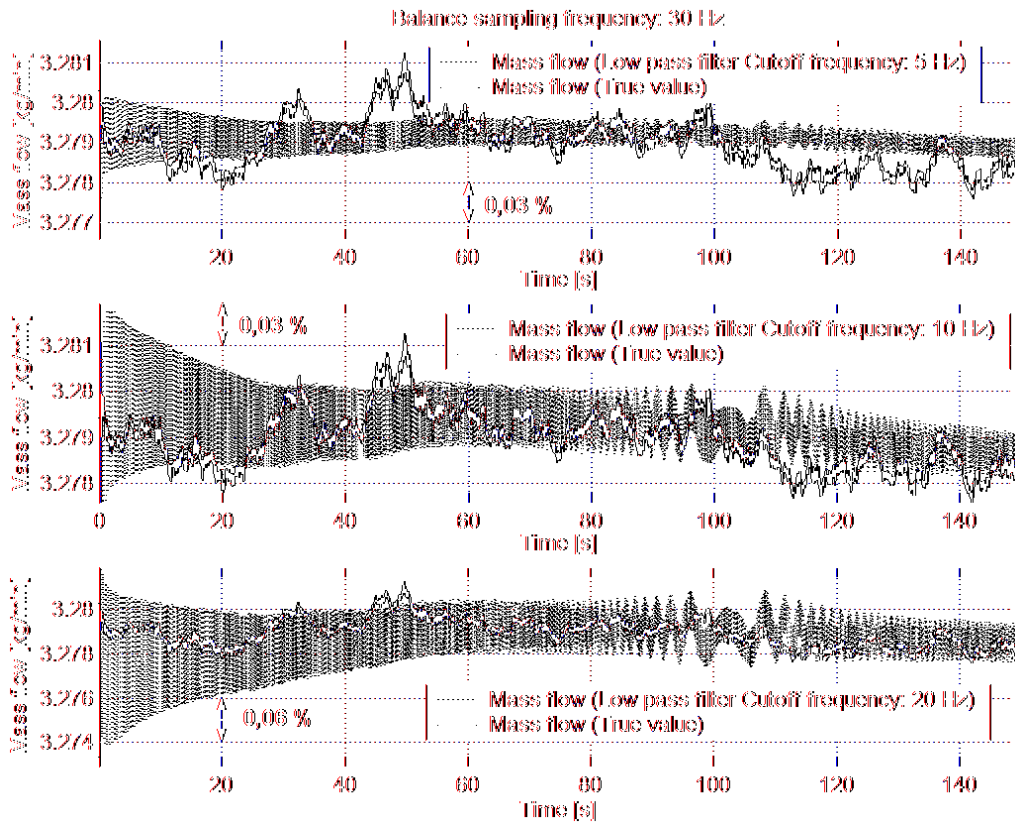


Fig. 5.14 Simulation of the balance output signal response at three different low pass filter cutoff frequencies (5 Hz, 10 Hz and 20 Hz) and a data sampling frequency of 30Hz

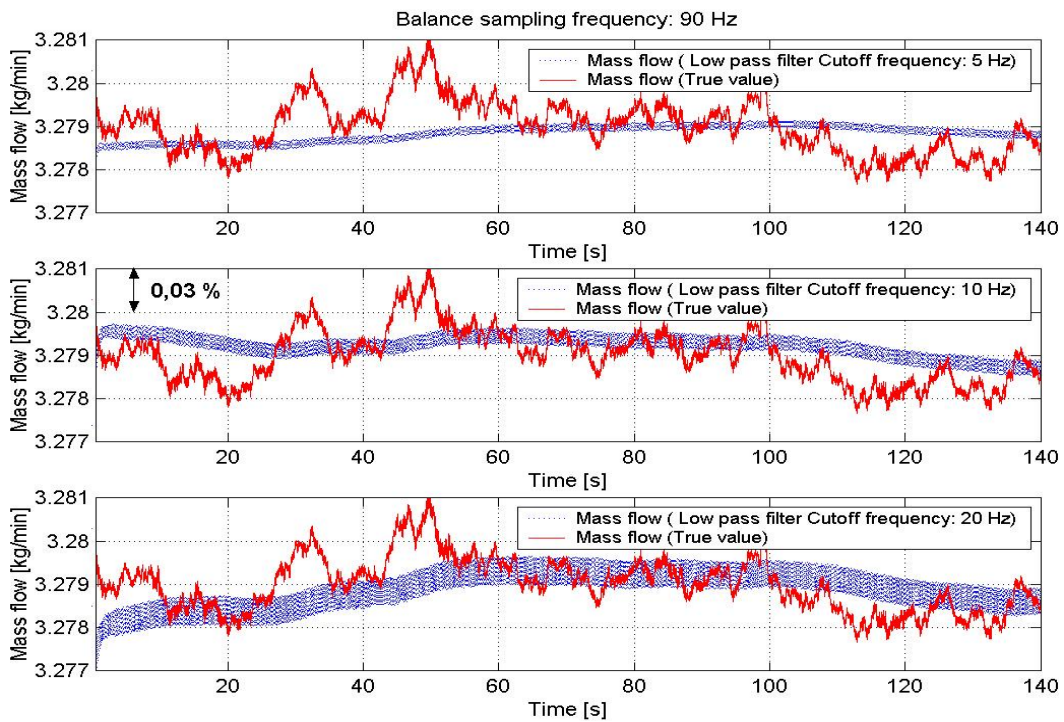


Fig. 5.15 Simulation of the balance output signal response at three different low pass filter cutoff frequencies (5 Hz, 10 Hz and 20 Hz) and a data sampling frequency of 90Hz

Fig. 5.16 exemplifies the filter response when the low pass filter is excluded from the output signal conditioning process. In this example, the estimated values at a balance sampling frequency of 30 Hz are satisfactory, despite the apparent influence of the measurement noise at the beginning of the measurement. On the other hand, the performance of the filter is outstanding when the system is able to sample data at 90 Hz. In this case, the estimate values converge in a few seconds after the start point of the collection process. Additionally, the filter keeps tracking the fluctuated mass flow rate, within a band of 0,05% with respect to the average magnitude.

The conclusion given by this analysis is that the accuracy and precision of the estimate values can be re-enhanced, if the balance output signal could skip the low pass filter, and the sampling frequency would be higher [16]. However, the criteria for an appropriate increment of the data sampling frequency will be closely related, for instance, with the level of stationary fluctuating flow at the primary standard and the balance time constant. Furthermore, as an important remark, these specific output signal characteristics can be currently provided only by *customized balances*.

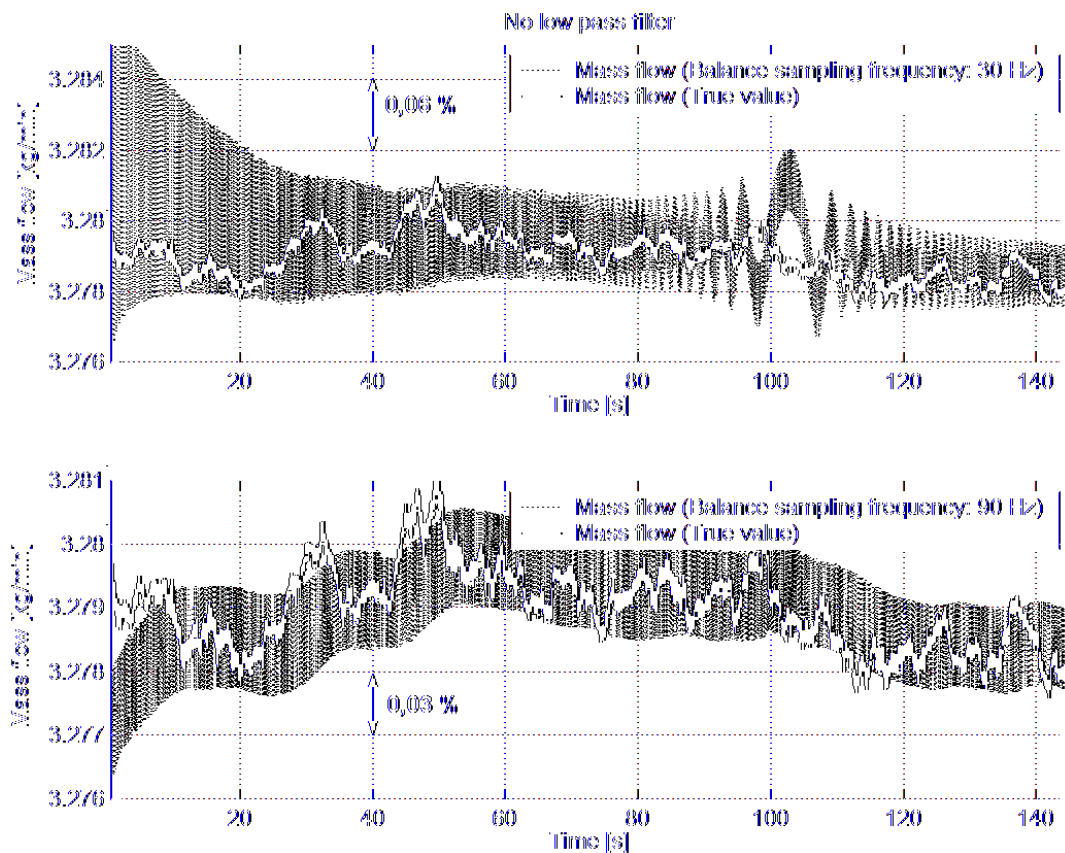


Fig. 5.16 Simulation of the balance output signal response at a data sampling rate of 30 Hz and 90 Hz without low pass filter

6. Experimental results

The content of this chapter addresses the theoretical, mechanical, and data acquisition set up of a prototype used as a dynamic weighing liquid flow standard. Furthermore, it presents a series of measurements performed at different mass flow rates, with the aim to experimentally determine the accuracy level of the process model algorithm described in **Chapter 4**.

For these series of tests, the reference system in use is a flowmeter with direct traceability to the PTB national standard for low liquid flow measurements [1]. This means, a measurement approach, in which a primary flow standard can provide a low-uncertainty characterization to the flowmeter output signal, and at the same time, a flowmeter that is capable of tracking the stationary and quasi-steady mass flow rate fluctuation in small time intervals, but within the uncertainty claimed after its calibration. The description of the transfer standard is also given in this chapter.

6.1 Transfer standard used for the liquid flow comparison

The transfer standard used for these experimental tests is a turbine flowmeter owned by the PTB calibration laboratory, which complies with all metrological requirements of reproducibility, repeatability, linearity, precision, and covers the measuring range demanded by the tests.

Regarding its working principle, the turbine flowmeter is a metering device, which converts the mechanical angular velocity of the rotor (generated by the mass flow) into an electrical frequency signal [2]. In other words, if the mass flow passing through the meter increases, the rotor angular velocity as well as the electrical frequency measured by an external pickoff will raise in the same manner (**Fig. 6.1**). Concerning its mechanical construction, the turbine rotor has to be held inside the stream, whereby supports are added to position the rotor bearing in the pipe as shown in **Fig. 6.1**. Additionally, such supports serve as a flow straightener that removes the swirls and/or disturbing flows caused by upstream pipe fittings and valves. Another good feature of the turbine meter is the high-sensitivity of the mechanical sensing element (rotor) to sudden changes of mass flow rate during a measurement run [3 and 4], despite some small response delay attributed to a retarding torque from the rotor [5].

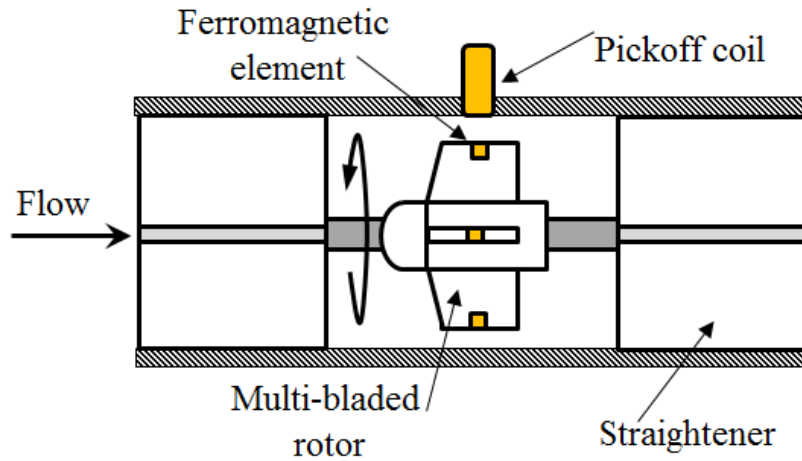


Fig. 6.1 Turbine flowmeter used as a transfer standard

The transfer standard is a 25-mm turbine flowmeter that has been previously calibrated by the PTB primary standard of liquid flow, within 2 kg/min to 10 kg/min. The results of this characterization are given in terms of a ratio called K factor, which represents the number of pulses read by the pickoff during the transfer of 1 L of water through the flowmeter (**Eq. 6.1**). The K factor of the transfer standard was defined to be equal to 12821 pulses/L, and on the other hand, the region of linearity of this flowmeter was found between 3 kg/min and 8 kg/min. This is the flow range that will be used during the measurement comparison, due to its relatively lower measurement uncertainty levels and repeatable results.

$$K_{Meter} = \frac{f_{Meter}}{\dot{V}_{PTB}} \quad (6.1)$$

Here f_{Meter} denotes the turbine rotor frequency in Hz, and \dot{V}_{PTB} represents the volumetric flow rate determined by the PTB primary flow standard during the characterization process. Meanwhile, during the dynamic flow measurement tests, the turbine flowmeter will be able to calculate the mass flow rate by using **Eq. 6.2**, which is a dependent function of the obtained turbine calibration factor K_{Meter} , $f_{Meter}(t_n)$, and the fluid density $\rho_w(\mathcal{G}_{Meter})$ at its location.

$$\dot{m}_{Meter}(t_n) = \frac{\rho_w(\mathcal{G}_{Meter}) \cdot f_{Meter}(t_n)}{K_{Meter} \cdot \left[\frac{1000 L}{1 m^3} \right]} \quad (6.2)$$

As for the measurement uncertainty attributed to the transfer standard, this can be determined by the combined measurement uncertainty of the small PTB liquid flow primary standard ($U_{PTB} = 0,05\%$) [1], in addition to the uncertainty of the transfer standard due to its repeatability ($U_{Meter_Rep} = 0,06\%$). Both values are referring to a 95% confidence level.

$$\begin{aligned} U_{Meter} &= \pm \sqrt{(U_{PTB})^2 + (U_{Meter_Rep})^2} \\ &= \pm 0,078\% \end{aligned} \quad (6.3)$$

On the other hand, the measurement uncertainty of the Dynamic Weighing Liquid Flow Standard prototype (DWLFS) is estimated by the combined uncertainty of the storage effect of the connecting volume U_{CV} (**Chapter 3**), and the uncertainty related to the time-varying estimate error given by the process model algorithm $U_e(t_n)$.

$$U_{DWLFS}(t_n) = \pm \sqrt{(U_{CV})^2 + (U_e(t_n))^2} \quad (6.4)$$

6.2 Data acquisition system

The data acquisition system and signal synchronization for the dynamic weighing liquid flow standard prototype (DAQ) is realized by a software written in Labview®, and a programmable automation controller known as NI CompactRIO® [6]. Such equipment comprises a dedicated 400-MHz microprocessor that serves to acquire synchronous real-time measurement data. Furthermore, the integrated high-performance FPGA (Field-Programmable Gate Array) allows the user to generate a reconfigurable hardware circuitry between the customized I/O modules (**Table 6.1**) connected to the measuring devices and the microprocessor. Moreover, a RS-232 serial port is employed to interface the high-precision balance to the CompactRIO®. The interfacing of the prototype measuring devices as well as the DAQ system is depicted by **Fig. 6.2**.

The I/O data transfer between the modules and the NI CompactRIO microprocessor is carried out by means of using a high-speed PCI bus for real-time analysis and data logging. Thereafter, the acquired data are sent to a networked host computer for visualization through via Ethernet. As for the acquired data, these are stored in an external hard disc plugged to a CompactRIO® full speed

USB port. In this instance, the speed of DAQ system can be only limited by the implemented sensors and the I/O modules, rather than its processing performance. For this application, the data sampling rate for all acquired signals is 250 Hz.

| Module | Signal type | Sensor | Input range | Sampling frequency | Resolution |
|---------|--------------|---------------------------------------|-------------------|--------------------|------------|
| NI 9233 | Analog Input | Accelerometer | $\pm 5V$ | 50 kHz | 24-Bit |
| NI 9203 | Analog Input | Laser displacement sensor | $\pm 20mA$ | 200 kHz | 16-Bit |
| NI 9401 | Digital I/O | Transfer standard (Turbine flowmeter) | $\pm 0 - 5V(TTL)$ | 10 MHz | 1 mV |

Table 6.1 Technical specifications of data acquisition modules [7, 8 and 9]

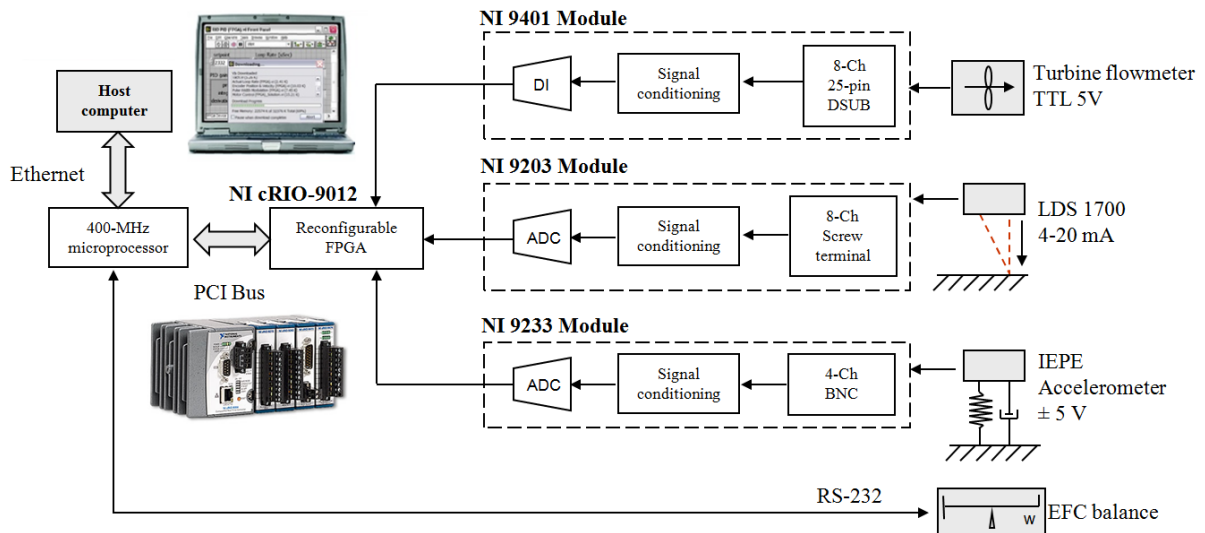


Fig. 6.2 FPGA system used as a DAQ and controller for dynamic-weighting measurements

6.3 Implementation of an accelerometer to detect the initial time of the measurement process

The task of the accelerometer mounted upon the balance platform is to monitor the z axis (weighing axis) acceleration at the initial stage of the measurement. This is with the aim to trigger out the start time of the filling process, when the water jet impacts for the first time the vessel. The start time is a very important process variable, because it enables the hydrodynamic force filter to calculate the estimate mass flow rate more accurately.

This technique is based on the physical fact that the incoming water jet will generate an impact on the balance platform, and eventually, the weighing system will have to react mechanically to such an impulse force in terms of a sudden acceleration [10].

If the weighing system output response were used instead, as the basis to trigger out the start time of the measurement process, then the estimate measurand values would take longer to stabilize. The explanation to this phenomenon lie on an smaller *time constant* and higher data sampling frequency of the accelerometer, in relation to its counterpart, the weighing system.

As a matter of definition, the difference in time between the EFC balance response and the acceleration response to the first water jet impact will be denoted as *time offset*. In **Section 6.5**, an experimental test exemplifies the magnitude of such a time offset effect.

The employed Brüel & Kjaer 4508 DeltaTron® accelerometer is a compact (1cm³), hermetic, and a light-weight (4,8 g) piezoelectric transducer. One of the remarkable features of this accelerometer is its low noise pre-amplifier [11] incorporated in the transducer, as well as the low-impedance cable used to prevent erroneous measurements due to voltage drops. The transducer is connected to a 4-Channel NI 9233 module [7], which is dedicated to serve as a power supply, A/D converter, amplifier, and digital filter for the accelerometer output signal.

Concerning its mounting, the accelerometer and its cable have to be properly fastened to the weighing platform in order to avoid measurement errors caused by the wiggle of the sensor and the triboelectric noise induced by the cable movement [12 & 13]. According to the PTB acceleration laboratory, the measurement uncertainty of this accelerometer is in the order of $\pm 0,2\%$ at a confidence level of 95%.

6.4 Usage of a non-contact laser displacement sensor to characterize the water jet impact height

The Micro-Epsilon NCDT 1710 Laser Displacement Sensor (LDS) is a measurement device responsible of determining the water jet impact height $\hat{h}_i(z)$, which is a key process variable for the experimental estimation of mass flow rate via hydrodynamic force filter.

As shown in **Fig. 6.3**, the LDS is mounted over the weighing system platform to monitor its oscillatory displacement with a resolution of 0,5 μm , at a data sampling frequency of 250 Hz, and a measurement uncertainty of 2 μm (95% confidence level). This device working under the triangulation measurement principle [14 and 15] is an appropriate sensor for this application, because it does not exert any undesired additional force upon the balance platform.

The characterization of the impact height $\hat{h}_i(z)$ was determined by filling the collection vessel at 10 different levels, measuring the corresponding distance between the nozzle outlet and the water surface, and recording the displacement of the calibrated balance at each level by using the LDS. Afterwards, these two variables are plotted to yield a characterization curve depicted by **Fig. 6.3**. Thus, the current water jet impact height is a function of the balance displacement (z), wherein its trend can be approximated by a quadratic curve-fitting equation, **Eq. 6.5**. The range of the water jet impact height is between 520 mm (distance from nozzle outlet to vessel bottom) and 250 mm (distance from nozzle outlet to the water surface at 10 L of the vessel capacity). As a remark, the non-linear representation of **Eq. 6.5** is due to the side wall shape of the vessel at the bottom.

$$h_i(z) = -1339 \cdot z^2 - 863,09 \cdot z + 515,82 \quad (6.5)$$

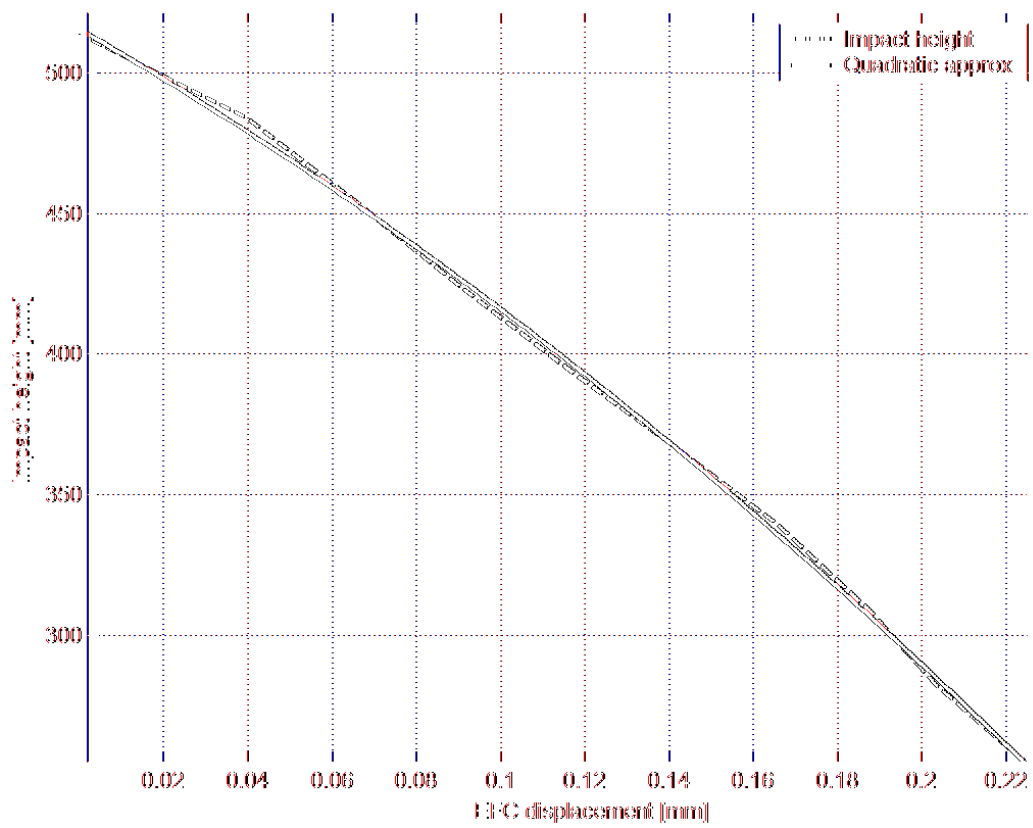
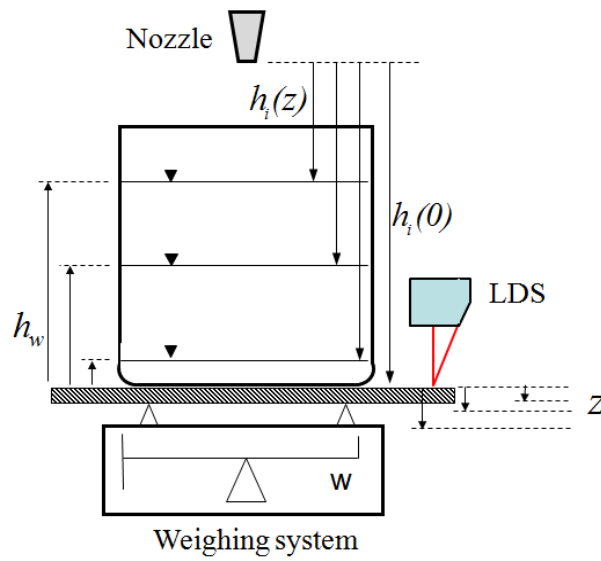


Fig. 6.3 Water jet impact height characterization as a function of the EFC balance platform displacement measured by the LDS

6.5 Characterization of the weighing system's stiffness and damping coefficients

The characterization of the weighing system spring coefficient was carried out by applying PTB reference masses upon the center of the balance platform (50 g, 100 g, 200 g, 500 g, 1 kg, 3 kg, 5 kg, 7 kg, 9 kg and 10 kg), and knowing the local acceleration of gravity to calculate the exerted force. Note that the accorded maximum loading of 10 kg is related to the maximum capacity of the collection vessel (10 L) used in the dynamic weighing liquid flow primary standard prototype, and the density of the water ($998,2 \text{ kg/m}^3 \times 0,01 \text{ m}^3 = 9,982 \text{ kg}$). Furthermore, the air temperature, relative humidity, and atmospheric pressure were recorded, in order to calculate the buoyancy force effect upon the reference masses.

After a set of reference masses are placed upon the balance, a laser displacement sensor records the displacement of the weighing platform. Once the loading from 0 kg to 10 kg is completed, a force-displacement graph is plotted (**Fig. 6.4**), and a curve fitting is applied in order to get a second order equation (**Eq. 5.3**) that approximately describes the data path.

During the characterization test, the maximum balance displacement recorded at a nominal load of 100 N was $2,7 \cdot 10^{-4} \text{ m}$. Then, as a result of such a characterization, the balance force-displacement curve shown in **Fig. 6.4** and described by **Eq. 6.6** depicts a slight non-linearity, attributed to the deflection of the balance beam, the rubber supports of the balance, and in a very minor degree due to the balance sensing element. Finally, the derivative of **Eq. 6.6** yields the weighing system stiffness coefficient (**Eq. 6.7**), wherein its magnitude covers a range from $2,774 \cdot 10^5 \text{ N/m}$ to $4,3 \cdot 10^5 \text{ N/m}$.

$$F_{Ref}(z) = 2,9337 \cdot 10^8 \cdot z^2 + 2,744 \cdot 10^5 \cdot z + 0,60935 \quad (6.6)$$

$$k_{Bal} = \frac{dF_{Ref}(z)}{dz} = 5,8674 \cdot 10^8 \cdot z + 2,744 \cdot 10^5 \quad (6.7)$$

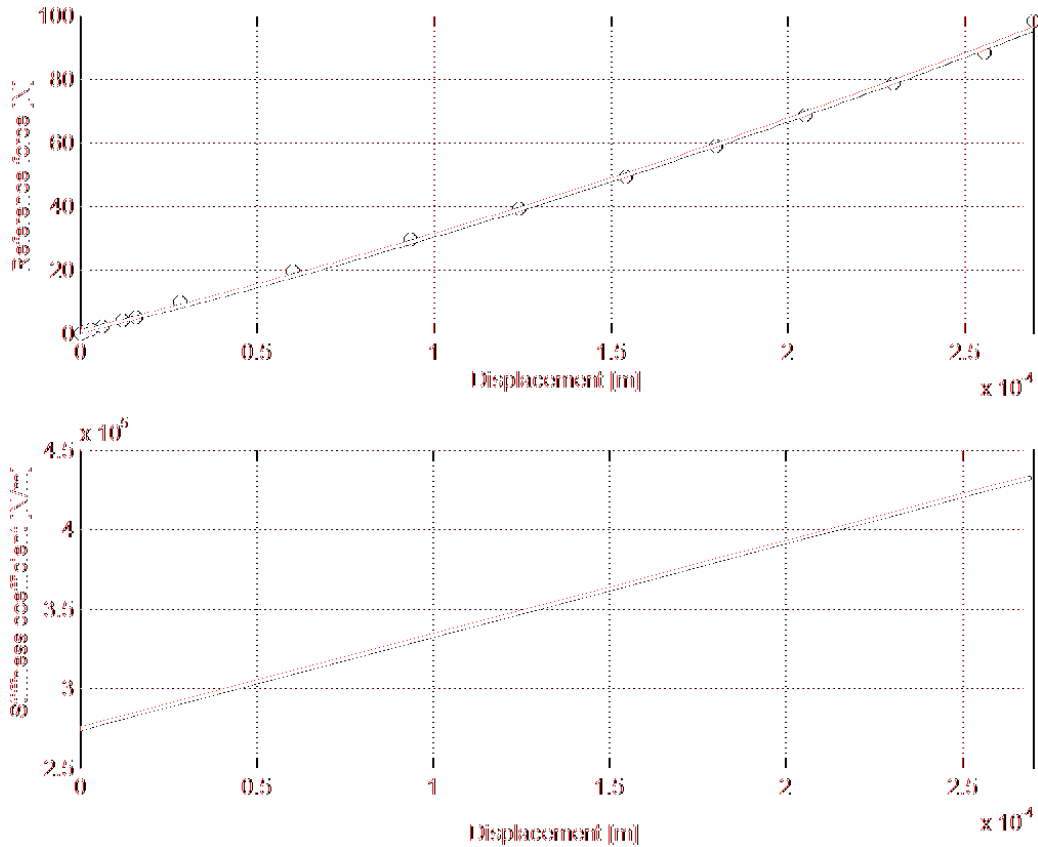


Fig. 6.4 Characterization of the weighing system stiffness coefficient

The determination of the weighing system damping coefficient was calculated in accordance to **Eq. 6.8** (previously described in **Chapter 3**), wherein such a system parameter is a function of the stiffness coefficient k_{Bal} , the total mass supported by the balance $m_T(t)$ (**Eq. 6.9**), and the characterized damped angular frequency of the balance along its weighing axis $\omega_d(m_T(t))$ depicted in **Fig. 5.4**, **Chapter 5**. Thus, according to **Fig. 6.5** the damping coefficient is within $0,12 \text{ N.s/m}$ and $0,26 \text{ N.s/m}$.

$$c_{Bal}(t) = 2 \cdot \left(k_{Bal} \cdot \hat{m}_T(t) - \omega_d^2(\hat{m}_T(t)) \cdot \hat{m}_T^2(t) \right)^{1/2} \quad (6.8)$$

$$\hat{m}_T(t) = m_v + m_p + m_w(0) + \hat{m}_{HF}(t) \quad (6.9)$$

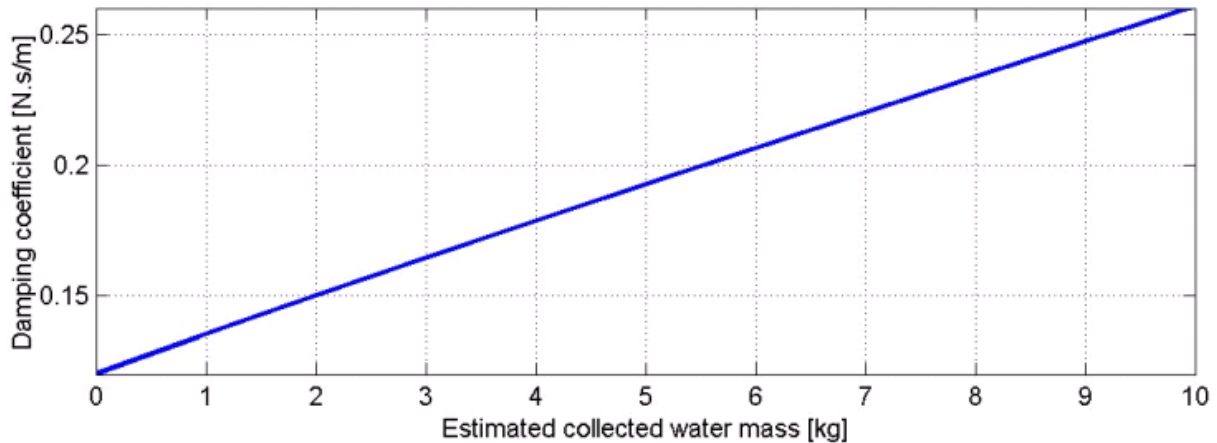


Fig. 6.5 Characterization of the weighing system damping coefficient (Eq. 6.8)

6.6 Results

A very important stage during this research was to validate the process model used to determine mass flow rate via dynamic-weighing. This task consisted in getting the results delivered by the transfer standard (turbine flowmeter), and thereafter comparing such reference measurements with the proposed approach. The set of experimental tests described in the following paragraphs below, correspond to two stages carried out in order to obtain the measurand mass flow rate (see **Fig. 6.6**).

1. Mass flow rate determination by means of an algorithm (Hydrodynamic force filter), which takes as an input the acquired signal from the balance force response and time, and it is responsible of quantifying and minimizing the effects from the hydrodynamic and buoyancy force from the measurement,
2. A subsequent filter algorithm called Measurement noise filter, uses the outcome from the Hydrodynamic force filter as an input signal, and deals with the attenuation of the measurement noise caused by the dynamic response of the weighing system. In this analysis, there are three different measurement noise filters proposed for this task (Moving average, Least-mean-Square adaptive, and a Kalman filter), with the aim to compare their ability to get rid of such a signal disturbance, and thus, delivering a more accurate estimate measurand.

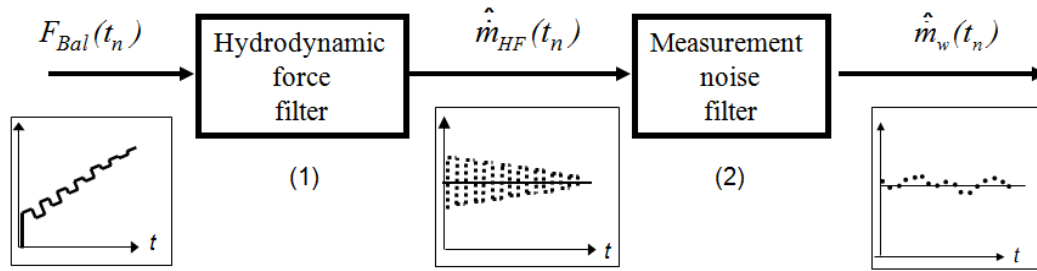


Fig. 6.6 Process model subsystem

6.6.1 Hydrodynamic force filter

In the measurement process, the hydrodynamic and buoyancy force have to be taken into account in order to avoid a significant systematic error in the determination of mass flow rate via dynamic weighing. With regard to the buoyancy force, this can be estimated by knowing the temperature-dependent density from the air and water. On other hand, the hydrodynamic force induces a larger undesired force magnitude to the measurement process caused by the time-varying force of the water jet impacting the collection vessel. **Fig. 6.7** describes an experimental test to prove the influence of this variable, and to estimate its force magnitude. The experiment consisted of starting the water collection process, and then bypassing the water jet from the collection vessel. The result is a difference in force magnitude between the fluid in motion (collected mass force + hydrodynamic force – buoyancy force), and the fluid at rest (collected mass force – buoyancy force), which concludes in an estimated hydrodynamic force [16].

Fig. 6.7 exemplifies such an estimate at a nominal mass flow rate of 8 kg/min. In this instance, the value of the hydrodynamic force at the initial stage of the filling process is 0,51 N, that decreases to 0,4 N (or 20 %) at the final stage of the collection, because of the reduction of the water jet impact height.

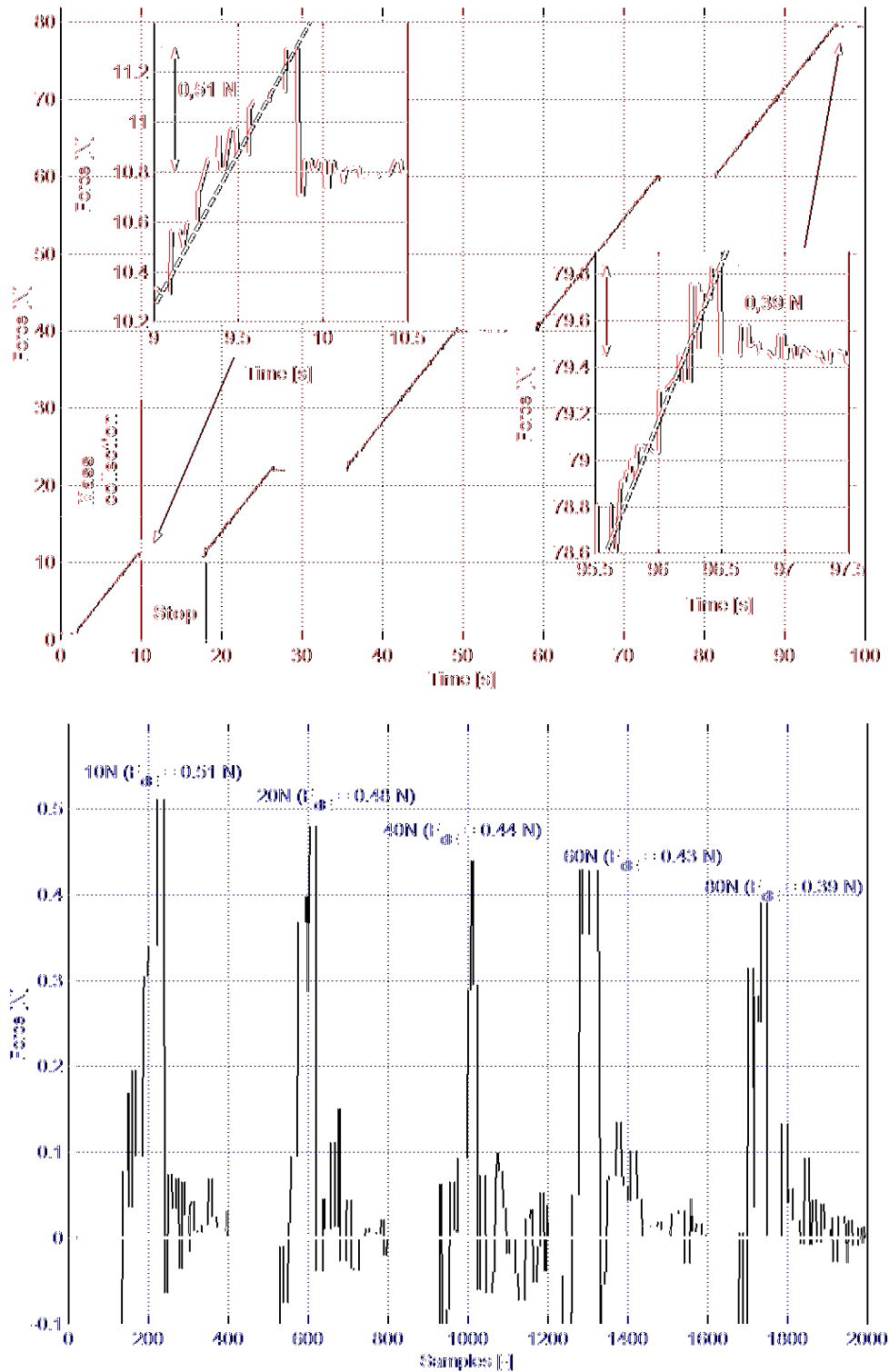


Fig. 6.7 Experimental estimation of the hydrodynamic force at 8 kg/min

6.6.2 Analytical and experimental estimation of the hydrodynamic force

The same type of experiment depicted in **Fig. 6.7** was performed at 3 kg/min, 5 kg/min and 8 kg/min but additionally, the hydrodynamic force was quantified by **Eq. 6.10** (**Chapter 4, Eq. 4.15**) and **Eq. 6.11**, with the aim to compare the agreement between the experimental and analytical approach. The results shown in **Fig. 6.8**, reveal that most of experimental measuring points at five different levels of collection, overlap with the values obtained by analytical means. The largest deviations between these two approaches to estimate the variable were: 1,7% at 3 kg/min, 1,4% at 5 kg/min, and 1,5% at 8 kg/min.

$$\begin{aligned} & \left[\frac{I}{\rho_w^2(\vartheta_w) \cdot A_n^2} \right] \cdot \hat{m}_{HF}^4(t_n) + \left[2 \cdot g \cdot \hat{h}_i(z) - g^2 \cdot \left(1 - \frac{\rho_A(\vartheta_A)}{\rho_w(\vartheta_w)} \right)^2 \cdot t_n^2 \right] \cdot \hat{m}_{HF}^2(t_n) + \dots \\ & \dots + \left[2 \cdot F_{Bal}(t_n) \cdot g \cdot \left(1 - \frac{\rho_A(\vartheta_A)}{\rho_w(\vartheta_w)} \right) \cdot t_n \right] \cdot \hat{m}_{HF}(t_n) - F_{Bal}^2(t_n) = 0 \end{aligned} \quad (6.10)$$

$$\hat{F}_d(t_n) = \hat{m}_{HF}(t_n) \cdot \left\{ \left(\frac{\hat{m}_{HF}(t_n)}{\rho_w(\vartheta_w) \cdot A_n} \right)^2 + 2 \cdot g \cdot \hat{h}_i(z) \right\}^{1/2} \quad (6.11)$$

wherein the estimate water jet impact height $\hat{h}_i(z)$ can be calculated by **Eq. 6.5**.

It is important to remark that the data scattering yield by the analytical form is highly spread during the first seconds of the process due to the balance reacting shock response. Nonetheless, such data spread (originated by the oscillatory response of the balance) does significantly decrease as the collected water level rises.

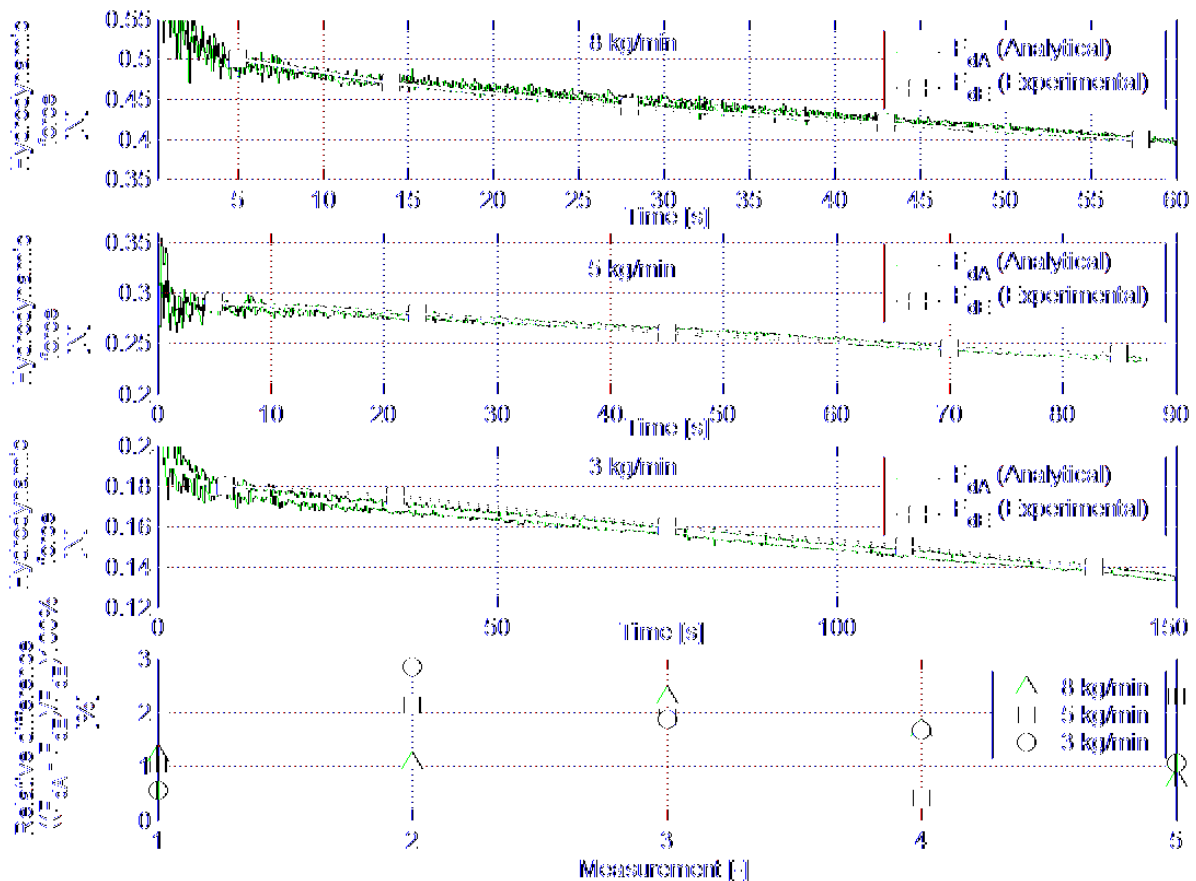


Fig. 6.8 Analytical and experimental estimation of the hydrodynamic force at 8, 5 and 3 kg/min

6.6.3 Estimation of the collected mass force

The estimation of the collected mass force is a key step for determining how good the measurement process model will approach to the real water mass collection, and subsequently the mass flow rate. The experimental results illustrated in **Fig. 6.9** show the balance force response at 8 kg/min. This signal, as previously demonstrated in **Fig. 6.8**, contains the undesired magnitude of the hydrodynamic and buoyancy force. Therefore, the task of the hydrodynamic force filter is to significantly reduce these dynamic process variables, thus yielding an estimate of the collected water mass. The removal of these dynamic forces is clearly seen in **Fig. 6.9** when comparing the slope of the balance force response and the given by the hydrodynamic force filter algorithm. As expected, the slopes are different because the attenuated dynamic variables vary in time. As observed in **Fig. 6.9**, the slope percent change of the hydrodynamic force filter output signal with respect to Balance output response (Non-treated process signal) at three different mass flow rates, were in the order of: 0,35 % at 8 kg/min, 0,28% at 5 kg/min, and 0,20% at 3 kg/min. The results here infer that the balance force response trends to converge the estimate collected mass force,

either at the lowest flow rates or at high levels of the collection process, associated with the shortened water jet impact height. Moreover, this outcome suggests a worthwhile design criterion of reducing as much as possible the distance from the discharging nozzle to the collection vessel bottom, with the goal to physically decrease the hydrodynamic force magnitude from the measurement process.

It is appropriate to highlight the term slope in this analysis, because in this measurement process the slope implies a mass flow rate calculation. **Fig. 6.10** clearly highlights the difference when the balance force response and hydrodynamic force filter output as quotients of time (mass flow rate). Note that the local acceleration of gravity $9,8125 \text{ m/s}^2$ [17] has been employed in order to present the data as an estimate of kg/min . The estimate mass flow rate obtained by the direct quotient of the balance output and time reveals a relative error of about 0,2 % in relation to the average reference value given by the transfer standard (**Fig. 6.10**).

On the other hand, a smaller relative error of 0,07% is attained by using the estimate collected water mass (Hydrodynamic force filter) to calculate the flow unit. After analyzing the tests at 3, 5, and 8 kg/min , it was concluded that the filter enable the measurements to improve by a factor between 2 and 3.

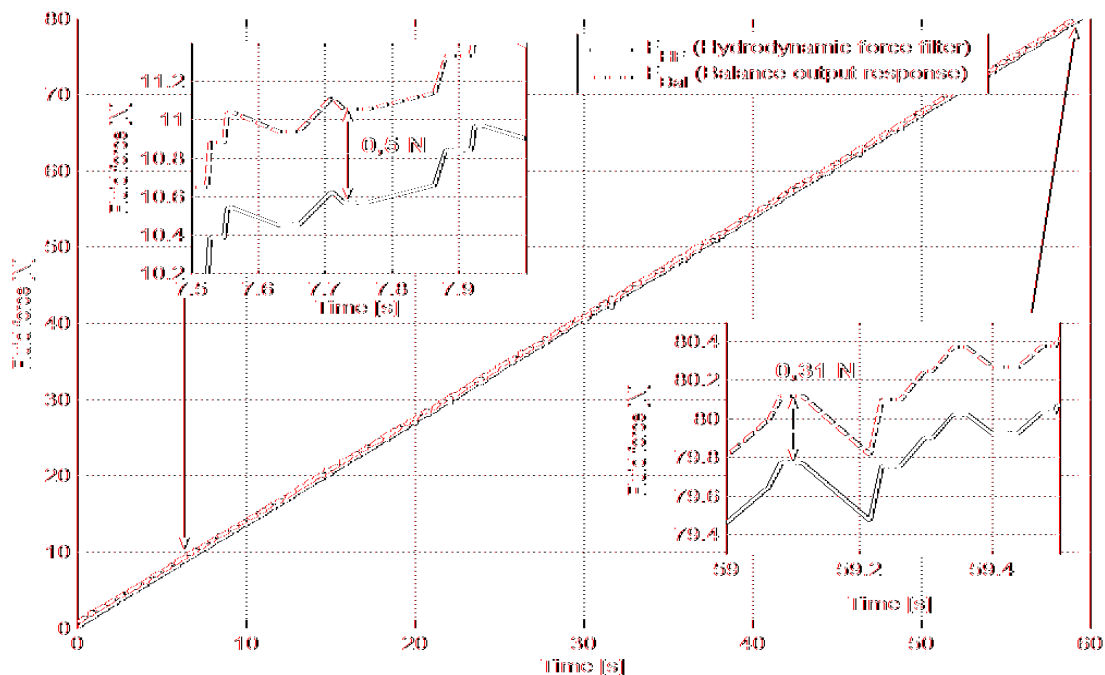


Fig. 6.9 Hydrodynamic force filter used to estimate the collected water mass at 8 kg/min

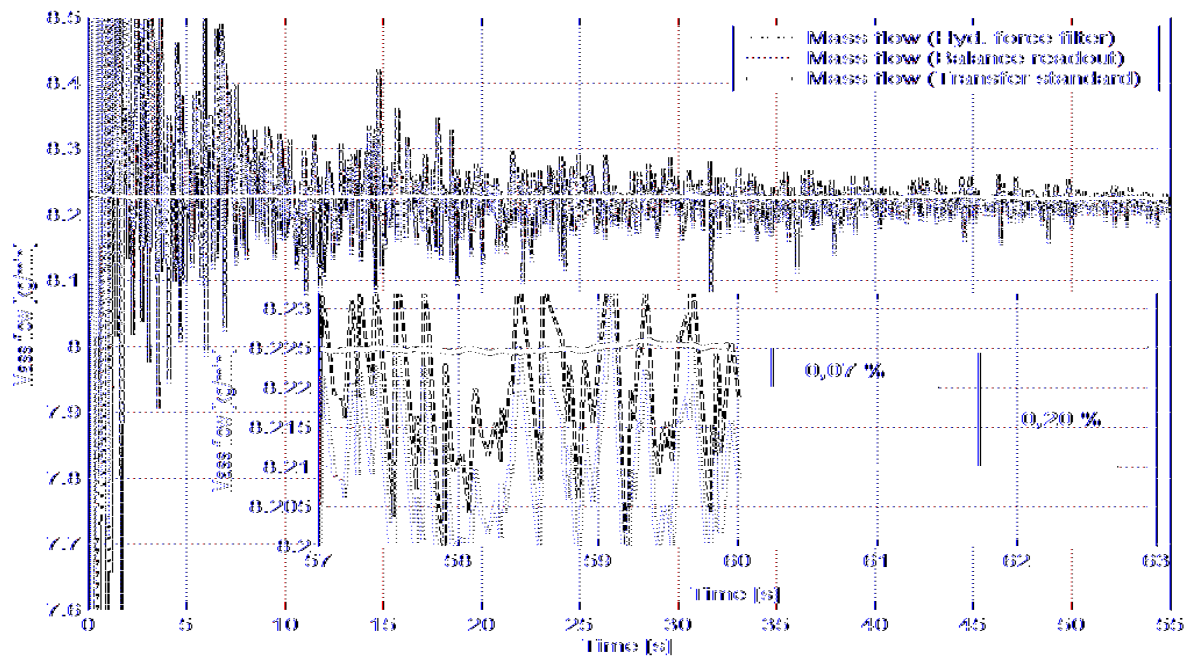


Fig. 6.10 Comparison of the average mass flow rate measurements via hydrodynamic force filter and balance output signal

As a remark, the scattered data seen in **Fig. 6.10** (caused largely by the time-discrete oscillatory response of the balance) will be treated by the following filter algorithm (see **Fig. 6.6**), which tackles the attenuation of the measurement noise.

6.6.4 Time offset correction

The experimental results shown in **Fig. 6.10** were possible because the data was corrected from the *time offset* originated by the balance response (**Section 6.4.2**). Such a correction enables the measurement process to recognize at which point the collection process indeed started, so then an initial time (or time zero) can be set for the calculations of mass flow rate. As previously discussed in **Section 6.4.2**, this technique works under the principle of sudden acceleration of the weighing system caused by the first impact of the water jet impacts upon the collection vessel. An example of this method is illustrated in **Fig. 6.11**, wherein an accelerometer mounted upon the weighing axis (perpendicular axis to the balance platform) measures the right moment of the impact at 2,616s instead of at 2,661s given by the balance readout. This means, 45 ms faster than the first step of the balance output response. The observed time delay between the two systems is will depend upon the accelerometer time constant, the internal filter of the balance, and the higher

sampling frequency of the accelerometer DAQ module (250 Hz), in relation to a 25-Hz data sampling frequency from the EFC balance.

In order to exemplify the relevance of this parameter, consider the first step response of the balance output signal as a reference mark for the process initial time. In this circumstance, the calculation of the estimated mass flow rate depicted in **Fig. 6.12** (with no time-offset correction), would nearly require half of its measurement time (29 s) in order to converge with the average reference value. The latter value agrees within an error band of 0,3% at 8 kg/min. On the other hand, the other two mass flow rates at 5 kg/min and 3 kg/min, depict an stabilization time at approximately 40% and 28% of their total measurement time, respectively. These numbers demonstrate that the time offset significantly affects the high mass flow rates, due to the relative short time of collection to compensate the weighing system time delay. As for the time-offset corrected signal, this would require about 2s to get stable (**Fig. 6.12**). Therefore, almost the entire set of data can be worth for analyzing.

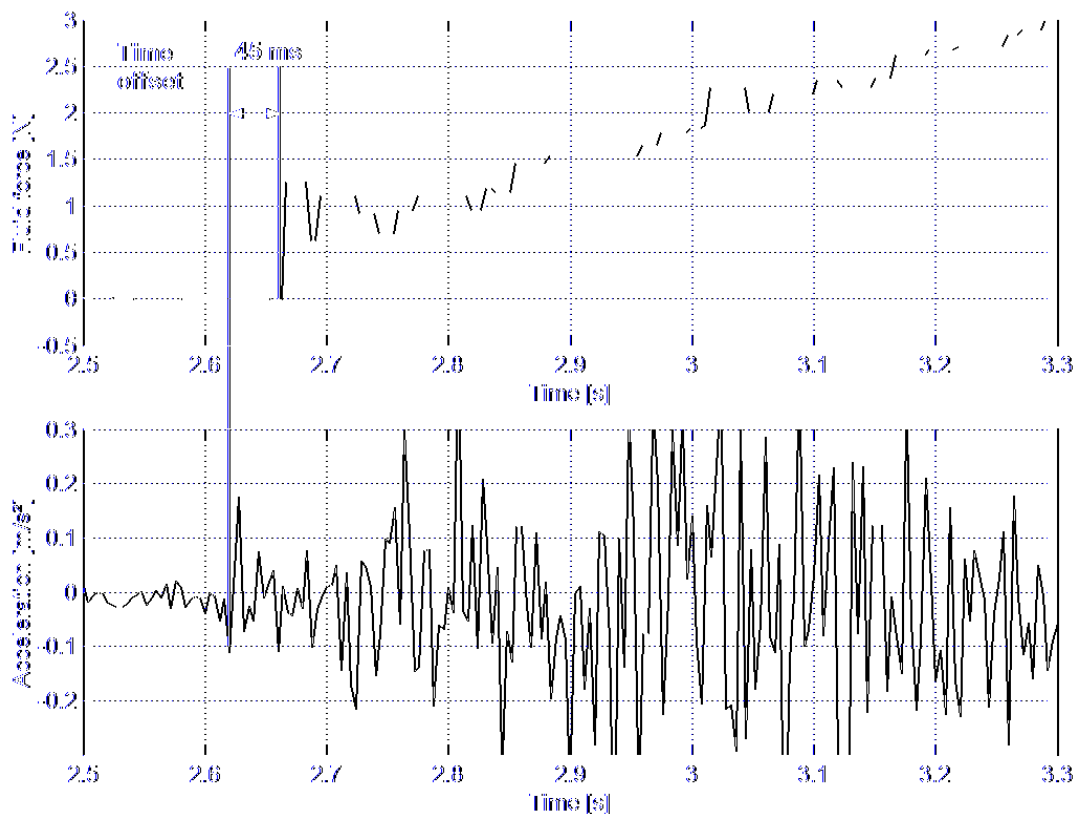


Fig. 6.11 Determination of the filling process initial time based on the sudden acceleration of weighing system when the water jet impacts for the first time

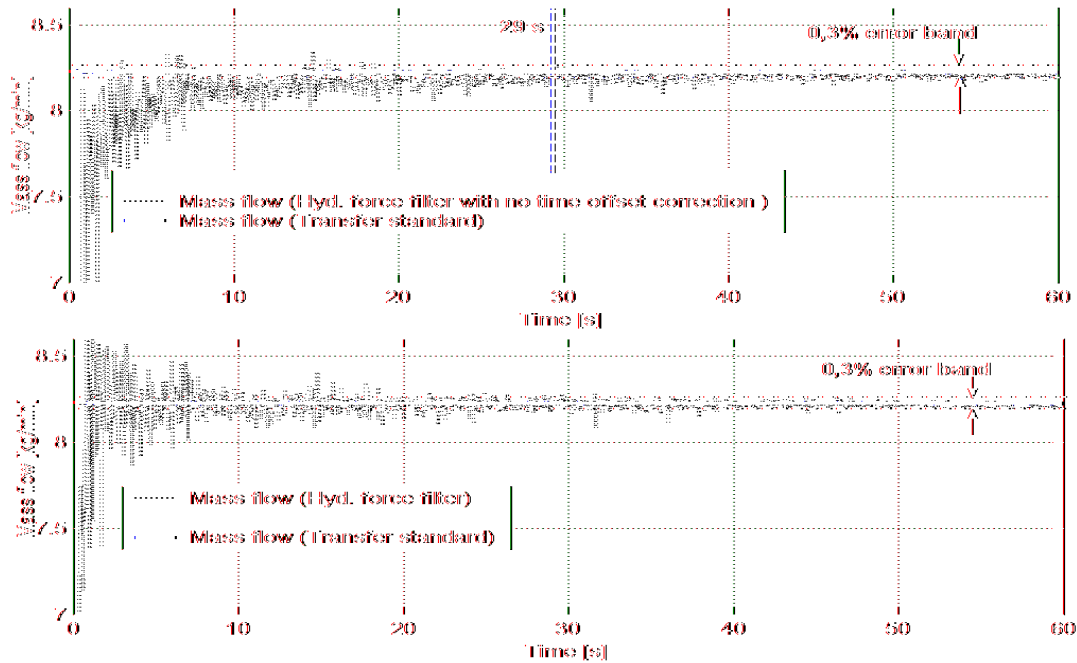


Fig. 6.12 Time-offset effect upon the hydrodynamic force filter's mass flow rate estimate values

Fig. 6.13 summarizes the three mass flow rates performed in this experiment with sets of three measurement points each. The aim of gathering this information is to observe how relevant is the minimization of the hydrodynamic force as well as the buoyancy force for the accuracy enhancement of the measurand. Below, there are some remarks extracted from these data.

At 8 kg/min, the mass flow rate values given by the balance readout are out of the $\pm 0,09\%$ uncertainty level of the transfer standard. Furthermore, the relative error yield by the hydrodynamic force filter is nearly in the limit of the uncertainty value of the transfer standard. However, when comparing the two calculation approaches: the Balance response $\hat{m}_{Bal}(t_n)$ (Eq. 4.1) and the hydrodynamic force filter $\hat{m}_{HF}(t_n)$, it is clear that the hydrodynamic force filter has improved the measurement accuracy by a factor of 2.

The measurements taken from both measuring methods at 5 kg/min show closeness to the reference value, within $\pm 0,06\%$ and $\pm 0,025\%$ for the balance readout and hydrodynamic force filter, respectively. At 3 kg/min, both measurement approaches were also within the claimed uncertainty level of $\pm 0,1\%$. However, the percent relative error between 0,02% and 0,05% turned out to be a bit larger than expected, when compared with the previous higher flow rate at 5 kg/min (narrow range between 0,02% to 0,025%).

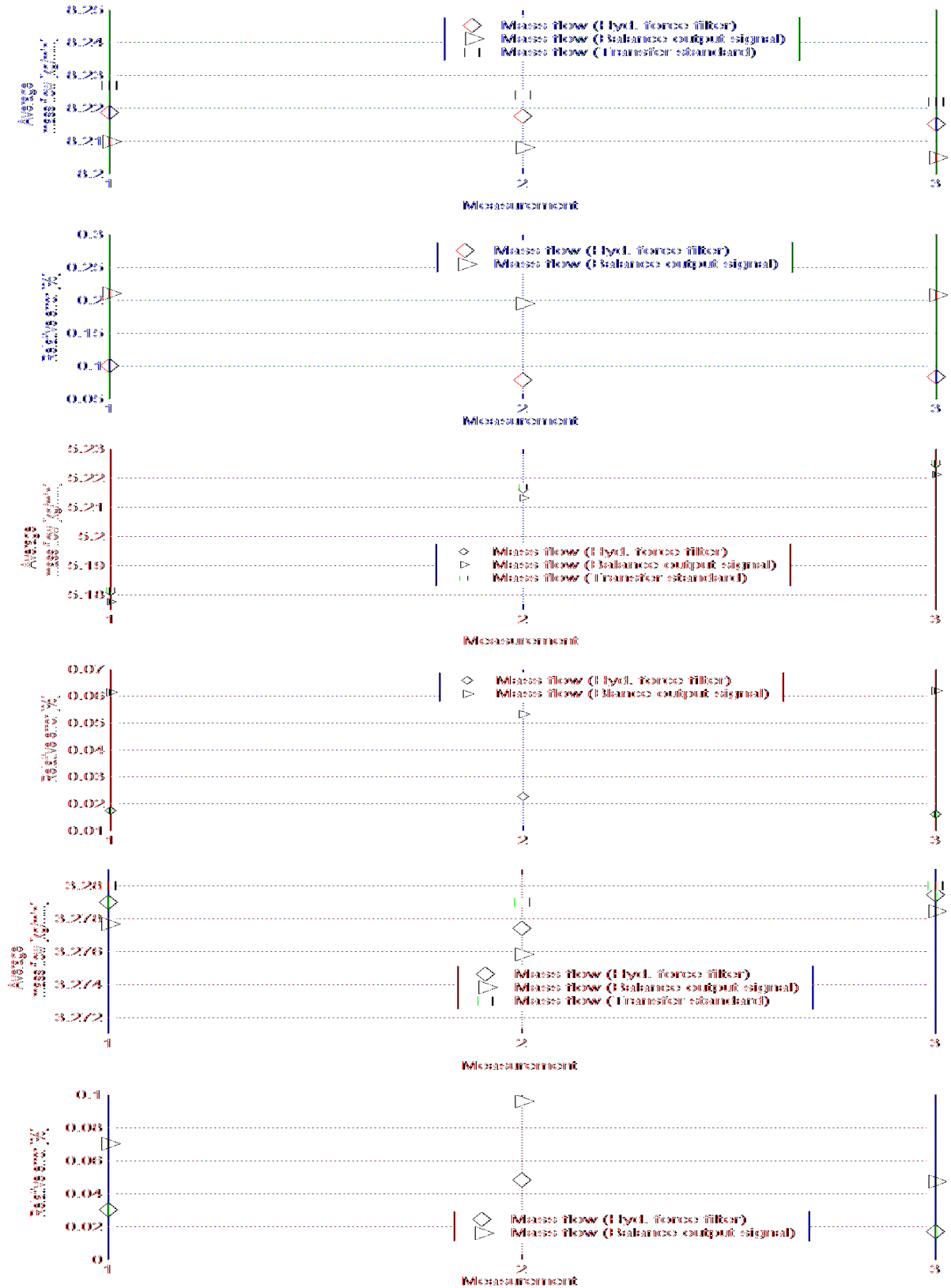


Fig. 6.13 Measurement comparison of estimate mass flow rates by means of using a hydrodynamic force filter and by direct balance output response

The fluctuating mass flow rate can be another contributing factor in the average relative error shown in **Fig. 6.13**, and particularly at 3 and 5 kg/min. This assumption can be explained by when comparing the possible correlation existing between the average percent relative error (**Fig. 6.14**), and the approximated level of fluid flow fluctuation measured by the transfer standard (**Fig. 6.14**). Here, the highest data dispersion is found in both cases at the lowest and highest flow rate (3 kg/min and 8 kg/min), and the smallest at the mid flow rate, 5 kg/min.

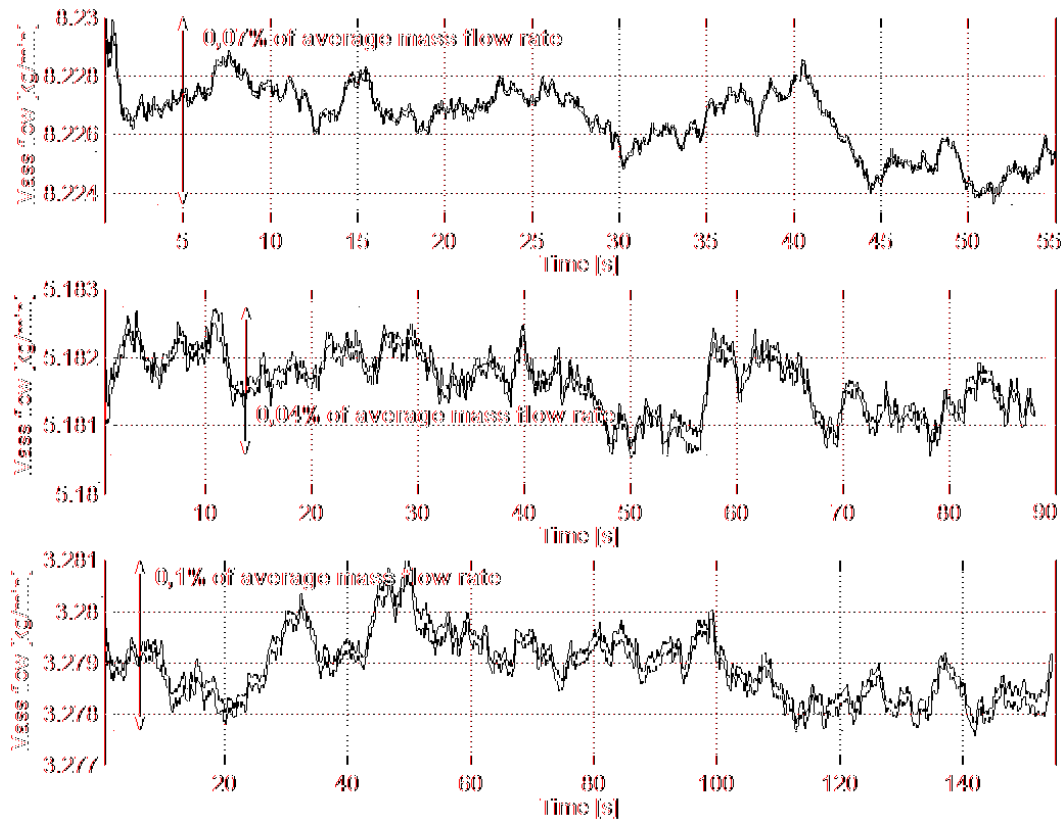


Fig. 6.14 Quasi-steady mass flow rate data measured by the transfer standard

The term average relative error is highlighted with the intention of illustrating how the estimate fluctuating mass flow rate depicted in **Fig. 6.14** can impact the measurand value of the transfer standard or a flowmeter. This situation is present in a major or a minor degree, even if the measurement process is intended to be carried out at a constant mass flow rate (an ideal condition that cannot be achieved so far by any liquid flow calibration facility). These observations are important to be kept in mind, especially in a static weighing system, which is unable to monitor this non-steady parameter, and its implications in terms of the measurement accuracy of the flowmeter under calibration.

6.6.5 Summary

Fig. 6.15 presents the results of the different approaches used to estimate the time-varying mass flow rate in the form of a histogram. Such approaches are listed below, in accordance to the block diagram of the process model subsystem shown in **Fig. 6.6**.

1. Balance force response (**Eq. 4.1**),
2. Hydrodynamic force filter,
3. Three proposed measurement noise filters:
 - a) *Central moving average*,
 - b) *Least-Mean-Square (LMS) adaptive filter*, and
 - c) *Linear Kalman filter*,
4. Flowmeter used as a transfer standard (measurand reference)

For instance, in **Fig. 6.15** the balance force response and the hydrodynamic force filter approaches feature equally wide data distribution, which is due to the fact that both signals have not been treated at this point by the influence of the measurement noise. As recalled, the measurement noise is referred as the noisy signal embedded in the balance output response, and it is considered to be mostly caused (but not entirely) by the dynamics of the weighing system, in response to the existing measurement process fluid-mechanical conditions. On the other hand, the difference seen between these two approaches is indeed in terms of their mean value, which in case of the hydrodynamic force filter turns out to be closer to the reference mean value, because its data have been corrected from the water jet impact force and the air buoyancy effects upon the measurand. At the first glance, **Fig. 6.15** could suggest that the percent relative difference between the hydrodynamic force filter and the transfer standard mean values is proportional to the operational mass flow rate. However, when looking more carefully at the percent relative difference of the hydrodynamic force filter data at 5 kg/min (0,018%), it turns out to be smaller than at 3 kg/min (0,03%), and therefore, it implies that such a statement cannot be simply taken for granted.

One of the possible explanations about why this relative difference magnitude is not fully (or necessarily) proportional to the mass flow rate can be related with the level of flow steadiness and its stationary condition. For example, the measurements carried out at 3 kg/min and 8 kg/min feature a multi-peak histogram, meaning that such mass flow rate data were not only quasi-steady

in the process, but also slightly shifting (decreasing) from its nominal mean value (**Fig. 6.14**). In this case, the given conditions imply that the largest peak in the data distribution corresponds to the flow rate that lasted longer during the measuring run, and whereby its mean value will trend to lie in that direction (out of the range midpoint as seen in **Fig. 6.15**). On the other, when looking at the measurement data at 5 kg/min, one can be inferred that a more steady and stationary flow is taking place, because the transfer standard reference data depict a more homogeneous distribution.

As for the LMS adaptive filter performance, it is observed that besides attenuating the induced measurement noise (compared to the hydrodynamic force filter), it turns out its mean value nearly coincides with the mean value of the central moving average filter, as shown in **Fig. 6.15**. One reason for this common behavior is that for this specific data processing task, both filter algorithms obtained a similar weighted average magnitude (with their corresponding coefficients) for the three selected mass flow rates.

Concerning the central moving average, it is demonstrated in **Fig. 6.15** that despite its limited number of estimate values, (in relation to its counterparts, LMS adaptive and Linear Kalman filters), it is able to deliver precise and accurate results. The latter statement applies even if the mean value of the central moving average was not overlapping the reference data at 8 kg/min (with a relative difference of 0,09%). This is because, in practice, the true mass flow mean value can lie within the claimed uncertainty of $\pm 0,1\%$, in relation to the transfer standard mean value. On the other hand, as already recalled in **Chapter 5**, the number of estimate values (17 at 8 kg/min, 22 at 5 kg/min, and 47 at 3 kg/min) given by the central moving average should not be a limitation, because 5 to 10 measurements per mass flow rate can be statistically sufficient to calibrate a flowmeter.

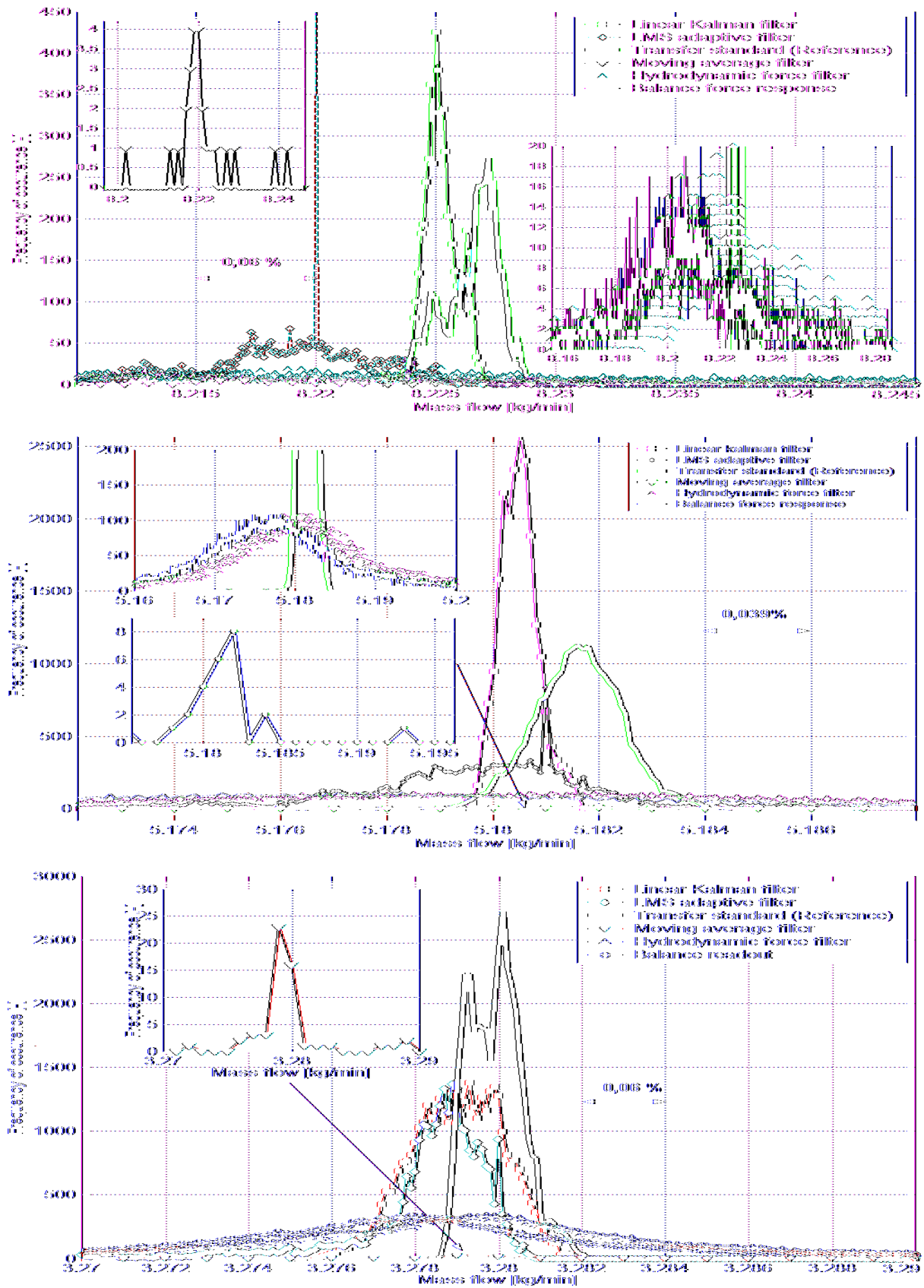


Fig. 6.15 Histograms summarizing the different mass flow rate estimation processes

In relation to the Linear Kalman filter, **Fig. 6.15** shows two narrow and large data distributions at 8 kg/min and 5 kg/min, which indicate that most likely a slightly larger variance was assigned to the measurement noise model of the filter. In other words, it is inferred that the estimate values were relying more on the measurement noise model than on the measurements. Furthermore, according to the narrow shape of the Kalman filter data distribution, it points out that the estimate values are behaving in a linear trend. The Kalman filter histogram at 3 kg/min is a good example of a more accurate designation of the measurement variance, and its effect upon the filter tracking response (**Fig. 6.15**). Another interesting observation made after analyzing the histograms is the apparent systematic difference between 0,02% to 0,03% is taking place between the Kalman filter and the reference data, at 3, 5 and 8 kg/min. At this moment, there is no sufficient information that could clarify such a consistent difference in magnitude. Nevertheless, a possible explanation to this behavior might be that the Kalman filter has not yet included the process noise model into its algorithm. In this instance, the process noise refers to the force effect of the internal flow-induced forces inside the collection vessel upon the balance output signal.

Table 6.2 shows the level of measurement uncertainty of some published results of flow calibration facilities which work within the frame dynamic *gravimetric flow measurements*:

| Flow laboratory | Type of system | Type of measurement | Flow range (kg/min) | Measurement uncertainty (95% confidence level) |
|---------------------------------------|------------------|---------------------|---------------------|--|
| Small NIST Cox bench [18] | ISO definition | Average flow | 0,5 to 8,0 | $\pm 0,12 \%$ |
| Large NIST Cox bench [18] | ISO definition | Average flow | 5,3 to 916 | $\pm 0,12 \%$ |
| NIST water flow primary standard [18] | Dynamic weighing | Time-varying flow | 300 to 720 | $\pm 0,036 \%$ |
| PTB Berlin [19] | ISO definition | Average flow | 500 to 3330 | $< \pm 0,05 \%$ |
| Rota Yokogawa GmbH [20] | Dynamic weighing | Time-varying flow | at 25 | $\pm 0,05 \%$ |
| PTB Braunschweig (proposal) | Dynamic weighing | Time-varying flow | 3,0 to 8,0 | $< \pm 0,1 \%$ |

Table 6.2 Current primary flow standards working under the dynamic weighing measurement principle

7. Conclusions and outlook

In this research work, a new method for the calibration of liquid flowmeters was presented, for its future application in liquid flow calibration laboratories. The characteristics, advantages and limitations of this new method have been described in terms of its principle of functionality as well as the next steps to be taken, in order to improve its current performance. This chapter summarizes all the conclusions and remarks of this ongoing long-term investigation.

First, it was necessary and feasible to *simulate the measurement process (Chapter 3)*, with the aim to understand the system's dynamic response, the main sources of noise in the process, their source, the role and significance of different process variables, and to verify the consistency of the experimental results. In this instance, the simulation applies to a 1 Degree-of-Freedom model, which despite analyzing the normal weighing axis (z axis), it highlights the most striking fluid-mechanical forces in the process: the water jet impact force, the collected mass force, the buoyancy force acting upon the system normal axis, and the normal reacting force of the weighing system

This calibration method can significantly *reduce the calibration time*, because it only requires a single measuring run (one collection per calibration point), and at the same time is capable of generating a large amount of measurement data for the characterization of a flowmeter. For example, the factor of calibration time reduction could be agreed to be five, if one considers that each calibration point (i.e. static weighing method) requires at least five measurements. This number is based on some calibration procedures [1], which consider that amount of data as statistically sufficient for a measurement uncertainty analysis (**Section 1.2**). Another advantage of this calibration method is the possibility to implement it in a static weighing liquid flow primary standard, without the necessity to modify the mechanical design of such a facility. This means that the user can perform a flowmeter calibration, either in a static or in a dynamic weighing mode by using a single facility. Moreover, in a dynamic weighing liquid flow primary standard, the thorough characterization and fast actuation of a diverter valve (**Chapter 2**) is not longer a system requisite, since the proposed calibration principle only requires the diverter valve to act as an ordinary bypass valve, to directs the fluid into the vessel, and bypasses it back to a supply tank when the collection is completed.

In the *hydrodynamic force filter*, the effect and quantification of the water jet turbulence as well as the viscous shear stress caused by the water jet-air interaction [2] were not included in the current analysis, due to the complexity in deriving an analytical model. However, as demonstrated in experimental tests, the simplified water jet impact force model (based on the Bernoulli equation, geometry and dimensions of the system) proves to be good enough in estimating the average impacting force of the water jet (**Chapter 6**). In this case, the average impact force can be calculated, due to the fact that the turbulent flow is quasi-steady [3]. In summary, even if such a force cannot be exactly quantified, it greatly helps in diminishing the unwanted hydrodynamic force effect from the process. This is clearly seen in **Chapter 5** and **Chapter 6**, wherein such a filter is compared with a mass flow rate calculation that overlooks the water jet impact force.

As for the three proposed *measurement noise filters*, the following observations were made. The central moving filter yields a limited number of estimates in relation to the LMS adaptive and the Kalman filter. Nevertheless, such a number can turn out to be sufficient and accurate enough, if compared with the number of data samples required in a regular calibration procedure. In regards to the LMS adaptive filter, it estimates the time-varying mass flow rate in a similar way the central moving average does, except that the adaptive filter can reproduce more estimates than the central moving average. On the other hand, in terms of their initial response, the LMS adaptive filter and the central moving average require some time to converge the reference values, and to overcome the high-amplitude overshoot response seen at the first 1/3 of the collection time. The third proposed algorithm, the linear Kalman filter requires less computational power than the LMS adaptive filter. Furthermore, as observed at the results in **Chapter 5** and **Chapter 6**, the Kalman filter seems to deal better with the high-amplitude measurement noise at the beginning of the process, as well as tracking and estimating more effectively the fluctuating mass flow rate. The usage of the average mass flow rate magnitude (obtained from the hydrodynamic force filter data) turned out to be an appropriate estimation parameter for the Kalman filter and the LMS adaptive filter because, as already mentioned, the process was carried out at quasi-steady flow conditions. And, as demonstrated in numerical and experimental results, the Kalman filter delivers the largest number of estimates with the lowest percent of relative error. Therefore, it was chosen as the measurement noise filter.

As for the experimental tests, *accuracy levels of less than $\pm 0,1\%$* are attainable by applying the dynamic weighing liquid flow calibration approach. However, it is worth recalling that this number is given in accordance to estimate mass flow rate values that stood within the claimed accuracy of the PTB transfer standard (used in the comparison test). Another interesting characteristic found in some experimental data was the similar time-varying mass flow rate measured by the two different approaches (the process model and the transfer standard), which suggests that in reality the flow might indeed follow such a particular path (**Chapter 6**). Nonetheless, in order to confirm this observation, it is necessary to compare the proposed calibration method with another high-accurate flow primary standard such as a piston prover (**Chapter 2**) or a Laser Doppler Anemometer system (LDA) [4].

According to numerical tests, the *accuracy and precision* of the measurements could be significantly enhanced if the data sampling frequency of the weighing system was increased, and the low pass filter avoided. This also raises the conclusion that a customized balance for this particular application would be the ideal case, by allowing the user to acquire the balance analog output signal without aliasing effects, understanding and treating more effectively the unwanted process and measurement noisy signals from the acquired data, and thus, obtaining a more accurate mass flow rate estimate. Furthermore, the concept of a customized balance would also help in the sense of getting a closer numerical representation of the physical weighing system, in terms of studying in depth the impact of the system dynamics upon the measurand determination (i.e. knowing the algorithm of the balance positioning control loop).

According to the mechanical frequency analysis presented in **Chapter 6**, it is demonstrated that the system is subjected to move not only along its weighing axis, but also to at least two additional translational and/or rotational axes. From the previous observations made and in the literature [5 and 6], it indicates that this behavior is caused by the acting radial fluid forces of a generated vortex inside the collection vessel, and the reacting orthogonal forces of the balance (due to the slight transverse sensitivity of its cell). To better understand this system condition and its influence on the balance output signal (mechanical crosstalk effect), it is necessary to analyze, in future, the system as a *2 or 3 Degrees-of-Freedom case*. The process requires that the model should include the time-varying acting moment (torque) generated by the normal and radial fluid forces [7] and their location, and the reacting time-varying moment of inertia of the system during its operation. In order to apply this concept, it is necessary to know (or to estimate) the

magnitude of these acting forces. Therefore, it will be required to quantify their magnitudes by using an experimental approach, such as the Particle Image Velocimetry (PIV) [8], and/or a numerical analysis via Computational Fluid Dynamics (CFD) [5]. In terms of its application, this process condition can be added into the Kalman filter; so that the algorithm will be able to take into account some of the *process noise* generated by the fluid dynamics as well as the recalled system measurement noise. This will benefit the calibration procedure in re-enhancing its current accuracy and precision.

As a next step in this research work, the mechanisms for effective *system's energy dissipation* [9] have to be investigated. A liquid flow primary standard has to be designed in such a way that its dimensional and geometrical characteristics (i.e. the vessel diameter and its height, the system's mass, the discharging nozzle cross section area, and its location), allow it to diminish the level of disturbance caused by the stored kinetic energy in the system (The higher the rate of energy dissipation, the lower the influence of the process and measurement noise upon the measurand). In practical terms, this rate of energy dissipation can be correlated with the system's inertial force or its oscillatory acceleration.

The influence of the *water surface waves* in the collection vessel and the *water jet mass* have not being treated in this research work. However, for the case of the water surface waves, this phenomenon cannot be disregarded for a future analysis because, as visually observed, this is an inherent process characteristic, which might influence (in some measure) the balance response [10]. On the other hand, it is more appropriate to first investigate the influence of the internal vortex because this process variable, in addition to the water jet impact is responsible (cause) for generating the surface waves (effect). Moreover, in accordance to the experiments carried out, the influence of the water jet mass (interpreted as a water mass column) was not observed, as Shinder et al. mention in its analysis [11]. However, this is not discarded, and it will be reconsidered in future experiments, in order to ensure whether that variable takes place in the measurement process or not.

Nomenclature

| | |
|------------------------|---|
| \mathbf{A} : | Transition matrix |
| A : | Arbitrary cross section area in a pipeline |
| A_{CV} : | Arbitrary area of the connecting volume wherein the mass flow passes through |
| A_{Meter} : | Cross section area of the flowmeter |
| A_n : | Cross section area o the nozzle outlet |
| A_{Piston} : | Inner cross section area of a piston prover |
| A_v : | Cross section area of the collection vessel |
| $c_{Bal}(t)$: | Damping coefficient of a mechanical system |
| \mathbf{E}_n : | Characteristic time-varying matrix |
| $e_{AF}(t_n)$: | Feedback error signal estimate (Adaptive filter) |
| $F_b(t)$: | Time-varying buoyancy force |
| $F_{Bal}(t)$: | Balance reacting force due to its stiffness coefficient |
| $F_{BalLPF}(t)$: | Time-varying oscillatory force response of the balance driven by the low pass filter |
| $F_c(t)$: | Weighing system damping force |
| $F_d(t)$: | Time-varying hydrodynamic force caused by the water jet impact |
| $F_{Inertial}(t)$: | Time-varying inertial force exerted by the weighing system |
| $F_m(t)$: | Fluid force due to time-varying collected mass and local acceleration of gravity |
| $F_q(t)$: | Additional fluid forced acting upon the weighing system (i.e. Vortex axial and water wave oscillatory forces) |
| $F_T(t)$: | Time-varying total fluid force |
| $\Sigma F_{Mech}(t)$: | Summation of weighing system mechanical forces |
| f_d : | Balance frequency response |
| f_{LPF} : | Low-pass filter cutoff frequency |

Nomenclature

| | |
|-----------------------------------|--|
| $f_{Meter}(t_n)$: | Turbine flowmeter rotor frequency |
| $G_{LPF}(f_d)$: | Low pass filter gain factor |
| g : | Local acceleration of gravity |
| \mathbf{H} : | Measurement matrix |
| $h(k)$: | Current k-number filter coefficient (Least-Mean Square adaptive filter) |
| $h_i(t)$: | Water jet impact height |
| $h_i(0)$: | Initial water jet impact height |
| $\hat{h}_i(t_n)$: | Discrete time-varying estimate of the water jet impact height |
| $\hat{h}_i(z)$: | Water jet impact height estimate as a function of the balance displacement |
| $h_{up}(k)$: | Update k-number filter coefficient (Least-Mean Square adaptive filter) |
| $h_w(t)$: | Increasing height of the water surface |
| \mathbf{I} : | Identity matrix |
| \mathbf{K}_n : | Kalman gain matrix |
| K_{Meter} : | Turbine flowmeter calibration factor |
| k_{Bal} : | Balance stiffness coefficient |
| M : | Number of filter coefficients |
| $\hat{m}(t)$: | Continuous time-varying estimate mass flow rate |
| $\overline{\hat{m}}_{Bal}(t_n)$: | Average discrete time-varying mass flow rate |
| $\hat{m}_{HF}(t_n)$: | Hydrodynamic force filter estimate of time-varying mass flow rate |
| m_{ISO} : | Reference mass used by an ISO dynamic gravimetric liquid flow primary standard |
| \dot{m}_K : | Mean mass flow rate (Kalman filter) |
| $\hat{m}_K(t_n)$: | Discrete time mass flow rate estimate (Kalman filter) |
| $\hat{m}_{MA}(t_n)$: | Discrete time-varying mass flow rate estimate via moving average filter |
| $\hat{m}_{MA}^+(t_n)$: | A priori discrete time-varying mass flow rate estimate via moving average filter |

Nomenclature

| | |
|--------------------------|---|
| $\hat{m}_{MA}^-(t_n)$: | A posteriori discrete time-varying mass flow rate estimate via moving average filter |
| $\dot{m}_{Meter}(t_n)$: | Mass flow rate measured by the flowmeter |
| m_p : | Weighing platform mass |
| m_{Total} : | Total fluid mass |
| $m_T(t)$: | Continuous time-varying total mass held by the balance elastic elements |
| m_{Tr1} : | Reference-mass triggering point (Start) according to ISO dynamic gravimetric liquid flow primary standard |
| m_{Tr2} : | Reference-mass triggering point (Stop) acc. to ISO dynamic gravimetric liquid flow primary standard |
| m_v : | Collection vessel mass |
| \dot{m}_w : | Mass flow rate |
| $m_w(t)$: | Continuous time-varying collected water mass |
| $\hat{m}_w(t_n)$: | Discrete time-varying estimate mass flow rate |
| \bar{m}_{wIN} : | Mass flow rate of a fluid entering a finite volume |
| \bar{m}_{wOUT} : | Mass flow rate of a fluid entering a finite volume |
| N_{AF} : | Number of input signal data |
| N_{MA} : | Number of data samples used by the moving average filter |
| \mathbf{P}_n^- : | Predicted estimate error covariance matrix |
| P_{AF} : | Average power of the input signal data set (Adaptive filter) |
| $p(\lambda)$: | Eigenvalue polynomial equation |
| \mathbf{R} : | Measurement noise covariance |
| t_{ISO} : | Collection time according to ISO dynamic gravimetric liquid flow primary standard |
| t_n : | Discrete time |
| t_{Piston} : | Piston stroke time |
| t_{Total} : | Total collection time |

Nomenclature

| | |
|--------------------------|--|
| $U_e(t_n)$: | Measurement uncertainty related to time-varying process model algorithm |
| U_{CV} : | Measurement uncertainty attributed to the connecting volume |
| \bar{u} : | Average fluid velocity at an arbitrary point |
| $u(t)$: | Mean velocity of the fluid at an arbitrary region across the connecting volume |
| $u_{Meter}(t)$: | Mean normal velocity at the flowmeter location |
| $u_i(t)$: | Normal impact velocity of the water jet |
| $u_n(t)$: | Mean normal velocity at the nozzle location |
| V_{CV} : | Connecting volume between weighing system and meter under calibration |
| \dot{V}_{PTB} : | Volumetric flow rate determined by the PTB primary flow standard |
| V_{Total} : | Total fluid volume |
| $V_w(t)$: | Time-varying collected water volume |
| $v(t_n)$: | Discrete time-varying measurement noise estimate |
| $\hat{v}(t_n)$: | Discrete time estimate measurement noise |
| $v_K(t_n)$: | Discrete time measurement noise (Kalman filter) |
| $\hat{\mathbf{x}}_n^-$: | Current mass flow rate estimate vector |
| $\hat{\mathbf{x}}_n$: | Corrected state estimate value |
| x_{Piston} : | Piston displacement |
| \dot{x}_{Piston} : | Piston velocity |
| \mathbf{y}_n : | Current measurement vector |
| z : | Balance normal displacement |
| \dot{z} : | Weighing system velocity |
| \ddot{z} : | Weighing system acceleration |
| ρ_A : | Air density |
| ρ_w : | Water density |
| $\rho_{w_{CV}}$: | Water density in the connecting volume |
| $\rho_{w_{Meter}}$: | Water density at the flowmeter location |

Nomenclature

| | |
|---------------------|---|
| $\rho_{w,n}$: | Water density at the nozzle outlet |
| ϑ_A | Air temperature |
| ϑ_w : | Water temperature |
| ω_d : | Damped angular frequency of the balance |
| ω_{LPF} : | Low-pass filter cutoff angular frequency |
| $\omega_n(t)$: | Time-varying system's natural angular frequency |
| $\theta_{LPF}(t)$: | Low pass filter phase shift |
| σ_K^2 : | Mass flow rate variance (Kalman filter) |
| β_w : | Volumetric thermal expansion coefficient of water |
| α_{CV} : | Linear expansion coefficient of the connecting pipe |
| $\lambda(t_n)$: | Discrete time-varying eigenvalues |
| Δ_{AF} : | Adaptive filter step size |
| ζ : | Critical damping fraction |

Acronyms

| | |
|----------------|--|
| <i>ISO</i> : | International Standardisation Organisation |
| <i>PTB</i> : | Physikalisch-Technische Bundesanstalt |
| <i>NIST</i> : | National Institute of Standards and Technology |
| <i>MUC</i> : | Meter Under Calibration |
| <i>CV</i> : | Connecting Volume |
| <i>LPF</i> : | Low Pass Filter |
| <i>EFC</i> : | Electromagnetic Force Compensation |
| <i>LMS</i> : | Least-Mean Square algorithm |
| <i>MA</i> : | Moving Average filter |
| <i>NLMS</i> : | Normal Least-Mean Square filter |
| <i>HF</i> : | Hydrodynamic Filter |
| <i>DWLFS</i> : | Dynamic Weighing Liquid Flow Standard |

References

Chapter 1

- [1] M. Rinker, G. Wendt, *Legal Metrology in the Field of Fluid Measurement Technology*, PTB-Mitteilungen **119** (2009), No. 1, Special Issue “Metering Energy and Fluid Flows”, Braunschweig, Germany, 2009, pp. 28-30

Chapter 2

- [1] O. Madsen, *Summary of finite control volume analysis in fluid mechanics*, Engineering mechanics II, Faculty of civil and environmental engineering, Massachusetts Institute of Technology (MIT), USA, April, 2006
- [2] The Instrumentation, Systems and Automation society (ISA), *The automation, systems and instrumentation dictionary*, Fourth edition, ISA, NC, USA, November, 2005
- [3] M. Reader-Harris, J. McNaught, *Impulse lines for differential pressure flowmeters: Best practice guide*, National Engineering Laboratory (NEL), Glasgow, UK, September, 2005
- [4] J. Bentley, *Principles of measurement systems*, Fourth edition, Pearson education limited, England, 2005
- [5] D. Spitzer, *Flow measurement: practical guides for measurement and control*, Second edition, The Instrumentation, Systems and Automation Society, ISA, USA, 2001
- [6] R. Arias, *Measurement uncertainty of an orifice plate flowmeter (In Spanish)*, National center of metrology (CENAM), Querétaro, México, April, 2001
- [7] R. Baker, *Flow measurement handbook: Industrial designs, operating principles, performance, and applications*, Cambridge University press, USA, 2000
- [8] R. Miller, *Flow measurement handbook*, Third edition, McGraw Hill professional, New York, NY, USA, March, 1996
- [9] S. Phillips, W. Estler, T. Doiron, K. Eberhardt, M. Levenson, *A careful consideration of the calibration concept*, Journal of research of the National Institute of Standards and Technology, NIST, Vol. 106, No. 2, Gaithersburg, MD, USA, April, 2001

References

- [10] Bureau International des Poids et Mesures (BIPM), *Concept of traceability and standards*, BIPM, Cedex, France, 2004, <http://www.bipm.org/en/convention/wmd/2004/>
- [11] P. Espina, *A question of accuracy: What does it mean to be traceable?*, NIST, Gaithersburg, MD, USA, 2000
- [12] Bureau International des Poids et Mesures (BIPM), *International vocabulary of metrology: Basic and General concepts and associated terms (VIM)*, BIPM, Cedex, France, 2008
- [13] G. Wendt, R. Engel, J. Riedel, *Ensuring the Traceability of Volume and Flow Measurements of Liquids*, PTB-Mitteilungen **119** (2009), No. 1., Special Issue “Metering Energy and Fluid Flows”, Braunschweig, Germany, pp. 23-27
- [14] W. Pöschel, R. Engel, *The concept of a new primary standard for liquid flow measurement at PTB Braunschweig*, The 9th International conference of flow measurement, FLOMEKO 1998, Lund, Sweden, June 15th-17th, 1998
- [15] A. Sleigh, C. Noakes, *Fluid dynamics: The momentum and Bernoulli equations*, CIVE 1400: Fluid Mechanics, Leeds University, UK, January, 2009
- [16] R. Engel, B. Mickan, *Aspects of traceability and comparisons in flow measurement*, 7th International Symposium on Fluid Flow Measurement (ISFFM), Alaska, USA, August 12th-14th, 2009
- [17] W. Pöschel, R. Engel, D. Dopheide, H. Kecke, R. Praetor, N. Weist, E. Kurras, *An unique fluid diverter design for water flow calibration facilities*, 10th International conference of flow measurement, FLOMEKO 2000, Salvador, Brazil, June 5th-8th, 2000
- [18] International Standard Organization, *ISO 4185, Measurement of liquid flow in closed conduits: Weighing method*, First edition, Ref. No: ISO 4185-1980(E), Switzerland, 1980
- [19] R. Paton, *Calibration and standards in flow measurement*, Reproduced from the Handbook of measuring system design, John Wiley and Sons, Ltd, UK, 2005
- [20] T. Yeh, J. Aguilera, J. Wright, *NIST Hydrocarbon liquid flow calibration services*, Chemical science and technology laboratory, NIST special publication 250-1039, USA, 2005
- [21] J. Kuttin, G. Bobovnik, I. Bajsic, *Dynamic effects in a clearance-sealed piston prover for gas flow measurements*, Metrologia 48, UK, January 2011

References

- [22] R. Arias, A. Loza, J. Lara, H. Luchsinger, *Dynamic calibration of a bi-directional prover for liquid flow measurements (In Spanish)*, National center of metrology (CENAM), Internal publication, Querétaro, México, 2000
- [23] M. van der Beek, *Euroloop: Measurement concepts for efficient calibrations and primary realization of accurate reference values in flow*, FLOMEKO 2003, Groningen, The Netherlands, 2003
- [24] N. Mathies, *Messunsicherheit einer gravimetrischen Kalt- und Warmwasser-Normalmessanlage für große Volumenströme*, Mensch und Buch Verlag, Berlin, 2005, p. 85
- [25] M. Shafer, F. Ruegg, *Liquid-flowmeter calibration techniques*, Transactions of ASME, October, USA, 1958, p. 1369
- [26] Küppers Elektromechnik GmbH, *Durchflußmeßgeräte kalibrieren*, Germany, 2010
- [27] V. Ivashenko, K. Podkopaev, T. Taranenko, V. Skorobogatov, *An automated standard test system flow liquid flow rates*, Translated from Izmeritel'naya Technika, No 4, Russia, April, 1976, pp. 36-38
- [28] R. Engel, *Dynamic weighing – Improvements in gravimetric liquid flowmeter calibration*, The 5th International symposium on fluid flow measurement, Arlington, VA, USA, 2002
- [29] X. Weilin, L. Huasheng, Y. Yongquan, W. Chigong, *Turbulent flow and energy dissipation in plunge pool of a high arch dam*, Journal of hydraulic research, Vol. 40, No. 4, UK, December, 2002
- [30] I. Shinder, I. Marfenko, *NIST calibration services for water flowmeters*, NIST special publication 250, National Institute of Standards and Technology (NIST), Gaithersburg, MD, August, 2006
- [31] I. Shinder, M. Moldover, *Accurately measuring unsteady water flows using a dynamic standard*, Measurement science conference, Anaheim, CA, USA, March, 2009
- [32] I. Shinder, M. Moldover, *Dynamic gravitational standard for liquid flow: Model and measurements*, International symposium on fluid flow measurements, Alaska, USA, August, 2009

Chapter 3

- [1] M. Kutz, *Mechanical Engineers' handbook*, Instrumentation, systems, controls, and MEMS, Third Edition, John Wiley & Sons, Inc., Hoboken, New Jersey, USA, 2006, p. 387
- [2] L. Brusquet, J. Oksman, *Improving the accuracy of tracer flow measurement techniques by using an inverse-problem approach*, Measurement science and technology journal, Vol. 10, UK, 1999, pp. 559-563
- [3] I. Shames, *Fluid Mechanics (Spanish)*, Third edition, McGraw Hill, USA, 1995, p. 9
- [4] M. Fogiel, *The fluid mechanics and dynamics problem solver*, Research and Education Association (REA), New York, USA, 1984, p. 294
- [5] Y.C. Fung, *A first course in continuum mechanics*, Prentice-Hall, Inc., Englewood Cliffs, N.J., USA, 1969, p.13
- [6] F. Jones, *Techniques and topics in flow measurement*, CRC Press, New York, USA, 2000, p. 71
- [7] R. Engel, *Dynamic weighing – Improvements in gravimetric liquid flowmeter calibration*, The 5th International symposium on fluid flow measurement, Arlington, VA, USA, 2002
- [8] A. Reichmuth, *Measuring mass and force with a balance*, Mettler Toledo, Vol.12, Greifensee, Switzerland, June, 1999
- [9] A. Reichmuth, *Adverse influences and their prevention in weighing: Design and working principles of laboratory balances, specifications of balances, and influences on balances and weighing samples*, Mettler Toledo, Vol. 13, Greifensee, Switzerland, May, 2001
- [10] U. Berli, M. Bönzli, *Electronic weighing principles*, Mettler Toledo, Greifensee, Switzerland, May, 1991
- [11] E. Manske, T. Fröhlich, R. Füßl, *Lehrmaterial zur Vorlesung Mess- und Sensortechnik*, Technische Universität Ilmenau, Fakultät für Maschinenbau, Institut für Prozessmess- und Sensortechnik, Ilmenau, Germany, December, 2010
- [12] J. Hartog, *Mechanics*, First edition, McGraw Hill, New York, USA, 1948, p.175
- [13] C. Harris, A. Piersol, *Shock and vibration handbook*, Fifth Edition, McGraw Hill, New York, USA, 2002, pp. 2.1-2.5 and 10.2

References

- [14] D. Findeisen, *System dynamics and mechanical vibrations*, Springer-Verlag, Heidelberg, Germany, 2000, p.30
- [15] S. Timoshenko, H. Young, *Engineering Mechanics*, Third edition, McGraw Hill, New York, USA, 1951, p. 303
- [16] F. Axisa, J. Antunes, *Modelling of mechanical systems: fluid structure interaction*, Volume 3, First edition, Elsevier Ltd., Oxford, Great Britain, 2007, p. 51
- [17] BIPM, *International vocabulary of metrology (VIM)*, France, 2008, p. 29
- [18] P. Gaydecki, *Foundation of digital design processing: Theory algorithms and hardware design*, IEEE, UK, 2004, p. 120
- [19] Thomson Delmar Learning, *Circuit analysis with devices: Theory and practice*, Chapter 22, 2007, p. 19
- [20] J. Wright, G. Mattingly, *NIST Calibration services for gas flow meters*, NIST Special publication 250-49, NIST, MD, USA, August, 1998, p. 3
- [21] D. Tritton, *Physical fluid dynamics*, Van Nostrand Reinhold (UK) Co, Ltd., Molly Millars Lane, Wokingham, Berkshire, England, 1982, p. 45
- [22] Y.C. Fung, *A first course in continuum mechanics*, Prentice-Hall, Inc., Englewood Cliffs, N.J., USA, 1969, p.11
- [23] T.T. Yeh, P. Espina, G. Mattingly, J. Aguilera, *An uncertainty analysis of a NIST hydrocarbon liquid flow calibration facility*, Proceedings of ASME HT/FED 04, 2004 Heat transfer/ Fluids engineering summer conference, Charlotte, N.C., USA, July, 2004
- [24] G. Elert, *The physics hypertextbook: Thermal expansion*, <http://physics.info/expansion/>, USA, 2010
- [25] M. Tanaka, R. Davis, A. Peuto, N. Bignell, *Recommended table for the density of water between 0 °C and 40 °C based on recent experimental reports*, Metrologia, Vol. 38, Issue 4, August, 2001
- [26] EURAMET, *Calibration of temperature block calibrators*, EURAMET Technical committee for thermometry, European Association of National metrology Institutes, EURAMET/cg-13/v.01, July, 2007, p. 10

- [27] R. Engel, H. Baade, *Model-based flow diverter analysis for an improved uncertainty determination in liquid flow calibration facilities*, Measurement science and technology, Volume:21, IOP Publishing, Ltd., UK, January, 2010

Chapter 4

- [1] W. Schmid, R. Arias, *Estimation of measurement uncertainty (Spanish)*, National center of metrology (CENAM), Querétaro, México, 2005, p.15
- [2] R. Davis, *A primer for mass metrology*, NBS special publication 700-1, Industrial measurement series, Gaithersburg, MD, USA, 1984, p. 8
- [3] A. Coehlo, *Signal processing and data filtering*, University of Santa Catarina (UFSC), Brazil, May, 2005, p.1
- [4] A. Prasad, *Introduction to error analysis*, Dept. of Mechanical engineering, Univ. of Delaware, USA, 2006, p.1
- [5] H. Fryer, *Concepts and methods of experimental statistics*, Allyn and Bacon, Inc. Boston, USA, 1966, p.4
- [6] P. Sydenham, *Static and dynamic characteristics of instrumentation*, CRC Press, University of South Australia, 2000, Section 3.2
- [7] M. Gläser, M. Borys, *Precision mass measurements*, Reports on progress in physics, No. 72, IOP Publishing, UK, 2009
- [8] L. Yao, *Linear and quadratic equation*, Chapter 1, Math 10, University of North Carolina, USA, 2005
- [9] S. Goode, *An introduction to differential equations and linear algebra*, Prentice Hall, New Jersey, USA, 1991, p. 283
- [10] C. Moler, *Numerical computing with MatLab®*, Chapter 10, The MathWorks, Inc, Natick, MA, USA, p. 17
- [11] D. Lay, *Linear algebra and its applications*, Second edition, Addison-Wesley, Massachusetts, USA, 2000, p. 311

References

- [12] J. Aguilera, T. Yeh, J. Wright, *Inside diameter measurements for the cylinder of a 20 L piston prover*, 6th International symposium on fluid flow measurement (ISFFM), Querétaro, México, May 16th-18th, 2006
- [13] NIST Statistical engineering division, *Engineering statistics handbook*, NIST, Maryland, USA, June, 2010, Section 6.4
- [14] A. Gelb, *Applied optimal estimation*, The Analytic Science Corporation (TASC), MIT Press, Cambridge, MA, USA, 1974, pp. 23, 102-119, 156
- [15] V. Stewart, *Echo cancelling*, Chapter 4, The Queen's University of Belfast, Ireland, 2000, p.59
- [16] P. Maybeck, *Stochastic models, estimation, and control, Volume 1*, Academic Press, Inc., New York, USA, 1979, pp. 5-15
- [17] S. Smith, *The scientist and engineering guide to digital signal processing*, chapter 15, California technical publications, California, USA, 2000, p. 278
- [18] Y. Chou, *Statistical analysis for business and economics*, Elsevier science Ltd., Amsterdam, The Netherlands, 1989, Section. 17.9
- [19] D. Hyde, *DPlot Graph software for scientist and engineers: Moving average*, HydeSoft Computing, Inc., Vicksburg, MS, USA, 2009
- [20] M. Van Exter, *Noise and signal processing*, Chapter 2, University Leiden, The Netherlands, August, 2003, p. 9
- [21] P. Gaydecki, *Foundation of digital design processing: Theory algorithms and hardware design*, IEEE, UK, 2004, pp. 120, 385-397
- [22] C. Feldbauer, F. Pernkopf, *Adaptive filters: A tutorial for the course in computational intelligence*, Institut für Grundlage der Informationverarbeitung, Technische Universität Graz, Austria, June, 2010
- [23] The MathWorks®, Inc., *Filter design Toolbox 4: User's Guide*, chapter 5, MatLab®, Natick, MA, September, 2010, pp. 5.20-5.24
- [24] A. Poularikas, Z. Ramadan, *Adaptive filtering primer with MatLab®*, Taylor and Francis Group, London, England, 2006, p. 2

References

- [25] The MathWorks®, Inc., *Filter design Toolbox 4: Getting started guide*, Chapter 5, MatLab®, Natick, MA, September, 2010, p. 5.4
- [26] K. Rekha, B. Nagabushan, K. Nataraj, *FPGA implementation of NLMS algorithm for identification of Unknown systems*, International journal of engineering science and technology, Vol. 2 (11) 2010, Chennai, India, 2010, p. 6397
- [27] National Instruments, *Least Mean Square (LMS) algorithms (Adaptive filter toolkit)*, Austin, TX, USA, June, 2008
- [28] C. Toker, *Recursive Least Squares (RLS) adaptive filters*, Chapter 9, Department of electrical and electronics engineering, Hacettepe University, Turkey, December, 2007
- [29] M. Junnti, *Communication signal processing: Recursive Least Squares (RLS) algorithm*, department of electrical and information engineering, University of Oulu, Finland, February, 2008
- [30] National Instruments, *Recursive Least Squares (RLS) algorithms (Adaptive filter toolkit)*, Austin, TX, USA, June, 2008
- [31] R. Kalman, *A new approach to linear filtering and prediction problems*, transactions of the ASME, Journal of basic engineering, 82 (series D), USA, 1960. pp. 35-45
- [32] J. Mandel, *The statistical analysis of experimental data*, Dover publications, Inc., New York, USA, 1984, p. 35
- [33] J. Taylor, *An introduction to error analysis: the study of uncertainty in physical measurements*, Second edition, University science books, Sausalito, CA, USA, 1997, pp. 137-141
- [34] V. Becerra, *Advanced system identification: the Kalman filter*, School of systems engineering, university of Reading, reading, UK, 2008
- [35] E. Crow, F. Davis, M. Maxfield, *Statistics manual*, US Naval ordnance test station, China lake, CA, USA, 1955, p. 14
- [36] G. Welch, G. Bishop, *An introduction to the Kalman filter*, Department of computer science, University of North Carolina, at Chapel Hill, NC, USA, July, 2006
- [37] G. Welch, *The Kalman filter learning tool: Dynamic and measurement models*, Department of computational science, University of North, USA, February, 2003

- [38] D. Simon, *Kalman filtering*, Department of electrical and computing engineering, Cleveland State University, Ohio, USA, June, 2001
- [39] B. Danforth, *Variance-Covariance matrix*, Department of computer science, University of North Carolina, at Chapel Hill, NC, USA, June, 2009
- [40] K. Van Laerhoven, *The Kalman filter*, School of computing and communications, Lancaster University, UK, August, 2004
- [41] A. Blumani, *Elementary statistics: A step by step approach*, Fifth edition, McGraw Hill, USA, 2004, p. 329

Chapter 5

- [1] E. Manske, T. Fröhlich, R. Füßl, *Lehrmaterial zur Vorlesung Mess- und Sensortechnik*, Technische Universität Ilmenau, Fakultät für Maschinenbau, Institut für Prozessmess- und Sensortechnik, Ilmenau, Germany, December, 2010
- [2] J. Aguilera, R. Engel, G. Wendt, *Dynamic-weighing liquid flow measurements – A description of the measurement process*, 1st International congress on mechanical metrology, Rio de Janeiro, Brazil, October, 2008
- [3] A. Crawshaw, A. Robinson, *The calibration of force transducers ‘On-the-fly’*, National Physical Laboratory, NPL Report CMAM 86, UK, September, 2002
- [4] J. Falcao, A. Nascimento, C. Mathias, *Dynamic pressure in plunge pool floors: Effect of air entrainment*, Department of civil engineering, Technical university of Lisbon, Portugal, 2001
- [5] A. Oota, T. Usuda, H. Nozato, T. Ishigami, T. Kikuchi, *Estimation of uncertainty of transverse sensitivity and vibration distribution of primary accelerometer calibration*, XIX IMEKO world congress, Fundamental and applied metrology, September 6th-11th, Lisbon, Portugal, 2009
- [6] R. Füßl, G. Jäger, *The influence of the force feed-in system on high-accuracy low force measurement*, XIX IMEKO world congress, Fundamental and applied metrology, September 6th-11th, Lisbon, Portugal, 2009

References

- [7] I. Choi, D. Choi, S. Kim, *Double force compensation method to enhance the performance of a null balance force sensor*, Japanese journal of applied physics, Vol. 41 (2002), pp. 3987-3993, part 1, N0 6A, June, 2002
- [8] Mettler Toledo®, *Proven weighing platforms WMH designed for automation*, Mettler Toledo, Greifensee, Switzerland, May, 2006
- [9] T. Pavlic, *Sources of Phase shift, Operational amplifiers and first-order circuits*, ECE 209: Circuits and electronics laboratory, Department of electrical and computing engineering, The Ohio state university, USA, 2009
- [10] R. Lyons, *Understanding digital signal processing*, Chapter 2, 3rd edition, Prentice Hall, USA, November, 2010
- [11] L. Bendig, M. Raudensky, J. Horsky, *Descaling with high pressure nozzles*, ILASS-Europe 2001, Zürich, Switzerland, September 2nd-6th, 2001
- [12] A. Gelb, *Applied optimal estimation*, The Analytic Science Corporation (TASC), MIT Press, Cambridge, MA, USA, 1974, pp. 23, 102-119, 156
- [13] B. Hall, *Mismatch uncertainty: Representation for complex calculations*, Measurement standards laboratory of New Zealand, 29th ANAMET Meeting, New Zealand, March, 2008
- [14] OIML, *Dynamic measuring systems for liquids other than water, Part 1: Metrological and technical requirements*, OIML R 117-1, A.6, Edition 2007 (E), Paris, France, 2007
- [15] J. Taylor, *An introduction to error analysis: the study of uncertainty in physical measurements*, Second edition, University science books, Sausalito, CA, USA, 1997, p. 123
- [16] P. Ribeiro, *Time-varying waveform distortion in power systems*, Chapter 15, First edition, Wiley and Sons, USA, September, 2009

Chapter 6

- [1] K. Holzer, *Untersuchung des Einflusses der Geschwindigkeitsverteilung der Strömung auf das Messverhalten von Wasserzählern*, Diplomarbeit Fachhochschule Braunschweig/Wolfenbüttel, Institut für Konstruktion und angewandten Maschinenbau, September, 2008, p. 6
- [2] D. Spitzer, *Flow measurement: practical guides for measurement and control*, Second edition, The Instrumentation, Systems and Automation Society, ISA, USA, 2001, p. 473
- [3] D. Wirklund, M. Peluso, *Flowmeter dynamic response characteristics part 1: Quantifying dynamic response*, International Symposium on Fluid Flow Measurement (ISFFM), Arlington, VA, USA, 2002
- [4] J. Riedel, H. Többen, *Untersuchungen zur Wiederholunsicherheit von Turbinenraddurchflussmessgeräten für Flüssigkeiten*, Technisches Messen 74, Germany, 2007
- [5] R. Baker, *Flow measurement handbook: industrial designs, operating principles, performance, and applications*, Cambridge University press, USA, 2000
- [6] National Instruments, *NI CompactRIO control and acquisition system*, NI, Austin, TX, USA, 2010
- [7] National Instruments, *NI 9233: 4-Channel, ± 5 V, 24-Bit IEPE Analog Input Module, operating instructions and specifications*, NI, Austin, TX, USA, 2008
- [8] National Instruments, *NI 9203: 8-Channel, ± 20 mA, 16-Bit Analog Input Module, operating instructions and specifications*, NI, Austin, TX, USA, 2008
- [9] National Instruments, *NI 9401: 8-Channel, TTL Digital Input/Output Module, operating instructions and specifications*, NI, Austin, TX, USA, 2008
- [10] Y. Fujii, *Optical method for accurate force measurement*, Society for Experimental Mechanics (SEM), CT, USA, 2004
- [11] Brüel and Kjaer, *Product data: Miniature DeltaTron® accelerometers, Types 4507 and 4508*, B&K, Naerum, Denmark, 2006
- [12] Brüel and Kjaer, *Primer on measuring vibration*, B&K, Naerum, Denmark, September, 1982, p. 19

References

- [13] Dytran Instruments, Inc., *Accelerometer mounting considerations*, Dytran Instruments, Inc., Chatsworth, CA, USA
- [14] E. Manske, T. Fröhlich, R. Füßl, *Lehrmaterial zur Vorlesung Mess- und Sensortechnik, technische Universität Ilmenau*, Fakultät für Maschinenbau, Institut für Prozessmess- und Sensortechnik, Ilmenau, Germany, December, 2010
- [15] R. Dorsch, G. Häusler, J. Hermann, *Laser triangulation: fundamental uncertainty in distance measurement*, Applied optics, Vol. 33, No. 7, USA, March, 1994
- [16] J. Aguilera, R. Engel, G. Wendt, *Dynamic-weighing liquid flow calibration system – realization of a model-based concept*, FLOMEKO 2007, Johannesburg, South Africa, September, 2007
- [17] Physikalisch-Technische Bundesanstalt, *Gravity Information System software (SIS)*, Mass division, Mechanics and acoustics department, PTB, Braunschweig, Germany, 2007, http://www.ptb.de/en/org/1/11/115/_index.htm
- [18] National Institute of Standards and Technology, Fluid metrology calibration services, Physical Measurement Laboratory (PML), NIST, Gaithersburg, Maryland, USA, <http://www.nist.gov/pml/div685/grp02/calibrations.cfm>
- [19] N. Mathies, *Messunsicherheit einer gravimetrischen Kalt- und Warmwasser-Normalmessanlage für große Volumenströme*, Mensch und Buch Verlag, Berlin, 2005, p. 87
- [20] R. Engel, *Dynamic weighing – Improvements in gravimetric liquid flowmeter calibration*, The 5th International symposium on fluid flow measurement, Arlington, VA, USA, 2002

Chapter 7

- [1] OIML, *Dynamic measuring systems for liquids other than water, Part 1: Metrological and technical requirements*, OIML R 117-1, A.6, Edition 2007 (E), Paris, France, 2007
- [2] G. Storr, M. Behnia, *Experiments with large diameter gravity driven impacting liquid jets*, *Experiments in fluids*, Vol. 27, Springer-verlag, Germany, 1999, pp. 60-69
- [3] T. Craft, *Simulation of turbulent flows*, TPFE MSc CFD-1, School of mechanical aerospace and civil engineering, The university of Manchester, U.K., November, 2010
- [4] Dantec dynamics, *Pipeflow profile measurements for NIST*, Publication note: LDA6, Dantec dynamics, Skovlunde, Denmark, 2000
- [5] X. Weilin, L. Huasheing, Y. Yongquan, *Turbulent flow and energy dissipation in plunge pool o f high arch dam*, *Journal of hydraulic research*, Vol. 40, No. 4, U.K., 2002
- [6] R. Füßl, G. Jäger, *The influence of the force feed-in system on high-accuracy low force measurement*, XIX IMEKO world congress, Fundamental and applied metrology, September 6th-11th, Lisbon, Portugal, 2009
- [7] V. Mik, *Normal impingement of a circular liquid jet onto a flat plate*, Proceedings of the international conference: Problems in fluid mechanics and hydrology, Vol. 1, Academy of science of the Czech republic, Prague, Czech republic, June 23-26 1999, p. 118
- [8] B. Thomas, Q. Yuan, S. Sivaramakrishnan, T. Shi, S. Vanka, M. Assar, *Comparison of four methods to evaluate fluid velocities in a continuous slab casting mold*, ISIJ International, Vol. 41, No. 10, USA, 2001, pp. 1262-1271
- [9] F. Axisa, J. Antunes, *Modelling of mechanical systems: Fluid structure interaction*, Volume 3, First edition, Elsevier, UK, 2007, p. 51
- [10] H. Nakamura, F. Kaminaga, K. Matsumura, *Self-induced sloshing of free surface caused by a free jet*, 7th International conference on nuclear engineering, ICONE-7268, JSME, Tokyo, Japan, 1999
- [11] I. Shinder, M. Moldover, *Dynamic gravitational standard for liquid flow: Model and measurements*, International symposium on fluid flow measurements, Alaska, USA, August, 2009